Invariant Mass Distributions of SUSY Cascade Decays

Anders Kvellestad

Department of Physics and Technology

University of Bergen

Master's Thesis in Theoretical Particle Physics

June 2011

Acknowledgements

First and foremost I would like to sincerely thank my supervisor Professor Per Osland for continuous help and guidance in the writing of this thesis. Thank you for introducing me to theoretical particle physics through three excellent courses, for patiently checking and rechecking my work, and for always taking time to answer my questions.

Also, I would like to thank Associate Professor Are Raklev at the University of Oslo for a short but most valuable discussion concerning this thesis.

I would further like to thank all the friendly people of the Bergen particle physics group for making the time here so memorable.

I am especially grateful for having spent these last couple of years together with such fine folks as Anders Haarr, Siri Fløgstad Svensson, Ørjan Dale, Ørnulf Amundsen, Siri Vaktdal and Eivind Larsen. It's been great wasting time with you.

Finally, I would like to thank family and friends, and especially Kaja, for all the support and encouragement you have provided.

Anders Kvellestad
Bergen, June 2011

Contents

Chapter 1

Introduction

1.1 Overview

As of today, the *Standard Model* (SM) constitutes our best description of the particle world. Based on the mathematics of quantum field theory, aided by experimentally determined parameters, the predictions of the SM are in astonishingly good agreement with experimental results. The basic structure of the SM in terms of forces and particle content is covered in this introduction, while the more mathematical treatment is given in Chapter 2.

Despite its tremendous success, there are good reasons to believe that there is more to nature than is accounted for in the SM, a topic we return to at the end of Chapter 2. Probably the most popular candidate for a theory going beyond the SM is the theory of *Supersymmetry* (SUSY). Its main motivations, concepts and possible phenomenological consequences are covered in Chapter 3.

If some form of SUSY is discovered experimentally, the next step will be to determine the parameters of the theory, most notably the masses of any new supersymmetric particles. For this purpose, studies of invariant mass distributions of SUSY decay chains might become an important tool. The main results of this thesis are presented in Chapters 4 – 6, in which analytical expressions for various such invariant mass distributions are derived and discussed. Concluding remarks, along with comments on possible expansions of the results given, can be found in Chapter 7.

Appendix A contains two supplementary results to the main result of Chapter 5, while in Appendix B an alternative derivation related to the result of Chapter 6 is

given. As all results in this thesis are in the form of differential decay rates, Appendix C contains an outline of how such observable distributions appear from the rather abstract language of quantum field theory.

We note that the results presented in this thesis are in principle independent of any specific experimental setting. Nevertheless, they are both motivated by and interpreted in the context of the proton-proton experiments currently running at the Large Hadron Collider (LHC) in Geneva.

1.2 Fundamental forces

The SM contains a consistent quantum description of three of the four known fundamental forces: the electromagnetic, the weak and the strong force. Gravity is left out of the picture, but this is of no direct consequence for the predictive power of the SM as gravitational effects are expected to be negligible all the way up to *Planck scale* energies, of the order of 10^{19} GeV. (In contrast, today's highest energy experiments, situated at the LHC, study particle collisions at energies around 10^4 GeV.) However, as physics at the Planck scale might dictate the structure of the particle world at much lower energies, it is a long-term goal of particle physics to obtain a complete theory where *all* forces are included.

Of the forces described by the SM, the electromagnetic force is perhaps the best-known. It binds atomic electrons to their nuclei and governs interactions between atoms and molecules, thus explaining most physical phenomena at our 'human length scale'. The classic example of a phenomenon due to the weak force is the beta-decay of unstable nuclei, in which a nuclear neutron decays into a proton, an electron and a neutrino. The weak force is the only fundamental force that has been shown to distinguish a particle interaction from its spatially inverted antiparticle interaction (CP violation), a key ingredient in the quest to explain the dominance of matter over anti-matter in the universe. Finally, the strong force is the force governing interactions of nuclear matter. It binds quarks together to form protons and neutrons, along with a wide range of more exotic composite particles known collectively as *hadrons*, and further dictates the interactions between these bound states.

In the Standard Model, all the above forces are described in terms of exchanges of spin-1 particles, called *gauge bosons*. The name refers to the mathematical description

Table 1.1: The gauge bosons of the Standard Model [1].

Interaction	Gauge Boson	Symbol	Charge [e]	Spin	Mass [GeV]
Strong	Gluon	g	0	1	0
Electromagnetic	Photon	γ	0	1	0
Weak	W boson	$W^{\pm}$	± 1	1	80.4
	Z boson	Z^0	0	1	91.2

in terms of *gauge theories*, which we cover in Chapter 2. The different gauge bosons are listed in Table 1.1.

Although usually referred to as two different forces, one of the cornerstones of the SM is the unified description of the electromagnetic and weak force in terms of a more fundamental *electroweak* force. Due to *electroweak symmetry breaking*, describing how the vacuum does not necessarily satisfy all the symmetries of the underlying theory (see Section 2.5), electromagnetism and weak interactions appear as two separate forces at low energies. This mechanism, thought to explain why the W and Z bosons are massive, introduces another boson to the theory, namely the much sought-after spin-0 *Higgs boson*.

1.3 Matter particles

According to the SM, the building blocks of matter acted upon by the above forces are spin-1/2 particles known as $fermions$. All ordinary atomic matter is build up of a few light fermions, while the heavier fermions only appear as unstable products of particle interactions. The set of known fermions can be divided into two subcategories: *leptons* and *quarks*. The leptons include the charged electron and its neutral electron neutrino, along with two 'heavier versions' of the electron (μ and τ) and their corresponding neutrinos. While the charged leptons feel both the electromagnetic and weak force, the neutrinos only interact through the weak force.

Similar to the leptons, the quarks can be grouped into three generations: The familiar up- and down-quarks make up the first generation, while the next two generations consist of heavier 'up-type' and 'down-type' quarks. Quarks are the only known particles to feel all three fundamental forces. The various types of quarks and leptons are

Table 1.2: The Standard Model leptons [1].

Lepton	Symbol	Charge [e]	Spin	Mass [MeV]
Electron	e	-1	1/2	0.511
Electron neutrino	ν_e	0	1/2	$< 2 \times 10^{-6}$
Muon	μ	-1	1/2	105.659
Muon neutrino	ν_μ	0	1/2	$< 2 \times 10^{-6}$
Tau	τ	-1	1/2	1.776×10^3
Tau neutrino	ν_τ	0	1/2	$< 2 \times 10^{-6}$

Table 1.3: The Standard Model quarks [1].

Quark	Symbol	Charge [e]	Spin	Mass [MeV]
Up	u	+2/3	1/2	(1.7 – 3.3)
Down	d	$-1/3$	1/2	(4.1 – 5.8)
Charm	c	+2/3	1/2	(1.18 – 1.34) $\times 10^3$
Strange	s	$-1/3$	1/2	(80 – 130)
Top	t	+2/3	1/2	(169.8 – 174.2) $\times 10^3$
Bottom	b	$-1/3$	1/2	(4.13 – 4.37) $\times 10^3$

often referred to as different quark/lepton *flavours*. The SM leptons and quarks are listed in Tables 1.2 and 1.3, along with a few of their basic properties. Finally, we note that for every particle there exists a corresponding antiparticle of the same mass and spin, but with opposite charge.[1]

1.4 Dynamics and kinematics

The observable results of particle interactions depend on the interplay of two conceptually different contributions: *dynamics* and *kinematics*. The dynamics constitutes the interaction mechanism, and is related to questions like 'what kind of particles are interacting?' and 'what properties of the particles cause the interaction?'. It is due

[1] It is still an open question whether the neutrinos are *Majorana particles*, in which case they are identical to the corresponding anti-neutrinos.

to differences in their dynamics that we can separate between the fundamental forces. Kinematics, on the other hand, governs the movement of initial- and final-state particles based on conservation laws for energy, momentum and angular momentum, without caring for the (dynamical) cause of the interaction. The rules of both dynamics and kinematics can be traced back to mathematical symmetries in the underlying theory, but while the dynamics depends on *internal* symmetries specific for each fundamental force, the kinematics is dictated by *external* (space-time) symmetries common for all interactions.

We underline this distinction as the derivations presented in Chapters 4 – 6 will be mostly of kinematical nature. The theoretical framework describing the interaction dynamics is presented in Chapters 2 and 3.

1.5 Notation and units

Throughout this thesis natural units in which $\hbar = c = 1$ are used. Further, the relativistic notation of four-vectors will be employed, although Lorentz indices will often be suppressed when there is no risk of ambiguity. The most important contravariant four-vectors are the spacetime four-vector x^μ and the energy-momentum four-vector P^μ, defined as

$$x^\mu \equiv \left(x^0, x^1, x^2, x^3\right) = \left(t\,, \boldsymbol{x}\right) \tag{1.1}$$

$$P^\mu \equiv \left(P^0, P^1, P^2, P^3\right) = \left(E, p^1, p^2, p^3\right) = \left(E, \boldsymbol{p}\right) \tag{1.2}$$

The metric tensor $g_{\mu\nu}$ is defined by the relations

$$g_{00} = -g_{11} = -g_{22} = -g_{33} = 1 \tag{1.3}$$

$$g_{\mu\nu} = 0 \quad \text{for } \mu \neq \nu \tag{1.4}$$

Covariant four-vectors are defined from the contravariant ones using the metric tensor:

$$x_\mu \equiv g_{\mu\nu}\, x^\nu = \left(x^0, -x^1, -x^2, -x^3\right) \tag{1.5}$$

The convention that repeated indices are summed will be used throughout the thesis. Furthermore, Greek indices run from 0 to 3 unless otherwise noted. For scalar products of two four-vectors, Lorentz indices will usually be suppressed:

$$P_1{}^\mu\, P_{2\mu} = E_1 E_2 - \boldsymbol{p}_1 \cdot \boldsymbol{p}_2 \equiv P_1 \cdot P_2 \tag{1.6}$$

Finally, we note that the following notation is used for the spacetime derivative:

$$\partial_\mu \equiv \frac{\partial}{\partial x^\mu} \tag{1.7}$$

Chapter 2

Gauge Theories and the Standard Model

Elementary particle physics is formulated mathematically in the language of quantum field theories. This framework successfully combines quantum mechanics and special relativity, avoiding the problems of negative-energy solutions found in early formulations of relativistic quantum theories. Simply put, quantum field theories describe the behaviour of mathematical fields that, due to imposed (anti)commutation relations, are interpreted as *operators*. By acting on *states* (e.g. the vacuum $|0\rangle$) these field operators 'create' and 'annihilate' particles, returning a final state that may differ in particle content relative to the initial state.

Needless to say, the quantum field theories of the SM and their physical manifestations is a far too comprehensive subject to be adequately covered within a single chapter. We therefore choose to focus on the key aspect of global and local symmetries, and illustrate their importance for understanding the structure of the SM gauge theories. The following chapter is largely based on Mandl & Shaw [2] and Barger & Phillips [3].

2.1 The gauge principle

The usual starting point of a quantum field theory is the Lagrangian density, $\mathcal{L}$, which for the theories considered here is restricted to being a function of the fields ($\psi_r(x)$) and their first spacetime derivatives ($\partial_\mu \psi_r(x)$). Postulating a Lagrangian density is equivalent to postulating the fields' equations of motion, as the latter can be obtained

from $\mathcal{L}$ through the Euler-Lagrange equation:

$$\frac{\partial \mathcal{L}}{\partial \psi_r} - \partial_\mu \left(\frac{\partial \mathcal{L}}{\partial(\partial_\mu \psi_r)} \right) = 0 \qquad r = 1, \ldots, N \tag{2.1}$$

The index r runs over all N fields contained in $\mathcal{L}$.

When postulating Lagrangian densities (or simply 'Lagrangians'), a prescription known as the *gauge principle* has proven very successful for obtaining theories for elementary particles. An important feature of such gauge theories is that observables calculated in perturbation theory remain finite to all orders, a property known as *renormalisability*. We will illustrate the gauge principle for the simplest of the quantum field gauge theories, Quantum Electrodynamics (QED)[1], describing the interactions of photons with charged fermions.

The gauge principle can be summarised as follows: First, starting from a Lagrangian $\mathcal{L}_0$ describing the free fermions, we identify *global* transformations of the fields that leave $\mathcal{L}_0$ unchanged. Second, we promote these transformations to *local* (gauge) transformations. Finally, we *demand* that the complete Lagrangian should still be invariant under the local transformations, a criterion that forces us to introduce interactions with spin-1 fields. In the QED case we will only need a single spin-1 field, namely the photon field $A^\mu(x)$.

The Lagrangian describing free fermions is:

$$\mathcal{L}_0 = \overline{\psi}(x) \left(i\gamma^\mu \partial_\mu - m \right) \psi(x) \tag{2.2}$$

Through the Euler-Lagrange equation in (2.1) this Lagrangian reproduces the Dirac equation of relativistic quantum mechanics. In the above expression, γ^μ represent four 4×4 matrices defined by the relations

$$\left\{ \gamma^\mu \, , \, \gamma^\nu \right\} = 2\, g^{\mu\nu} \tag{2.3}$$

$$\gamma^{\mu\dagger} = \gamma^0 \gamma^\mu \gamma^0 \tag{2.4}$$

Further, $\overline{\psi}(x)$ is known as the *Dirac adjoint* and is defined by

$$\overline{\psi}(x) \equiv \psi^\dagger(x) \gamma^0 \tag{2.5}$$

[1] Historically, the gauge principle was inspired by QED, not the other way around.

Corresponding to the dimension of the gamma matrices, the fermion field $\psi(x)$ is a four-component spinor field. The four degrees of freedom can be attributed to the fact that we are simultaneously describing both particles and antiparticles, with each type having two possible spin states. Following the prescription of the gauge principle, we observe that the global transformations

$$\begin{aligned} \psi(x) &\to \psi'(x) = U(\alpha)\,\psi(x) \equiv e^{-i\alpha}\psi(x) \\ \overline{\psi}(x) &\to \overline{\psi}'(x) = \overline{\psi}(x)\,U^{\dagger}(\alpha) \equiv \overline{\psi}(x)e^{i\alpha} \end{aligned} \tag{2.6}$$

leave $\mathcal{L}_0$ invariant. Here α is an arbitrary real number. In the terminology of group theory, the above phase transformations belong to the group of global $U(1)$ transformations, where the group name indicates that the elements $U(\alpha)$ are 1×1 'matrices' satisfying the *unitarity* condition $U^{\dagger}(\alpha) = U^{-1}(\alpha)$. We now make the above transformations local:

$$\begin{aligned} \psi(x) &\to \psi'(x) = U(\alpha(x))\,\psi(x) \equiv e^{-iq\alpha(x)}\psi(x) \\ \overline{\psi}(x) &\to \overline{\psi}'(x) = \overline{\psi}(x)\,U^{\dagger}(\alpha(x)) \equiv \overline{\psi}(x)e^{iq\alpha(x)} \end{aligned} \tag{2.7}$$

Note that due to the derivative ∂_μ appearing in (2.2), $\mathcal{L}_0$ is *not* invariant under these gauge transformations:

$$\begin{aligned} \mathcal{L}_0 \to \mathcal{L}_0' &= \overline{\psi}'(x)\left(i\gamma^\mu\partial_\mu - m\right)\psi'(x) \\ &= \overline{\psi}(x)e^{iq\alpha(x)}\left(i\gamma^\mu\partial_\mu - m\right)e^{-iq\alpha(x)}\psi(x) \\ &= \overline{\psi}(x)\left(i\gamma^\mu[\partial_\mu - iq\partial_\mu\alpha(x)] - m\right)\psi(x) \\ &\neq \mathcal{L}_0 \end{aligned} \tag{2.8}$$

Now the invariance of the Lagrangian can be restored in two steps: First, we introduce a vector field $A_\mu(x)$ through substituting the derivative ∂_μ in (2.2) with the *covariant derivative* $D_\mu \equiv \partial_\mu + iqA_\mu(x)$:

$$\mathcal{L}_0 \to \mathcal{L} = \overline{\psi}(x)\left(i\gamma^\mu D_\mu - m\right)\psi(x) \tag{2.9}$$

Second, we require the gauge transformation of $A_\mu(x)$ to be of such a form that

$$\overline{\psi}(x)D_\mu\psi(x) \to \overline{\psi}'(x)D'_\mu\psi'(x) = \overline{\psi}(x)D_\mu\psi(x) \tag{2.10}$$

which immediately implies invariance of $\mathcal{L}$. By comparing the definition of D_μ with the term $-iq\partial_\mu\alpha(x)$ upsetting the invariance of $\mathcal{L}_0$ in (2.8), we find that $A_\mu(x)$ must

transform according to

$$A_\mu(x) \;\rightarrow\; A'_\mu(x) \;=\; A_\mu(x) + \partial_\mu \alpha(x) \tag{2.11}$$

With the *electromagnetic strength tensor* $F^{\mu\nu}$ defined by

$$F^{\mu\nu} \;\equiv\; \partial^\nu A^\mu(x) - \partial^\mu A^\nu(x) \tag{2.12}$$

we can further add to $\mathcal{L}$ the gauge invariant term $-(1/4)F^{\mu\nu}F_{\mu\nu}$ describing free photons. We have thus arrived at the complete QED Lagrangian

$$\begin{aligned} \mathcal{L}_{QED} \;&=\; \overline{\psi}(x)\left(i\gamma^\mu D_\mu - m\right)\psi(x) \;-\; \frac{1}{4}F^{\mu\nu}F_{\mu\nu} \\ &=\; \overline{\psi}(x)\left(i\gamma^\mu \partial_\mu - m\right)\psi(x) \;-\; \frac{1}{4}F^{\mu\nu}F_{\mu\nu} \;-\; q\overline{\psi}(x)\gamma^\mu\psi(x)A_\mu(x) \end{aligned} \tag{2.13}$$

which is left invariant under the coupled gauge transformations

$$\psi(x) \;\rightarrow\; \psi'(x) \;=\; e^{-iq\alpha(x)}\psi(x) \tag{2.14}$$

$$\overline{\psi}(x) \;\rightarrow\; \overline{\psi}'(x) \;=\; \overline{\psi}(x)e^{iq\alpha(x)} \tag{2.15}$$

$$A_\mu(x) \;\rightarrow\; A'_\mu(x) = \; A_\mu(x) + \partial_\mu \alpha(x) \tag{2.16}$$

We note that a hypothetical photon mass term, which for the Hermitian ($A^{\mu\dagger} = A^\mu$) spin-1 field $A^\mu(x)$ would be of the form $(1/2)m^2 A_\mu(x)A^\mu(x)$, is *not* gauge invariant.

To summarize the above derivation: By postulating invariance of the Lagrangian under $U(1)$ gauge transformations of the fermion fields, we were led to introduce interactions with a massless, spin-1 field. The coupled transformation of the spin-1 field was specified as a consequence of the invariance postulate. Finally, a gauge invariant term describing the non-interacting spin-1 field was added. As we cover in Section 2.4, gauge invariant theories for the strong and the unified electroweak interactions can be obtained in a similar way.

2.2 Symmetries and conservation laws

There is an important link between mathematical symmetries and physical conservation laws. The original result, proved by Emmy Noether in 1915, states that the invariance of the Lagrangian under a continuous, one-parameter set of transformations implies a conserved quantity. In field theory, where one usually works with a Lagrangian density,

the conservation law comes in the form of a continuity equation for a four-dimensional *current density*:

$$\partial_\mu f^\mu(x) \;=\; 0 \tag{2.17}$$

The four-current density $f^\mu(x)$ (usually referred to simply as a 'four-current') is a function of the fields included in $\mathcal{L}$, given by

$$f^\mu(x) \;=\; \frac{\partial \mathcal{L}}{\partial(\partial_\mu \psi_r(x))}\delta\psi_r(x) \tag{2.18}$$

where $\delta\psi_r(x)$ denotes the change in the field $\psi_r(x)$ due to the symmetry transformation. The zeroth component, $f^0(x)$, is interpreted as a charge density over a three-dimensional volume, while the components $f^1(x)$, $f^2(x)$ and $f^3(x)$ make up a three-dimensional current density. If we define a charge $F^0(t)$ as

$$F^0(t) \;\equiv\; \int \mathrm{d}^3\boldsymbol{x}\, f^0(x) \tag{2.19}$$

equation (2.17) implies that

$$\begin{aligned} \frac{\partial}{\partial t}F^0(t) \;&=\; \int \mathrm{d}^3\boldsymbol{x}\; \partial_0 f^0(x) \\ &=\; -\int \mathrm{d}^3\boldsymbol{x}\; \partial_k f^k(x) \\ &=\; -\oint_{S(\infty)} \mathrm{d}^2 S\, \left(\hat{\boldsymbol{n}}\cdot\boldsymbol{f}(x)\right) \;=\; 0 \end{aligned} \tag{2.20}$$

Here we have used Gauss' divergence theorem along with the common assumption that the fields, and hence $\boldsymbol{f}(x)$, vanish at infinity. Thus we see that the charge F^0 defined from the current density $f^\mu(x)$ is conserved.

In the case of QED, studied in the previous section, the global transformations defined in (2.46) are precisely such continuous, one-parameter (α) symmetry transformations as are covered by Noether's theorem. The conserved four-current, denoted by $s^\mu(x)$, can be expressed as

$$s^\mu(x) \;=\; q\overline{\psi}(x)\gamma^\mu\psi(x) \tag{2.21}$$

and the corresponding conserved charge is the well-known electric charge:

$$Q \;=\; q\int \mathrm{d}^3\boldsymbol{x}\; s^0(x) \;=\; -e\int \mathrm{d}^3\boldsymbol{x}\; \psi^\dagger(x)\psi(x) \tag{2.22}$$

Above we have used the relation $\overline{\psi}(x)\gamma^0 = \psi^\dagger(x)\gamma^0\gamma^0 = \psi^\dagger(x)$, and $e = -q$ denotes the elementary electric charge. By expanding the fields in terms of creation and annihilation operators and performing the $\boldsymbol{x}$-integration over all space, the charge operator Q can be re-expressed in terms of *number operators* for particles and antiparticles:

$$Q \;=\; -e\sum_{r,\boldsymbol{p}} \left[N_r(\boldsymbol{p}) - \overline{N}_r(\boldsymbol{p})\right] \tag{2.23}$$

When acting on a state, the operators $N_r(\boldsymbol{p})$ and $\overline{N}_r(\boldsymbol{p})$ respectively return the number of particles and antiparticles in spin state r ($r = 1, 2$) with three-momentum $\boldsymbol{p}$. Thus, Q operates in the intuitive way of counting the total number of particles and subtracting the total number of antiparticles.

2.3 A note on chirality and helicity

Before taking on the unified electroweak theory (Section 2.4.1), we introduce the important concepts of *chirality* and *helicity* in the context of fermion fields. These concepts will also be important for the results presented in Chapter 6.

In order to explain experimental observations of parity (spatial inversion) violation, the theory of weak interactions was developed as a *chiral theory*. This allows for an asymmetric treatment of the *left-chiral* and *right-chiral* parts of a fermion field, defined using the chirality projection operators P_L and P_R:

$$\begin{aligned} P_L \;&\equiv\; \frac{1}{2}(1-\gamma_5) \\ P_R \;&\equiv\; \frac{1}{2}(1+\gamma_5) \end{aligned} \tag{2.24}$$

With $\gamma_5 \equiv i\gamma^0\gamma^1\gamma^2\gamma^3$, P_L and P_R satisfy the general requirements for projection operators:

$$\begin{aligned} P_L^2 \;&=\; P_L \\ P_R^2 \;&=\; P_R \\ P_L + P_R \;&=\; 1 \end{aligned} \tag{2.25}$$

As γ_5 satisfies the anticommutation relation $\{\gamma_5, \gamma^\mu\} = 0$, we obtain an additional useful relation for P_L and P_R:

$$P_L\gamma^\mu \;=\; \gamma^\mu P_R \tag{2.26}$$

Using the above operators, the left-chiral and right-chiral parts of a field $\psi(x)$ are simply given by

$$\psi_L(x) \;=\; P_L\,\psi(x) \qquad\qquad \psi_R(x) \;=\; P_R\,\psi(x) \tag{2.27}$$

In terms of annihilation and creation operators, the field $\psi_L(x)$ annihilates left-chiral particles and creates left-chiral antiparticles. Correspondingly, $\psi_R(x)$ annihilates right-chiral particles and creates right-chiral antiparticles.

While chirality is a rather abstract concept, helicity is defined as the projection of a particle's spin along the direction of its three-momentum $\boldsymbol{p}$. A spin projection parallel to $\boldsymbol{p}$ is referred to as *right-handed* (or *positive*) helicity, while a projection antiparallel to $\boldsymbol{p}$ is referred to as *left-handed* (or *negative*) helicity. Operators for projecting out the right- and left-handed helicity components of a fermion field can be defined as

$$\begin{aligned} \Pi^R(\boldsymbol{p}) \;&=\; \frac{1}{2}\left(1 + \frac{\boldsymbol{\sigma}\cdot\boldsymbol{p}}{|\boldsymbol{p}|}\right) \\ \Pi^L(\boldsymbol{p}) \;&=\; \frac{1}{2}\left(1 - \frac{\boldsymbol{\sigma}\cdot\boldsymbol{p}}{|\boldsymbol{p}|}\right) \end{aligned} \tag{2.28}$$

where $\boldsymbol{\sigma} = (\sigma^{23}, \sigma^{31}, \sigma^{12})$ contains the four-dimensional generalisations of the two-dimensional Pauli matrices (σ_k):

$$\sigma^{ij} \;=\; \begin{pmatrix} \sigma_k & 0 \\ 0 & \sigma_k \end{pmatrix} \qquad i,j,k \;=\; 1,2,3 \;\text{ (cyclic)} \tag{2.29}$$

From $\Pi^L(\boldsymbol{p})$ and $\Pi^R(\boldsymbol{p})$ the left- and right-helicity parts of a field are obtained as

$$\psi_{L_H}(x) \;=\; \Pi^L(\boldsymbol{p})\,\psi(x) \qquad\qquad \psi_{R_H}(x) \;=\; \Pi^R(\boldsymbol{p})\,\psi(x) \tag{2.30}$$

Note that for these fields the helicity label corresponds to the helicity of the particle annihilated by the field. The created antiparticle has the opposite helicity.

By using properties of the Dirac spinors $u_r(\boldsymbol{p})$ and $v_r(\boldsymbol{p})$ $(r = 1, 2)$ contained in the field $\psi(x)$, along with the relation $\sigma^{ij} = -\gamma^0\gamma_5\gamma^k$, it can be shown that in the limit of a massless particle we have

$$\frac{\boldsymbol{\sigma}\cdot\boldsymbol{p}}{|\boldsymbol{p}|}u_r(\boldsymbol{p}) \;=\; \gamma_5\,u_r(\boldsymbol{p}) \qquad\qquad \frac{\boldsymbol{\sigma}\cdot\boldsymbol{p}}{|\boldsymbol{p}|}v_r(\boldsymbol{p}) \;=\; \gamma_5\,v_r(\boldsymbol{p}) \tag{2.31}$$

Thus, in the ultra-relativistic limit the effects of the chirality and helicity projection operators acting on fermion fields are equivalent. With $\psi_L = \psi_{L_H}$, the left-chiral and

left-helicity particles destroyed by these fields are identical. Similarly, the left-chiral antiparticle created by ψ_L is identical to the right-helicity antiparticle created by ψ_{L_H}. Consequently, in the limit $v = c$, chirality and helicity are of equal and opposite sign for particles and antiparticles, respectively.

2.4 The gauge theories of the Standard Model

2.4.1 The unified electroweak theory

All fermions of the SM feel the weak force. However, we will in the following only consider leptonic fields as this is sufficient to illustrate the structure of the electroweak theory. In Section 2.1 we saw that the fermionic mass term of the QED Lagrangian was $U(1)$ gauge invariant, whereas this was not the case for a hypothetical photon mass term. As electroweak theory is based on invariance under a larger $SU(2) \times U(1)$ group of transformations, it turns out that not even fermionic mass terms are gauge invariant. Therefore, all particles must initially be treated as massless. Non-zero masses will later be introduced in a gauge invariant way through spontaneous symmetry breaking and Yukawa couplings (Section 2.5).

In what follows we will derive the structure of the electroweak interactions using the gauge principle presented in Section 2.1. We start from the Lagrangian $\mathcal{L}_0$ describing free, massless leptons, now also including the neutrinos:

$$\mathcal{L}_0 \;=\; \overline{\psi}_l(x)\left(i\gamma^\mu\partial_\mu\right)\psi_l(x) \;+\; \overline{\psi}_{\nu_l}(x)\left(i\gamma^\mu\partial_\mu\right)\psi_{\nu_l}(x) \tag{2.32}$$

For clarity, we will henceforth write the fields simply as ψ rather than $\psi(x)$. The properties of the chirality projection operators given in (2.25) and (2.26) allow us to re-express each of the two terms of $\mathcal{L}_0$ as

$$\begin{aligned}
\overline{\psi}\left(i\gamma^\mu\partial_\mu\right)\psi \;&=\; \overline{\psi}\left(i\gamma^\mu\partial_\mu\right)(P_L + P_R)\psi \\
&=\; \overline{\psi}\left(i\gamma^\mu\partial_\mu\right)(P_L^2 + P_R^2)\psi \\
&=\; \overline{\psi}\left(i\gamma^\mu\partial_\mu\right)P_L^2\psi \;+\; \overline{\psi}\left(i\gamma^\mu\partial_\mu\right)P_R^2\psi \\
&=\; \overline{\psi}P_R\left(i\gamma^\mu\partial_\mu\right)P_L\psi \;+\; \overline{\psi}P_L\left(i\gamma^\mu\partial_\mu\right)P_R\psi \\
&=\; \overline{\psi}_L\left(i\gamma^\mu\partial_\mu\right)\psi_L \;+\; \overline{\psi}_R\left(i\gamma^\mu\partial_\mu\right)\psi_R
\end{aligned} \tag{2.33}$$

As mentioned in the previous section, the electroweak theory treats left- and right-chiral fermion fields differently. By combining the left-chiral charged leptons with their

respective left-chiral neutrinos to form doublets, while keeping the right-chiral fields as singlets, $\mathcal{L}_0$ becomes

$$\mathcal{L}_0 \;=\; \overline{\Psi}_l^L \big(i\gamma^\mu \partial_\mu\big)\, \Psi_l^L \;+\; \overline{\psi}_l^R \big(i\gamma^\mu \partial_\mu\big)\, \psi_l^R \;+\; \overline{\psi}_{\nu_l}^R \big(i\gamma^\mu \partial_\mu\big)\, \psi_{\nu_l}^R \tag{2.34}$$

where the doublet Ψ_l^L is defined as

$$\Psi_l^L \;\equiv\; \begin{pmatrix} \psi_{\nu_l}^L \\ \psi_l^L \end{pmatrix} \tag{2.35}$$

Next, we observe that $\mathcal{L}_0$ is invariant under the global $SU(2)_L$[1] transformations that transform the left-chiral doublets as

$$\begin{aligned} \Psi_l^L \;&\rightarrow\; \Psi_l^{L\prime} = \; U(\alpha)\, \Psi_l^L \;\equiv\; \exp\!\left[\frac{i\alpha_j \sigma_j}{2}\right] \Psi_l^L \\ \overline{\Psi}_l^L \;&\rightarrow\; \overline{\Psi}_l^{L\prime} = \; \overline{\Psi}_l^L\, U^\dagger(\alpha) \equiv\; \overline{\Psi}_l^L \exp\!\left[\frac{-i\alpha_j \sigma_j}{2}\right] \end{aligned} \tag{2.36}$$

and leave the right-chiral singlets unchanged. Here α_j are three arbitrary parameters, while σ_j denotes the three Hermitian 2×2 Pauli matrices

$$\sigma_1 \;=\; \begin{pmatrix} 0 & 1 \\ 1 & 0 \end{pmatrix} \qquad \sigma_2 \;=\; \begin{pmatrix} 0 & -i \\ i & 0 \end{pmatrix} \qquad \sigma_3 \;=\; \begin{pmatrix} 1 & 0 \\ 0 & -1 \end{pmatrix} \tag{2.37}$$

The three Pauli matrices are referred to as the *generators* of the $SU(2)$ group, meaning that any group element can be constructed from combinations of these three matrices. As the Pauli matrices do not commute, neither do two general $SU(2)$ elements. In group theory this property is referred to as $SU(2)$ being *non-Abelian*. Due to their transformation properties under $SU(2)$, Ψ_l^L is often called a *weak isospinor* while the right-chiral singlets are called *weak isoscalars*.

The transformations in (2.36) can be considered as three continuous, one-parameter transformations, and are thus covered by Noether's theorem. Consequently, there are three conserved four-currents with three correspondingly conserved charges. The currents, which can be obtained from the general expression (2.18), are:

$$J_i^\mu \;=\; \frac{1}{2}\, \overline{\Psi}_l^L \gamma^\mu \sigma_i \Psi_l^L \qquad\qquad i = 1, 2, 3 \tag{2.38}$$

[1]The group name specifies that the elements U are 'special' ($\det U = 1$) and unitary ($U^\dagger = U^{-1}$). Further, they can be expressed as 2×2 matrices in the *fundamental representation* of $SU(2)$.

The above (Hermitian) currents are referred to as *weak isospin currents*, and the conserved *weak isospin charges* are

$$I_i^W \;=\; \int \mathrm{d}^3\boldsymbol{x}\; J_i^0 \;=\; \frac{1}{2}\int \mathrm{d}^3\boldsymbol{x}\; \Psi_l^{L\dagger}\sigma_i\Psi_l^L \qquad\qquad i=1,2,3 \tag{2.39}$$

The first two currents of (2.38) can be combined to form the currents J^μ and $J^{\mu\dagger}$ given by

$$J^\mu \;=\; 2\big(J_1^\mu - iJ_2^\mu\big) \;=\; \overline{\psi}_l\gamma^\mu(1-\gamma_5)\psi_{\nu_l} \tag{2.40}$$

$$J^{\mu\dagger} \;=\; 2\big(J_1^\mu + iJ_2^\mu\big) \;=\; \overline{\psi}_{\nu_l}\gamma^\mu(1-\gamma_5)\psi_l \tag{2.41}$$

while the third current can be expanded in the form

$$J_3^\mu \;=\; \frac{1}{2}\Big(\overline{\psi}_{\nu_l}^L\gamma^\mu\psi_{\nu_l}^L - \overline{\psi}_l^L\gamma^\mu\psi_l^L\Big) \tag{2.42}$$

The currents J^μ and $J^{\mu\dagger}$ mix electrically charged and neutral fields, thus implying that any interaction must occur through a charged force carrier to satisfy overall charge conservation. J_3^μ, on the other hand, couples only fields of the same particle type, a consequence of σ_3 being diagonal. Therefore, J^μ and $J^{\mu\dagger}$ are referred to as *charged currents*, while J_3^μ is called a *neutral current*. The observation that J_3^μ exhibits a structure similar to the QED current s^μ in (2.21) serves as a first hint of the coming unification.

Analogously to equation (2.23) for the electrical charge operator Q, the third weak isospin charge I_3^W can be expanded in terms of number operators for the charged leptons ($N_r^{l_L}(\boldsymbol{p})$) and neutrinos ($N_r^{\nu_L}(\boldsymbol{p})$):

$$I_3^W \;=\; \frac{1}{2}\sum_{r,\boldsymbol{p}}\Big\{\big[N_r^{\nu_L}(\boldsymbol{p}) - \overline{N}_r^{\nu_L}(\boldsymbol{p})\big] - \big[N_r^{l_L}(\boldsymbol{p}) - \overline{N}_r^{l_L}(\boldsymbol{p})\big]\Big\} \tag{2.43}$$

By letting I_3^W act on the single particle states $|l^-,L\rangle$, $|\nu_l\,,L\rangle$, $|l^-,R\rangle$ and $|\nu_l\,,R\rangle$ we obtain the I_3^W eigenvalues for the various chiral particle states:

$$\begin{aligned} I_3^W\;\big|l^-,L\big\rangle &= -\frac{1}{2}\;\big|l^-,L\big\rangle \\ I_3^W\;|\nu_l\,,L\rangle &= \;\;\frac{1}{2}\;|\nu_l\,,L\rangle \\ I_3^W\;\big|l^-,R\big\rangle &= \;\;0 \\ I_3^W\;|\nu_l\,,R\rangle &= \;\;0 \end{aligned} \tag{2.44}$$

As we also know the eigenvalues for the electrical charge operator Q acting on these states, we can define a new charge operator known as *hypercharge*:

$$Y \equiv Q/e - I_3^W \tag{2.45}$$

With Y defined this way, the left-chiral particle states both have eigenvalue $-1/2$, while the right-chiral l^- and ν_l states have eigenvalues -1 and 0, respectively. Next, consider the global $U(1)_Y$ transformations (given for a general lepton field)

$$\begin{aligned} \psi &\rightarrow \psi' = U(\beta)\,\psi \equiv \exp\big[i\beta Y\big]\psi \\ \overline{\psi} &\rightarrow \overline{\psi}' = \overline{\psi}\,U^\dagger(\beta) \equiv \overline{\psi}\exp\big[-i\beta Y\big] \end{aligned} \tag{2.46}$$

where β is an arbitrary real number and Y is the hypercharge of the particle state annihilated by the field ψ. Under these transformations the free field Lagrangian in (2.34) is invariant. Thus, $\mathcal{L}_0$ is left invariant under the combined $SU(2)_L \times U(1)_Y$ transformations, implying that both I_3^W and Y are conserved charges. The well-known conservation of electric charge Q can therefore be viewed as a consequence of the combined $SU(2)_L \times U(1)_Y$ invariance of $\mathcal{L}_0$.

Following the general prescription presented in Section 2.1 we now promote the symmetry transformations of $\mathcal{L}_0$ from global to local transformations. The resulting $SU(2)_L$ gauge transformations can be expressed as

$$\begin{aligned} \Psi_l^L &\rightarrow \Psi_l^{L\prime} = U(\alpha(x))\,\Psi_l^L \equiv \exp\left[\frac{ig\sigma_j\alpha_j(x)}{2}\right]\Psi_l^L \\ \overline{\Psi}_l^L &\rightarrow \overline{\Psi}_l^{L\prime} = \overline{\Psi}_l^L\,U^\dagger(\alpha(x)) \equiv \overline{\Psi}_l^L \exp\left[\frac{-ig\sigma_j\alpha_j(x)}{2}\right] \end{aligned} \tag{2.47}$$

where we recall that right-chiral fields are left unchanged by $SU(2)_L$. Similarly, the $U(1)_Y$ gauge transformations for a general lepton field are given by

$$\begin{aligned} \psi &\rightarrow \psi' = U(\beta(x))\,\psi \equiv \exp\big[ig'Y\beta(x)\big]\psi \\ \overline{\psi} &\rightarrow \overline{\psi}' = \overline{\psi}\,U^\dagger(\beta(x)) \equiv \overline{\psi}\exp\big[-ig'Y\beta(x)\big] \end{aligned} \tag{2.48}$$

In the above transformations, $\alpha_j(x)$ and $\beta(x)$ are four arbitrary real differentiable functions, while g and g' are constant parameters. We note that $\mathcal{L}_0$ is not invariant under the above gauge transformations.

An invariant Lagrangian can now be regained by introducing spin-1 fields through covariant derivatives D^μ, and further require that the spin-1 fields transform such that

the following $SU(2)_L \times U(1)_Y$ invariance relations are satisfied:

$$\overline{\Psi}_l^L \, D^\mu \, \Psi_l^L \;\rightarrow\; \overline{\Psi}_l^{L'} \, D^{\mu\prime} \, \Psi_l^{L'} \;=\; \overline{\Psi}_l^L \, D^\mu \, \Psi_l^L \tag{2.49}$$

$$\overline{\psi}_l^R \, D^\mu \, \psi_l^R \;\rightarrow\; \overline{\psi}_l^{R'} \, D^{\mu\prime} \, \psi_l^{R'} \;=\; \overline{\psi}_l^R \, D^\mu \, \psi_l^R \tag{2.50}$$

$$\overline{\psi}_{\nu_l}^R \, D^\mu \, \psi_{\nu_l}^R \;\rightarrow\; \overline{\psi}_{\nu_l}^{R'} \, D^{\mu\prime} \, \psi_{\nu_l}^{R'} \;=\; \overline{\psi}_{\nu_l}^R \, D^\mu \, \psi_{\nu_l}^R \tag{2.51}$$

Corresponding to the number of group generators, we introduce three spin-1 fields, W_j^μ, for the $SU(2)_L$ transformations and one spin-1 field, B^μ, for the $U(1)_Y$ transformation. Analogous to the QED case, the covariant derivatives are given the form

$$D^\mu \, \Psi_l^L \;=\; \left(\partial^\mu \;+\; \frac{ig\sigma_j}{2} W_j^\mu \;+\; ig' Y B^\mu \right) \Psi_l^L \tag{2.52}$$

$$D^\mu \, \psi_l^R \;=\; \left(\partial^\mu \;+\; ig' Y B^\mu \right) \psi_l^R \tag{2.53}$$

$$D^\mu \, \psi_{\nu_l}^R \;=\; \left(\partial^\mu \;+\; ig' Y B^\mu \right) \psi_{\nu_l}^R \tag{2.54}$$

In order to satisfy (2.49) – (2.51), the three fields W_j^μ must be invariant under $U(1)_Y$ and transform under $SU(2)_L$ (with infinitesimal $\alpha_j(x)$) according to

$$W_i^\mu \;\rightarrow\; W_i^{\mu\prime} \;=\; W_i^\mu - \partial^\mu \alpha_i(x) - g \epsilon_{ijk} \alpha_j(x) W_k^\mu \tag{2.55}$$

Comparing this transformation to the $U(1)$ transformation of A^μ in (2.11), we note that the last term in the above expression appears as a consequence of $SU(2)$ being non-Abelian, in contrast to the Abelian group $U(1)$. Here ϵ_{ijk} is the completely antisymmetric structure constant of $SU(2)$[1]. Similarly, the field B^μ is required to be invariant under $SU(2)_L$ and transform under $U(1)_Y$ as

$$B^\mu \;\rightarrow\; B^{\mu\prime} \;=\; B^\mu - \partial^\mu \beta(x) \tag{2.56}$$

We have now arrived at an $SU(2)_L \times U(1)_Y$ gauge invariant Lagrangian describing massless leptons and lepton-boson interactions:

$$\mathcal{L}^L \;=\; \overline{\Psi}_l^L \big(i\gamma^\mu D_\mu \big) \, \Psi_l^L \;+\; \overline{\psi}_l^R \big(i\gamma^\mu D_\mu \big) \, \psi_l^R \;+\; \overline{\psi}_{\nu_l}^R \big(i\gamma^\mu D_\mu \big) \, \psi_{\nu_l}^R \tag{2.57}$$

[1]The Pauli matrices satisfy the commutation relation $[\sigma_i, \sigma_j] = 2i\epsilon_{ijk}\sigma_k$.

From (2.52) – (2.54) we see that the form of the covariant derivative depends on the hypercharge of the field it is acting on:

$$D^\mu \Psi_l^L \;=\; \left(\partial^\mu \;+\; \frac{ig\sigma_j}{2} W_j^\mu \;-\; \frac{ig'}{2} B^\mu\right) \Psi_l^L \tag{2.58}$$

$$D^\mu \psi_l^R \;=\; \left(\partial^\mu \;-\; ig' B^\mu\right) \psi_l^R \tag{2.59}$$

$$D^\mu \psi_{\nu_l}^R \;=\; \partial^\mu \psi_{\nu_l}^R \tag{2.60}$$

To complete the process outlined in Section 2.1, we now add gauge invariant terms describing the free boson fields. For B^μ this term is

$$-\frac{1}{4}\, B_{\mu\nu}\, B^{\mu\nu} \tag{2.61}$$

with $B^{\mu\nu}$ defined as

$$B^{\mu\nu} \;\equiv\; \partial^\nu B^\mu \;-\; \partial^\mu B^\nu \tag{2.62}$$

This is completely analogous to the $U(1)$ gauge invariant term $-(1/4)F^{\mu\nu}F_{\mu\nu}$ describing free photons in QED. Due to the occurrence of the last term in (2.55), the invariant Lagrangian term describing the free W_i^μ fields has a more complicated structure:

$$-\frac{1}{4}\, F_{i\,\mu\nu}\, F_i^{\mu\nu} \tag{2.63}$$

where $F_i^{\mu\nu}$ is defined to be

$$F_i^{\mu\nu} \;\equiv\; \partial^\nu W_i^\mu \;-\; \partial^\mu W_i^\nu \;+\; g\epsilon_{ijk} W_j^\mu W_k^\mu \tag{2.64}$$

Consequently, $-\frac{1}{4}\, F_{i\,\mu\nu}\, F_i^{\mu\nu}$ includes terms that in perturbation theory will be interpreted as interactions involving three or four gauge bosons. The complete electroweak Lagrangian for massless leptons and gauge bosons can now be written as:

$$\begin{aligned} \mathcal{L} \;=\;& \overline{\Psi}_l^L \big(i\gamma^\mu D_\mu\big)\, \Psi_l^L \;+\; \overline{\psi}_l^R \big(i\gamma^\mu D_\mu\big)\, \psi_l^R \;+\; \overline{\psi}_{\nu_l}^R \big(i\gamma^\mu D_\mu\big)\, \psi_{\nu_l}^R \\ & -\frac{1}{4}\, B_{\mu\nu}\, B^{\mu\nu} \;-\; \frac{1}{4}\, F_{i\,\mu\nu}\, F_i^{\mu\nu} \end{aligned} \tag{2.65}$$

In equations (2.40) and (2.41) the weak isospin currents J_1^μ and J_2^μ were combined into the charged currents J^μ and $J^{\mu\dagger}$. Correspondingly, the Hermitian fields W_1^μ and

W_2^μ can be combined to form the non-Hermitian fields W^μ and $W^{\mu\dagger}$ representing the physical $W^\pm$ bosons:

$$W^\mu = \frac{1}{\sqrt{2}}\left(W_1^\mu - iW_2^\mu\right) \tag{2.66}$$

$$W^{\mu\dagger} = \frac{1}{\sqrt{2}}\left(W_1^\mu + iW_2^\mu\right) \tag{2.67}$$

Further, we define two Hermitian fields A^μ and Z^μ by the linear combinations

$$W_3^\mu = \cos\theta_W\, Z^\mu + \sin\theta_W\, A^\mu \tag{2.68}$$

$$B^\mu = -\sin\theta_W\, Z^\mu + \cos\theta_W\, A^\mu \tag{2.69}$$

where the mixing angle θ_W is known as the *Weinberg angle*. By rewriting the lepton-boson interaction terms of $\mathcal{L}$ using the gauge fields W^μ, $W^{\mu\dagger}$, A^μ, Z^μ and the currents J^μ, $J^{\mu\dagger}$, s^μ, J_3^μ, it can be shown that A^μ can be interpreted as the QED photon field given that

$$g\sin\theta_W = g'\cos\theta_W = e \tag{2.70}$$

Finally, the Z^μ field represents the physical Z^0 boson.

2.4.2 Quantum chromodynamics

The mathematical description of the strong force in terms of a gauge theory is known as Quantum Chromodynamics (QCD). In the SM the strong force is restricted to interactions of quarks and gluons. Inspired by the results of scattering experiments performed during the 1950's and 60's, *the quark model* was introduced to explain the observed spectra of produced hadrons. Further, to solve an apparent conflict with the Pauli exclusion principle for some of the hadron states, as well as explain why no free quarks were observed, the concept of *colour* was introduced. The basic assumption is that all quarks can exist in one of three colour states - red, green or blue - with antiquarks existing in *anticolour states*. By introducing these additional quantum numbers, the problem related to the Pauli principle was solved. Furthermore, the non-observation of free quarks was alleviated by postulating that hadrons only can exist in *colour neutral* states. Such states can be formed either by three quarks with one quark of each colour, or by a quark and an antiquark forming a colour-anticolour state.

Based on the above ideas, QCD was formulated as a theory invariant under $SU(3)$ transformations. Using the fundamental representation in which the group elements are 3×3 matrices, this enables a description of quark fields in terms of *colour triplets*

$$\Psi^f \equiv \begin{pmatrix} \psi_r^f \\ \psi_g^f \\ \psi_b^f \end{pmatrix} \tag{2.71}$$

where the index f refers to quark flavour. The free quark fields are described by the Lagrangian

$$\mathcal{L}_0 = \overline{\Psi}^f \left(i\gamma^\mu \partial_\mu - m_f \right) \Psi^f \tag{2.72}$$

Here we include the quark mass term $-m_f \overline{\Psi}^f \Psi^f$ since this term will remain invariant under $SU(3)_C$ transformations. However, as the complete SM requires invariance under $U(1)_Y \times SU(2)_L \times SU(3)_C$ and such fermion mass terms violate $SU(2)_L$, also quark masses must eventually be introduced through Yukawa couplings with the Higgs field.

The above Lagrangian is invariant under the global $SU(3)_C$ transformations given by

$$\begin{aligned} \Psi^f &\rightarrow \Psi^{f\prime} = U(\alpha)\, \Psi^f \equiv \exp\left[\frac{i\alpha_i \lambda_i}{2}\right] \Psi^f \\ \overline{\Psi}^f &\rightarrow \overline{\Psi}^{f\prime} = \overline{\Psi}^f\, U^\dagger(\alpha) \equiv \overline{\Psi}^f \exp\left[\frac{-i\alpha_i \lambda_i}{2}\right] \end{aligned} \tag{2.73}$$

Here a_i are eight arbitrary real parameters while λ_i are the eight $SU(3)$ group generators in the form of 3×3 matrices[1]. According to Noether's theorem, the invariance of $\mathcal{L}_0$ under the above transformations imply eight conserved currents and charges. Using (2.18) we find the currents to be of the form

$$S_i^\mu = \frac{1}{2} \overline{\Psi}^f \gamma^\mu \lambda_i \Psi^f \qquad i = 1, 2, \ldots, 8 \tag{2.74}$$

The conserved charges are correspondingly given by

$$\hat{F}_i = \int \mathrm{d}^3\boldsymbol{x}\; S_i^0 = \frac{1}{2} \int \mathrm{d}^3\boldsymbol{x}\; \Psi^{f\dagger} \lambda_i \Psi^f \qquad i = 1, 2, \ldots, 8 \tag{2.75}$$

[1] Analogous to the Pauli matrices of $SU(2)$, the eight matrices λ_i satisfy the commutation relation $[\lambda_i, \lambda_j] = 2i f_{ijk} \lambda_k$. Here a sum over the repeated index $k = 1, 2, \ldots, 8$ is implied and f_{ijk} are the totally antisymmetric structure constants of $SU(3)$.

We here take a moment to comment on the connection between these eight colour charges and the postulate that hadrons only exist in colour neutral states. This assumption, known as *confinement*, can be expressed mathematically as the requirement

$$\hat{F}_i \left| n_r, n_g, n_b, \overline{n}_r, \overline{n}_g, \overline{n}_b \right\rangle \;=\; 0 \tag{2.76}$$

where $\left| n_r, n_g, \ldots, n_{\overline{b}} \right\rangle$ is a general hadron state consisting of n_r red quarks, n_g green quarks, etc. As the two matrices λ_3 and λ_8 are diagonal and thus do not mix different colour states, the corresponding charge operators $\hat{F}_3$ and $\hat{F}_8$ can be interpreted straightforwardly in terms of number operators:

$$\hat{F}_3 \;=\; \frac{1}{2} \sum_{f,s,\boldsymbol{p}} \left[(N_r - \overline{N}_r) - (N_g - \overline{N}_g) \right] \tag{2.77}$$

$$\hat{F}_8 \;=\; \frac{1}{2\sqrt{3}} \sum_{f,s,\boldsymbol{p}} \left[(N_r - \overline{N}_r) + (N_g - \overline{N}_g) - 2(N_b - \overline{N}_b) \right] \tag{2.78}$$

Here the summation indices f, s, $\boldsymbol{p}$ denote flavour, spin, and three-momentum, respectively. In order for $\hat{F}_3$ and $\hat{F}_8$ to both satisfy the constraint in (2.76), we note that single quark states, qq diquark states and other states which sum to a fractional electric charge are excluded. On the other hand, the colour neutral *baryon states* of the form $q_r q_g q_b$ and $\overline{q}_r \overline{q}_g \overline{q}_b$, and *meson states* of the form $q_c \overline{q}_c$ are allowed, in agreement with observations.

Although here presented as a postulate, colour confinement is widely believed to result from the property that the strong force does *not* decrease with distance. As a consequence, the effective potential between two quarks moving apart increases proportional to their separation r. In the case of two high-energy quarks, it will at some point be energetically favourable to create a quark-antiquark pair from the vacuum making the overall state colour neutral, and as this process repeats *jets* of colour neutral hadrons are formed from the original quarks.

To obtain the desired $SU(3)$ gauge theory we first make the transformations in (2.79) local:

$$\begin{aligned} \Psi^f \;&\rightarrow\; \Psi^{f\prime} = \; U(\alpha(x))\, \Psi^f \;\equiv\; \exp\!\left[\frac{i g_s \lambda_i \alpha_i(x)}{2} \right] \Psi^f \\ \overline{\Psi}^f \;&\rightarrow\; \overline{\Psi}^{f\prime} = \; \overline{\Psi}^f\, U^\dagger(\alpha(x)) \equiv\; \overline{\Psi}^f \exp\!\left[\frac{-i g_s \lambda_i \alpha_i(x)}{2} \right] \end{aligned} \tag{2.79}$$

Next, we introduce eight vector fields G_i^μ (gluon fields) through substituting the derivative in $\mathcal{L}_0$ with the covariant derivative

$$D^\mu \;=\; \partial^\mu + \frac{ig_s\lambda_i}{2}G_i^\mu \tag{2.80}$$

To regain invariance of the Lagrangian the (infinitesimal) transformations of the gluon fields must be of the form

$$G_i^\mu \;\rightarrow\; G_i^{\mu\prime} \;=\; G_i^\mu - \partial^\mu\alpha_i(x) - g_s f_{ijk}\alpha_j(x)G_k^\mu \tag{2.81}$$

where f_{ijk} are the structure constants of $SU(3)$. Similar to the transformations of the W_i^μ fields in (2.55), the last term in the above expression appears as a consequence of $SU(3)$ being non-Abelian. Finally, a $SU(3)$ gauge invariant term describing the free gluon fields is given by

$$-\frac{1}{4}\,G_{i\,\mu\nu}\,G_i^{\mu\nu} \tag{2.82}$$

where $G_i^{\mu\nu}$ is defined as

$$G_i^{\mu\nu} \;\equiv\; \partial^\nu G_i^\mu \;-\; \partial^\mu G_i^\nu \;+\; g_s f_{ijk}G_j^\mu G_k^\nu \tag{2.83}$$

The $SU(3)$ gauge invariant Lagrangian defining QCD is thus

$$\mathcal{L} \;=\; \overline{\Psi}^f\left(i\gamma^\mu D_\mu - m_f\right)\Psi^f \;-\; \frac{1}{4}\,G_{i\,\mu\nu}\,G_i^{\mu\nu} \tag{2.84}$$

Several aspects of the strong interaction can be inferred directly from the above Lagrangian. First, the quark-gluon interaction terms depend on the matrices λ_i. As these matrices in general are not diagonal they will mix different quark colour fields. Thus, in a quark-gluon interaction a quark of a given colour state can be annihilated while a quark of different colour state is created. Since the eight colour charges $\hat{F}_i$ are to be conserved in any such interaction, the gluons can be viewed as representing colour states defined by the λ_i matrices. This colour property of the gluons is also evident in the term $-(1/4)G_{i\,\mu\nu}G_i^{\mu\nu}$ which includes three- and four-gluon self-interactions. Finally, we note that the strong interaction is *flavour independent* in that it treats all quark flavours identically.

2.5 Electroweak symmetry breaking

In the previous sections the $U(1)_Y \times SU(2)_L$ invariant electroweak theory and the $SU(3)_C$ invariant theory of QCD have been studied. In order to obtain invariant Lagrangians, all gauge bosons, and for the electroweak theory also the fermions, were assumed massless. Nevertheless, it is known from experiments that both the fermions and the $W^{\pm}$ and Z^0 bosons are indeed massive. A gauge invariant way of introducing particle masses is therefore needed if the SM is to remain $U(1)_Y \times SU(2)_L \times SU(3)_C$ invariant.

A mechanism known as *spontaneous symmetry breaking* provides a solution to this problem. The main concept is that the physical vacuum needs not satisfy all the symmetries of the underlying theory. It turns out that when a symmetry is spontaneously broken, the gauge bosons corresponding to that particular symmetry acquire mass. As the photon is massless while the $W^{\pm}$ and Z^0 are massive, we seek to break $U(1)_Y \times SU(2)_L$ down to the $U(1)_{\text{em}}$ symmetry of QED. Similarly, the $SU(3)_C$ symmetry is kept unbroken as gluons are believed to be massless.

For spontaneous symmetry breaking to occur in a system, the ground state must be degenerate. Under the transformations that leave the underlying theory unchanged, the degenerate ground states transform amongst themselves. Further, each ground state must have an associated non-zero quantity that enables us to distinguish the degenerate states. (Otherwise there would be no way of telling they were degenerate in the first place.) In quantum field theory, the lowest energy state is per definition the vacuum state $|0\rangle$, and the quantity discriminating various vacuum states is taken to be the *vacuum expectation value* (*vev*) $\langle 0|\Phi(x)|0\rangle$ of a quantum field $\Phi(x)$. As the vacuum states are required to be Lorentz-invariant and the *vev* must be non-zero, $\Phi(x)$ must necessarily be a *scalar* (spin-0) field. Further, requiring that the vacuum states are invariant under spacetime translations, the *vev* of $\Phi(x)$ must be a constant:

$$\langle 0|\Phi(x)|0\rangle \;=\; c \;\neq\; 0 \tag{2.85}$$

For simplicity, we will in the following consider classical field theory, in which the fields are *not* operators and the ground states are classified by the corresponding field values. The fields can later be quantised in order to regain the interpretation in terms of operator fields.

To be able to break the $SU(2)$ symmetry, the scalar field $\Phi(x)$ is defined to be a doublet

$$\Phi(x) \equiv \begin{pmatrix} \phi_a(x) \\ \phi_b(x) \end{pmatrix} \tag{2.86}$$

where $\phi_a(x)$ and $\phi_b(x)$ are two complex scalar fields. This doublet is known as the *Higgs field*. Similar to the transformations of the lepton doublet $\Psi_l^L(x)$, the Higgs field transforms under $SU(2)_L$ and $U(1)_Y$ respectively as

$$\begin{aligned} \Phi(x) \rightarrow \Phi'(x) &= U(\alpha(x))\,\Phi(x) \equiv \exp\left[\frac{ig\sigma_j\alpha_j(x)}{2}\right]\Phi(x) \\ \Phi^\dagger(x) \rightarrow \Phi^{\dagger\prime}(x) &= \Phi^\dagger(x)\,U^\dagger(\alpha(x)) \equiv \Phi^\dagger(x)\exp\left[\frac{-ig\sigma_j\alpha_j(x)}{2}\right] \end{aligned} \tag{2.87}$$

and

$$\begin{aligned} \Phi(x) \rightarrow \Phi'(x) &= U(\beta(x))\,\Phi(x) \equiv \exp\big[ig'Y\beta(x)\big]\Phi \\ \Phi^\dagger(x) \rightarrow \Phi^{\dagger\prime}(x) &= \Phi^\dagger(x)\,U^\dagger(\beta(x)) \equiv \Phi^\dagger(x)\exp\big[-ig'Y\beta(x)\big] \end{aligned} \tag{2.88}$$

Next, $\Phi(x)$ is introduced in the overall theory by including the $SU(2)_L \times U(1)_Y$ gauge invariant Lagrangian:

$$\mathcal{L}^H = \big[D^\mu\Phi(x)\big]^\dagger\big[D_\mu\Phi(x)\big] - \mathcal{V} \tag{2.89}$$

Here the covariant derivative is given by

$$D^\mu\,\Psi_l^L = \left(\partial^\mu + \frac{ig\sigma_j}{2}W_j^\mu + ig'YB^\mu\right)\Psi_l^L \tag{2.90}$$

while the *Higgs potential* $\mathcal{V}$ is defined as

$$\mathcal{V} \equiv \mu^2\Phi^\dagger(x)\Phi(x) + \lambda\big[\Phi^\dagger(x)\Phi(x)\big]^2 \tag{2.91}$$

with μ^2 and λ as constant parameters. As we are doing classical field theory, the ground state corresponds to the field values that minimise the total energy density $\mathcal{H} = \mathcal{T} + \mathcal{V}$, where the kinetic term $\mathcal{T}$ is the first term of $\mathcal{L}^H$. From the requirement that the ground state should be Lorentz invariant, we know that the fields W_j^μ and B^μ of $\mathcal{T}$ must vanish. Further, as the ground state value of $\Phi(x)$ should be constant to ensure translational invariance, the derivative $\partial^\mu\Phi(x)$ must disappear. Therefore, the overall lowest energy

state corresponds to the constant field value Φ_0 that minimises the potential $\mathcal{V}$. With Φ_0 expressed as

$$\Phi_0 \;=\; \begin{pmatrix} \phi_{a0} \\ \phi_{b0} \end{pmatrix} \tag{2.92}$$

$\mathcal{V}(\Phi_0)$ can be expanded as

$$\mathcal{V}(\Phi_0) \;=\; \mu^2\Big[|\phi_{a0}|^2 + |\phi_{b0}|^2\Big] + \lambda\Big[|\phi_{a0}|^2 + |\phi_{b0}|^2\Big]^2 \tag{2.93}$$

If both parameters μ^2 and λ are positive, $\mathcal{V}$ has a unique minimum for $\phi_{a0} = \phi_{b0} = 0$, and spontaneous symmetry breaking cannot occur. However, if μ^2 is taken to be negative (despite the confusing notation), the potential takes on a 'Mexican hat' shape over the $(|\phi_{a0}|, |\phi_{b0}|)$-plane, with a circle of degenerate minima defined by

$$|\phi_{a0}|^2 + |\phi_{b0}|^2 \;=\; \frac{-\mu^2}{2\,\lambda} \;\equiv\; \frac{v^2}{2} \tag{2.94}$$

With all ground states being equivalent, we now choose the particular ground state situated on the $|\phi_{b0}|$-axis, with $\mathrm{Re}(\phi_{b0}) = v/\sqrt{2}$ and $\mathrm{Im}(\phi_{b0}) = 0$:

$$\Phi_0 \;=\; \begin{pmatrix} 0 \\ v/\sqrt{2} \end{pmatrix} \tag{2.95}$$

As Φ_0 clearly is not invariant under $SU(2)_L \times U(1)_Y$ transformations this symmetry has been spontaneously broken.

Analogous to the $\Psi_l^L(x)$ doublet, the upper and lower components of $\Phi(x)$ correspond to the I_3^W values $+1/2$ and $-1/2$, respectively. The $U(1)_{\mathrm{em}}$ symmetry can now be kept unbroken by assigning hypercharge $Y = 1/2$ to the Higgs field. Due to the definition of Y in (2.45), this is equivalent to assigning the electric charge $Q/e = +1$ to the upper component and $Q/e = 0$ to the lower component. Consequently, Φ_0 is left invariant under $U(1)_{\mathrm{em}}$ gauge transformations of the form

$$U(\alpha(x)) \;=\; \exp\big[-iQ\alpha(x)\big] \tag{2.96}$$

Next, we perform a coordinate change by rewriting the general Higgs field $\Phi(x)$ in terms of its deviation from Φ_0

$$\Phi(x) \;=\; \frac{1}{\sqrt{2}} \begin{pmatrix} \eta_1(x) + i\eta_2(x) \\ v + \sigma(x) + i\eta_3(x) \end{pmatrix} \tag{2.97}$$

where $\sigma(x)$ and $\eta_i(x)$ are four real scalar fields. Expanding $\mathcal{L}^H$ in terms of these fields gives rise to a multitude of terms, whereas several of the terms containing the $\eta_i(x)$ fields lead to problems in light of quantisation and perturbation theory. A closer examination shows that these fields are 'unphysical' in the sense that they do not correspond to physical particles in the quantised theory. The resolution to this problem is to choose a particular gauge where these fields vanish. That is, we perform the $SU(2)$ transformation needed to bring the upper component of $\Phi(x)$ to zero, followed by the $U(1)$ transformation that makes the lower component real. This gauge is known as *unitary gauge*, and the resulting Higgs field is given as

$$\Phi(x) \;=\; \frac{1}{\sqrt{2}} \begin{pmatrix} 0 \\ v + \sigma(x) \end{pmatrix} \tag{2.98}$$

Of course, all other fields are also transformed according to their respective transformation properties. By expanding $\mathcal{L}^H$ in terms of the transformed fields, and additionally rewriting the gauge fields W_i^μ and B_i^μ in terms of the 'physical' fields $W^{\mu\dagger}$, W^μ, Z^μ and A^μ, the resulting Lagrangian contains the following second order terms:

$$\begin{aligned} \mathcal{L}^H \;=\; & \frac{1}{2}\big[\partial_\mu \sigma(x)\big]\big[\partial^\mu \sigma(x)\big] \;-\; \frac{1}{2}\big(-2\,\mu^2\big)\big[\sigma(x)\big]^2 \\ & + \Big(\frac{vg}{2}\Big)^2 W_\mu^\dagger(x) W^\mu(x) \;+\; \frac{1}{2}\left(\frac{vg}{2\cos\theta_W}\right)^2 Z_\mu(x) Z^\mu(x) \\ & + \big(\text{higher order terms}\big) \end{aligned} \tag{2.99}$$

The first line is interpreted as the kinetic term and the mass term of a neutral scalar particle σ known as the *Higgs particle*, while the second line is interpreted as mass terms for the $W^\pm$ and Z^0 particles, respectively. The masses are given explicitly as

$$m_H = \sqrt{-2\,\mu^2} \qquad m_W = \frac{vg}{2} \qquad m_Z = \frac{vg}{2\cos\theta_W} = \frac{m_W}{\cos\theta_W} \tag{2.100}$$

To summarise: By introducing a complex scalar doublet $\Phi(x)$ with a non-vanishing *vev*, the $SU(2)_L \times U(1)_Y$ symmetry was spontaneously broken down to the $U(1)_{\text{em}}$ symmetry. Combining this with a transformation to the unitary gauge, we obtained a theory where three of the four degrees of freedom originally contained in $\Phi(x)$ were 'converted' to give masses to the $W^\pm$ and Z^0 bosons. Due to the non-zero masses of $W^\pm$ and Z^0, measured respectively to 80.4 GeV and 91.2 GeV, interactions mediated by these particles are suppressed at energies below this mass scale. This suppression

explains why the electromagnetic and weak interactions appear as two separate forces at low energies. The last degree of freedom in $\Phi(x)$ predicts the existence of the famous Higgs particle, which so far has eluded detection.

Without going into much detail, we note that mass terms for the SM fermions are introduced in the Lagrangian by adding gauge invariant *Yukawa couplings* which couple the fermion fields to the Higgs field. For example, the Yukawa couplings for the leptons are given by

$$-\lambda_l \Big[\overline{\Psi}_l^L(x)\, \psi_l^R(x)\, \Phi(x) \;+\; \Phi^\dagger(x)\, \overline{\psi}_l^R(x)\, \Psi_l^L(x) \Big] \tag{2.101}$$

where λ_l is a coupling constant. By expanding the doublets and combining the chiral fields using the properties of the projection operators P_L and P_R, these terms can be seen to yield a lepton mass term and an interaction term with the physical Higgs boson:

$$\begin{aligned} &- \frac{\lambda_l v}{\sqrt{2}}\, \overline{\psi}_l(x)\, \psi_l(x) \;-\; \frac{\lambda_l}{\sqrt{2}}\, \sigma(x)\, \overline{\psi}_l(x)\, \psi_l(x) \\ \equiv\; &- m_l\, \overline{\psi}_l(x)\, \psi_l(x) \;-\; \frac{m_l}{v}\, \sigma(x)\, \overline{\psi}_l(x)\, \psi_l(x) \end{aligned} \tag{2.102}$$

2.6 Shortcomings of the Standard Model

Although a most successful theory for the energies probed by experiments so far, the SM is still troubled with several theoretical shortcomings. In the following a few of the most important such problems will be introduced, with special emphasis on the *hierarchy problem*.

The hierarchy problem: Assuming the SM is correct, fits of the unknown Higgs mass using constraints from electroweak precision data (e.g. M_W, M_Z) indicate a m_H value below ~ 200 GeV at 99% confidence level (Fig. 2.1) [4]. Theoretically the physical Higgs mass squared can be expressed as

$$m_H^2 \;=\; \left(m_H^0\right)^2 + \Delta m_H^2 \tag{2.103}$$

where m_H^0 denotes the 'bare' (non-renormalised) Higgs mass as given by the Lagrangian parameter μ^2 in (2.100). Further, Δm_H^2 represents corrections due to loop diagrams for all the massive fermions and bosons in the SM, including the Higgs itself. For a

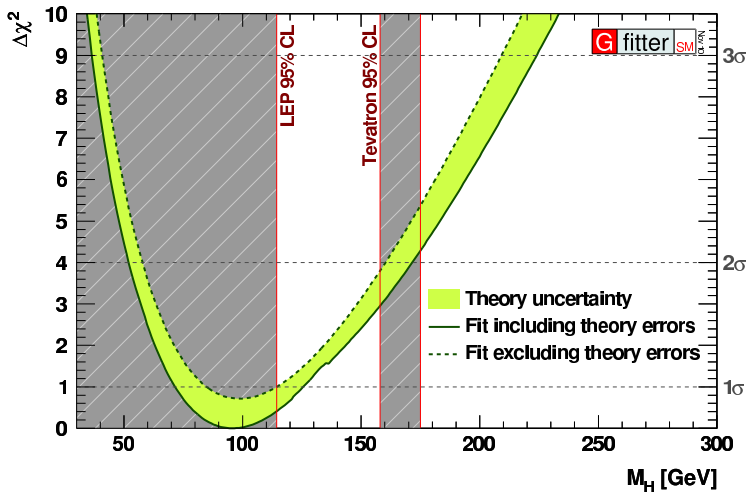

Figure 2.1: Fit of the SM Higgs mass to electroweak precision data, excluding direct Higgs searches. The figure is taken from [4].

fermion loop with the loop integral cut off at a momentum scale Λ, the contribution to m_H^2 takes the form [5]

$$\left(\Delta m_H^2\right)_f \;=\; -\frac{|\lambda_f|^2}{8\pi^2}\,\Lambda^2 + \ldots \tag{2.104}$$

Here $\lambda_f = \sqrt{2}m_l/v$ is the strength of the fermion-Higgs coupling, as seen in (2.102), and the terms left out are at most logarithmically dependent on Λ. (The largest fermion contribution is due to the top quark for which $\lambda_t \sim 1$.) The contribution from a boson loop exhibits the same quadratic dependence on Λ but with an opposite overall sign.

The cut-off parameter Λ can be interpreted as the energy scale at which physics beyond the SM becomes important, rendering further 'extrapolation' invalid. If this scale is large compared to the weak scale of ~ 100 GeV, e.g. with Λ being the Planck scale ($\sim 10^{19}$ GeV), the radiative corrections will naturally bring m_H up to the order of Λ. There is no apparent symmetry between the fermion and boson masses of the SM that could lead to an internal cancellation of the contributions to Δm_H^2. Therefore, in order to cancel the radiative corrections and end up with a physical Higgs mass around the experimentally preferred scale, the value of the bare mass m_H^0 would have to be extremely *fine-tuned*. This seemingly unnatural requirement is often referred to as the fine-tuning problem.

Free parameters: The SM depends on at least 19 parameters to be determined experimentally. From the theoretical point of view a theory with fewer free parameters seems preferable.

***CP* violation:** Some processes are observed to differ in probability relative to the parity transformed antiparticle processes, a phenomenon known as CP violation. In the SM this is a well-established feature of the weak interaction. According to the *Sakharov conditions*, CP violation is one of three ingredients necessary to produce a matter-dominated universe, starting from equal amounts of matter and antimatter [6]. However, relative to the observed matter-antimatter discrepancy, the small amount of CP violation in the SM seems insufficient. A related problem, known as the *strong CP problem*, is the question why strong interactions do not seem to violate CP.

Dark matter: Astrophysical and cosmological observations indicate that the universe consists of large amounts of a weakly-interacting and presumably non-baryonic form of matter. This *dark matter* is believed to make up $\sim 22\%$ of the energy density of the universe. The observational evidence for the existence of dark matter includes measurements of galactic rotational curves [7], gravitational lensing effects [8] and measurements of the cosmic background radiation [9]. The neutrinos, being both massive and only weakly interacting, constitute the only SM candidate for particle dark matter. SM neutrinos are, however, very low in mass, and can thus only account for a small fraction of the total dark matter. Moreover, the relativistic velocities of neutrinos come in conflict with the dark matter properties required for structure formation on small cosmological scales [10]. The existence of dark matter therefore hints towards a form of matter not described by the SM.

Grand unification: *Grand Unified Theories* (GUTs) are based on the postulate that the $U(1)_Y \times SU(2)_L \times SU(3)_c$ gauge group of the SM is a subgroup of some larger symmetry group. A general prediction of such theories is that the gauge couplings describing the strengths of the various interactions should unify at some high energy scale Λ_{GUT}, usually around 10^{16} – 10^{19} GeV. Extrapolations of the SM gauge couplings towards Λ_{GUT} show that such unification cannot occur with SM physics alone [11]. Although not a direct problem for the SM itself, this is by many viewed as an indication for

physics beyond the SM.

Further shortcomings: If indeed it is possible to formulate a 'theory of everything' one would need a consistent description of quantum gravity, which the SM does not include. Further, there is no SM explanation for the expansion-driving *dark energy* thought to make up $\sim 73\%$ of the total energy density of the universe [9].

Chapter 3

Supersymmetry and Cascade Decays

In Section 2.6 the need for theories that go beyond the SM was motivated. Numerous alternative theories have been proposed, but perhaps the most popular candidates are theories based on the idea of supersymmetry (SUSY). This chapter will form a phenomenological introduction to SUSY, with special emphasis on decay chains of supersymmetric particles. First, however, the general principle behind SUSY is presented, along with some important motivations for expecting that SUSY might be realised at energies within experimental reach. Sections 3.1 – 3.5 are mainly based on Martin [5] and Aitchison [12].

3.1 General concept

As noted in Section 1.4, the SM obeys both internal symmetries, namely invariance under the $U(1)_Y \times SU(2)_L \times SU(3)_C$ gauge group, and external spacetime symmetries of translation and change of reference frame. The spacetime symmetry group, known as the *Poincaré group*, is defined as the group of all transformations of the form

$$x^\mu \rightarrow x^{\mu\prime} = \Lambda^\mu_{\ \nu} x^\nu + a^\mu \tag{3.1}$$

that leaves the spacetime interval $(x-y)^2$ invariant. Here $\Lambda^\mu_{\ \nu}$ represents a Lorentz transformation while a^μ is a constant translation. The generators of Lorentz transfor-

mations, $M_{\mu\nu}$, and spacetime translations, P_μ, satisfy the *Poincaré algebra*:

$$\big[\, P^\mu \,, P^\nu \,\big] \;=\; 0 \tag{3.2}$$

$$\big[\, M^{\mu\nu} \,, P^\rho \,\big] \;=\; i\big(g^{\nu\rho}P^\mu - g^{\mu\rho}P^\nu\big) \tag{3.3}$$

$$\big[\, M^{\mu\nu} \,, M^{\rho\sigma} \,\big] \;=\; i\big(g^{\nu\rho}M^{\mu\sigma} + g^{\mu\sigma}M^{\nu\rho} - g^{\nu\sigma}M^{\mu\rho} - g^{\mu\rho}M^{\nu\sigma}\big) \tag{3.4}$$

Further, these generators commute with the generators of the internal SM symmetries [1].

The concept of SUSY evolved from attempts at extending the Poincaré group by including additional internal symmetries in a *non-trivial* way, that is, without all generators of the internal transformations commuting with the Poincaré generators. Through the work of Coleman, Mandula [13] and Haag, Lopuszanski, Sohnius [14], it became clear that the only way a non-trivial extension can be obtained is by allowing the additional symmetry group to be defined from *anti*commutation relations. Consequently, the group generators are fermionic operators described by spinors. In the following we consider a *minimal* extension of the Poincaré algebra in terms of a single, two-component SUSY generator Q_a (Weyl spinor) and its Hermitian conjugate $\overline{Q}_{\dot{a}}$. (The bar and dotted indices are used to indicate that the Hermitian conjugate of Q_a is a right-handed Weyl spinor.) The *supersymmetric* Poincaré algebra is then given by the anticommutation relations

$$\big\{\, Q_a \,, Q_b \,\big\} \;=\; \big\{\, \overline{Q}_{\dot{a}} \,, \overline{Q}_{\dot{b}} \,\big\} \;=\; 0 \tag{3.5}$$

$$\big\{\, Q_a \,, \overline{Q}_{\dot{a}} \,\big\} \;=\; 2\big(\sigma^\mu\big)_{a\dot{a}}P_\mu \tag{3.6}$$

and the commutation relations

$$\big[\, Q_a \,, P^\mu \,\big] \;=\; \big[\, \overline{Q}_{\dot{a}} \,, P^\mu \,\big] \;=\; 0 \tag{3.7}$$

$$\big[\, Q_a \,, M^{\mu\nu} \,\big] \;=\; \frac{1}{2}\big(\sigma^{\mu\nu}\big)_a^{\;b}Q_b \tag{3.8}$$

$$\big[\, \overline{Q}_{\dot{a}}, M^{\mu\nu} \,\big] \;=\; \frac{1}{2}\big(\overline{\sigma}^{\mu\nu}\big)_{\dot{a}}^{\;\dot{b}}\overline{Q}_{\dot{b}} \tag{3.9}$$

[1] We recall that the generators of the $U(1)_Y$, $SU(2)_L$ and $SU(3)_C$ groups satisfy the following commutation relations:

$$U(1)_Y\colon\ [Y,Y]=0 \qquad SU(2)_L\colon\ [\sigma_i\,,\sigma_j]=2i\epsilon_{ijk}\sigma_k \qquad SU(3)_C\colon\ [\lambda_a\,,\lambda_b]=2if_{abc}\lambda_c$$

where $i,j,k=1,2,3$ and $a,b,c=1,\ldots,8$.

In addition, the SUSY generators commute with the generators of the SM gauge group. In the above notation, $a, b = 1, 2$ and $\dot{a}, \dot{b} = 1, 2$ are distinct indices and Hermitian conjugation is defined as

$$\overline{Q}_{\dot{a}} \equiv (Q_a)^\dagger = (Q^\dagger)_{\dot{a}} \tag{3.10}$$

$$Q^a = (\overline{Q}^{\dot{a}})^\dagger \tag{3.11}$$

The two-dimensional σ^μ and $\sigma^{\mu\nu}$ are given by

$$\sigma^\mu = \left(1\,, \sigma^1\,, \sigma^2\,, \sigma^3\right) \qquad \overline{\sigma}^\mu = \left(1\,, -\sigma^1\,, -\sigma^2\,, -\sigma^3\right) \tag{3.12}$$

$$\sigma^{\mu\nu} \equiv \frac{i}{2}\left(\sigma^\mu\overline{\sigma}^\nu - \sigma^\nu\overline{\sigma}^\mu\right) \qquad \overline{\sigma}^{\mu\nu} \equiv \frac{i}{2}\left(\overline{\sigma}^\mu\sigma^\nu - \overline{\sigma}^\nu\sigma^\mu\right) \tag{3.13}$$

where σ^i are the usual two-dimensional Pauli matrices, written out explicitly in (2.37).

Without going into detail concerning the above algebra, we illustrate a few central properties of the SUSY generators: Let $|m\,, +1/2\rangle$ denote a fermion state of mass m and spin $+1/2$ along the z-axis. With $M^{12} = J^3$ being the z-component of the angular momentum operator and assuming the fermion is on mass-shell, we have

$$J^3\,|m\,, +1/2\rangle = \frac{1}{2}\,|m\,, +1/2\rangle \tag{3.14}$$

$$P^\mu P_\mu\,|m\,, +1/2\rangle = m^2\,|m\,, +1/2\rangle \tag{3.15}$$

From the definition of $\sigma^{\mu\nu}$ in (3.13) it follows that $\sigma^{12} = \sigma^3$. Thus, for J^3 the commutator in (3.8) becomes

$$\left[\,Q_a\,, J^3\,\right] = \frac{1}{2}\left(\sigma^3\right)_a^{\ b} Q_b \tag{3.16}$$

By choosing $a = 1$ and summing over b we obtain

$$\left[\,Q_1\,, J^3\,\right] = \frac{1}{2}Q_1 \tag{3.17}$$

The spin effect of Q_1 can now be deduced by acting with J^3 on the state $Q_1\,|m\,, +1/2\rangle$:

$$\begin{aligned} J^3\left(Q_1\,|m\,, +1/2\rangle\,\right) &= \left(Q_1 J^3 - \frac{1}{2}Q_1\right)|m\,, +1/2\rangle \\ &= \left(\frac{1}{2} - \frac{1}{2}\right)\left(Q_1\,|m\,, +1/2\rangle\,\right) \end{aligned} \tag{3.18}$$

Evidently, the effect of the SUSY operator Q_1 is to lower the spin by 1/2. Further, since Q_1 commutes with the generators of the gauge group, we know that all other quantum numbers remain unchanged. From the commutator in (3.7) it follows that

$$\left[\, Q_a \,, P^\mu P_\mu \,\right] \;=\; 0 \tag{3.19}$$

By letting $P^\mu P_\mu$ act on the state $Q_1 \,|m\,, +1/2\rangle$ and using the on-shell relation (3.15), we find

$$\begin{aligned} P^\mu P_\mu \, Q_1 \,|m\,, +1/2\rangle \;&=\; Q_1 P^\mu P_\mu \,|m\,, +1/2\rangle & (3.20)\\ &=\; m^2 \, Q_1 \,|m\,, +1/2\rangle & (3.21) \end{aligned}$$

Clearly the two states $|m\,, +1/2\rangle$ and $Q_1 \,|m\,, +1/2\rangle$ have identical mass, implying that $Q_1 \,|m\,, +1/2\rangle \propto |m\,, 0\rangle$. For consistency with the limit $m \to 0$ we note that the resulting state $|m\,, 0\rangle$ must be interpreted as a scalar, since a massless spin-1 state only can have spin eigenvalues ± 1.

The above example illustrates the general effect of the SUSY operators: A state is transformed to a mass degenerate state with spin altered by $\pm 1/2$. This can be illustrated schematically as

$$Q\,|\text{fermion}\rangle \;=\; |\text{boson}\rangle \qquad\qquad Q\,|\text{boson}\rangle \;=\; |\text{fermion}\rangle \tag{3.22}$$

Now two important observations can be made: First, there are no two SM particles that differ in spin by 1/2 with the remaining quantum numbers being equal. Therefore, any theory invariant under SUSY transformations necessarily predicts the existence of several new particles. Second, as *unbroken* SUSY predicts that a particle and its 'supersymmetric partner' are mass degenerate, SUSY must be a *broken* symmetry if it is to exist. This is analogous to the broken $SU(2)_L \times U(1)_Y$ symmetry of the SM.

To keep track of all the new states predicted by SUSY some categorisation and naming conventions are needed: Fermions and bosons that can be transformed into each other by some combination of the SUSY operators Q and $\overline{Q}$ are referred to as *superpartners*, and they are combined to form *supermultiplets*. Since the SUSY operators commute with the gauge group generators, the SM and SUSY members of a supermultiplet will have identical gauge quantum numbers. This implies that the left- and right-chiral fermion states of the SM form separate supermultiplets. It can further

be shown that the number of fermionic and bosonic degrees of freedom balance within a supermultiplet. As the left-chiral electron (e_L) represents two fermionic degrees of freedom, it is consequently accompanied by a complex scalar ($\widetilde{e}_L$), representing two bosonic degrees of freedom. Here we have introduced the common notation of using a tilde to denote a superpartner of a SM particle. Two types of supermultiplets are differentiated: *Chiral supermultiplets* are formed from a two-component (Weyl) fermion and the corresponding complex scalar, e.g. e_L and $\widetilde{e}_L$. *Gauge supermultiplets* contain a spin-1 gauge boson and its fermionic superpartner. Note that the bosonic and fermionic degrees of freedom balance as the gauge bosons are massless before spontaneous symmetry breaking.

The naming convention for scalar superpartners of SM fermions is to add the prefix "s-" to the name of the SM particle, e.g. the superpartner of the electron is the *selectron*. For fermionic superpartners of SM bosons it is customary to use the suffix "-ino" together with the boson name, e.g. the superpartner of the W boson is the *wino* while the Higgs bosons are partnered by the *Higgsinos*. (Note that more than one scalar Higgs particle is present in SUSY theories.) In addition, the term *sparticle* is used as a general label for any new 'supersymmetric particle'.

3.2 Motivations

Although no sparticles have yet been discovered, there are good reasons to expect that SUSY might be a symmetry of nature. This is due to the fact that SUSY theories offer viable solutions to several of the SM problems presented in Section 2.6. Furthermore, it can be motivated that if SUSY exists it should be manifest around the experimentally accessible TeV scale. A few of the most important such motivations are presented below, but the list is far from exhaustive.

The most common argument for the realisation of SUSY is that it presents a natural solution to the SM hierarchy problem. We recall that radiative corrections to the squared Higgs mass depend quadratically on the cut-off parameter Λ, which can be interpreted as the scale where physics beyond the SM becomes important. Unless there is an extreme fine-tuning of parameters, such corrections will bring the Higgs mass up to the order of Λ, in conflict with the weak-scale Higgs mass preferred by experimental

data. For diagrams containing a fermion loop the contributions to m_H^2 are of the general form

$$\left(\Delta m_H^2\right)_f \;=\; -\frac{|\lambda_f|^2}{8\pi^2}\,\Lambda^2 + \ldots \tag{3.23}$$

where the ellipsis represents terms that grow logarithmically with Λ. Contributions from diagrams with a boson loop are of the same general structure, but with opposite sign. For example, the contribution from a scalar loop is:

$$\left(\Delta m_H^2\right)_s \;=\; \frac{\lambda_s}{16\pi^2}\,\Lambda^2 + \ldots \tag{3.24}$$

The quadratically divergent terms of (3.23) and (3.24) will cancel exactly if there for every fermion exists *two* scalars with the coupling λ_s satisfying

$$\lambda_s \;=\; |\lambda_f|^2 \tag{3.25}$$

This is precisely what happens with unbroken SUSY, and the cancellation holds to all orders of perturbation theory. The cancellation of quadratic terms also holds for theories with *softly* broken SUSY, in which relation (3.25) still holds although $m_f \neq m_s$. However, with the masses no longer being degenerate, the logarithmic terms from $\left(\Delta m_H^2\right)_f$ and $\left(\Delta m_H^2\right)_s$ yield contributions of the form

$$\propto\; \left(m_f^2 - m_s^2\right)\ln\Lambda \tag{3.26}$$

Thus, the mass differences between SM particles and their superpartners cannot be too large if theories with softly broken SUSY is to avoid fine-tuning. This is generally regarded as the main motivation for SUSY to be manifest around the TeV energy scale. (Nevertheless, if SUSY particles are discovered around 1 TeV it still remains to be explained why their mass scale is so close to the weak scale.)

Further arguments in favour of TeV-scale SUSY is found in the evolution of the SM gauge couplings. Introducing superpartners for the SM particles around the scale of 1 TeV affects the evolution of the gauge couplings such that an apparent unification takes place around the scale $Q \sim 10^{16}$ GeV (Fig. 3.1). Although this may well be accidental, it is generally regarded as a strong hint towards grand unified theories incorporating SUSY.

Additionally, SUSY theories provide several candidates for particle dark matter, including the *neutralino* — a mass state mixture of the neutral wino, bino and higgsinos — and the *gravitino* — the spin-3/2 partner of a spin-2 graviton in theories with *local* supersymmetry.

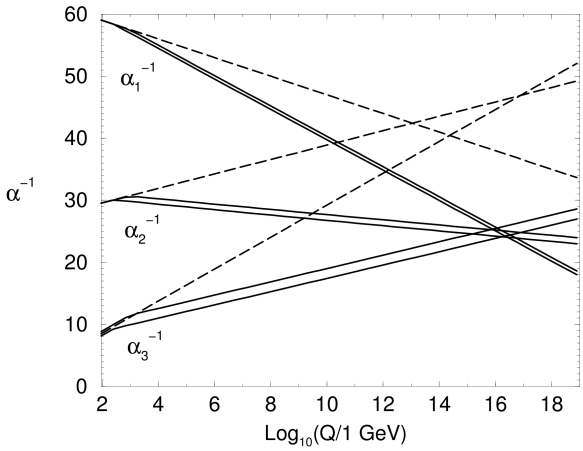

Figure 3.1: Example of unification of gauge couplings within the MSSM (Section 3.4). Evolution of inverse gauge couplings are shown for the SM (dashed lines) and the MSSM (solid lines). Double solid lines are due to variation of both the initial value of the strong coupling ($\alpha_3(M_Z)$) and the lower mass scale for SUSY particles. The figure is taken from [5].

3.3 Supersymmetry breaking

As already noted, SUSY must be broken in order to produce the mass differences between SM and SUSY particles required by experiment. In Section 2.5 we saw an example of spontaneous symmetry breaking, in which the vacuum state does not obey the full symmetry of the $\mathcal{L}$. An alternative way of breaking a symmetry, known as *explicit symmetry breaking*, is to introduce additional terms in $\mathcal{L}$ that do not satisfy the given symmetry. Explicit symmetry breaking can be used to construct effective phenomenological theories in cases where the underlying symmetry-breaking mechanism is unknown.

There are several alternative theories concerning how SUSY can be broken. However, a common assumption is that SUSY breaking takes place in a *hidden sector* of fields that, at most, have very small direct couplings to the fields of our detectable *visible sector*. With SUSY spontaneously broken by a non-zero *vev* in the hidden sector, the effects are mediated to the visible sector through some interaction common for both sectors. Below we mention two of the most popular such theories: *Planck-scale-mediated supersymmetry breaking* (PMSB) is based on the postulate that interactions

common to both sectors are gravitationally sized, that is, suppressed by powers of the Planck mass, $M_P \sim 10^{18}$ GeV. Another alternative is *Gauge-mediated supersymmetry breaking* (GMSB), in which the common interaction is assumed to be the gauge interactions known from the SM. A postulated *messenger field* interacting with the gauge bosons and gauginos can thus connect the non-zero *vev* of the hidden sector to the fields of the visible sector. This way, interactions with messenger fields at one- and two-loop level can give contributions to the gaugino and sfermion masses, respectively. The masses of the SM particles, however, are protected by the SM gauge invariance and only gain masses through electroweak symmetry breaking.

Whichever mechanism is responsible for breaking SUSY, an effective phenomenological theory can be constructed from an originally invariant theory by adding terms that explicitly violate SUSY. This is done in the *minimal supersymmetric standard model* (MSSM), which we introduce next.

3.4 The Minimal Supersymmetric Standard Model

The MSSM is based on a *minimal* extension of the Poincaré algebra by including one SUSY generator and its conjugate. This is known as $N = 1$ supersymmetry. The Lagrangian density is divided in a SUSY invariant part ($\mathcal{L}_{\text{SUSY}}$) and a part containing the SUSY breaking terms ($\mathcal{L}_{\text{soft}}$):

$$\mathcal{L}_{\text{MSSM}} = \mathcal{L}_{\text{SUSY}} + \mathcal{L}_{\text{soft}} \tag{3.27}$$

As the mechanism for breaking SUSY is unknown, $\mathcal{L}_{\text{MSSM}}$ includes all viable SUSY breaking terms that satisfy a few phenomenologically motivated constraints: First, only terms that softly break SUSY are allowed in $\mathcal{L}_{\text{soft}}$. This includes the sfermion and gaugino mass terms needed to produce mass splittings within the supermultiplets. Second, the complete $\mathcal{L}_{\text{MSSM}}$ is required to be $U(1)_Y \times SU(2)_L \times SU(3)_C$ gauge invariant. Finally, only interactions conserving *R-parity* (P_R) are allowed. The concept of R-parity and its important phenomenological consequences will be introduced in the following section.

The terms in $\mathcal{L}_{\text{SUSY}}$ are highly constrained by the requirements of both gauge and SUSY invariance, with parameters mostly determined by already measured SM parameters. On the other hand, the terms in $\mathcal{L}_{\text{soft}}$ introduce ~ 120 new parameters,

Table 3.1: The particle spectrum of the MSSM. Mixing is assumed to be negligible for the first two sfermion generations. SM fermions and bosons are not included.

Name	Spin	$\mathbf{P_R}$	Gauge Eigenstates	Mass Eigenstates
Higgs bosons	0	+1	$H_u^0 \;\; H_d^0 \;\; H_u^+ \;\; H_d^-$	$h^0 \;\; H^0 \;\; A^0 \;\; H^\pm$
squarks	0	-1	$\widetilde{u}_L \;\; \widetilde{u}_R \;\; \widetilde{d}_L \;\; \widetilde{d}_R$	(same)
			$\widetilde{s}_L \;\; \widetilde{s}_R \;\; \widetilde{c}_L \;\; \widetilde{c}_R$	(same)
			$\widetilde{t}_L \;\; \widetilde{t}_R \;\; \widetilde{b}_L \;\; \widetilde{b}_R$	$\widetilde{t}_1 \;\; \widetilde{t}_2 \;\; \widetilde{b}_1 \;\; \widetilde{b}_2$
sleptons	0	-1	$\widetilde{e}_L \;\; \widetilde{e}_R \;\; \widetilde{\nu}_e$	(same)
			$\widetilde{\mu}_L \;\; \widetilde{\mu}_R \;\; \widetilde{\nu}_\mu$	(same)
			$\widetilde{\tau}_L \;\; \widetilde{\tau}_R \;\; \widetilde{\nu}_\tau$	$\widetilde{\tau}_1 \;\; \widetilde{\tau}_2 \;\; \widetilde{\nu}_\tau$
neutralinos	1/2	-1	$\widetilde{B}^0 \;\; \widetilde{W}^0 \;\; \widetilde{H}_u^0 \;\; \widetilde{H}_d^0$	$\widetilde{\chi}_1^0 \;\; \widetilde{\chi}_2^0 \;\; \widetilde{\chi}_3^0 \;\; \widetilde{\chi}_4^0$
charginos	1/2	-1	$\widetilde{W}^\pm \;\; \widetilde{H}_u^+ \;\; \widetilde{H}_d^-$	$\widetilde{\chi}_1^\pm \;\; \widetilde{\chi}_2^\pm$
gluino	1/2	-1	$\widetilde{g}$	(same)
goldstino (gravitino)	1/2 (3/2)	-1	$\widetilde{G}$	(same)

so further assumptions on the nature of SUSY breaking are usually employed to improve predictability. A much studied such theory is known as *minimal supergravity* (mSUGRA) in which PMSB is invoked with the additional assumption of parameter unification at the Planck scale. This leads to a highly predictive theory completely determined by four Planck-scale parameters and a sign.

All presently undiscovered particles within the MSSM are listed in Table 3.1, along with their corresponding spin and R_P eigenvalues. Due to effects from SUSY breaking and electroweak symmetry breaking, the mass eigenstates are in general mixtures of the gauge eigenstates. This is evident for third-generation sleptons and squarks, as well as for the gauginos. As the amount of L-R mixing for sfermions can be shown to be proportional to the mass (or more precisely, the Yukawa coupling) of the corresponding SM fermion, mixing is assumed negligible for the first two generations. All mixed mass

eigenstates are numbered according to increasing mass, e.g., $\widetilde{t}_1$ being the lighter of the two stops.

For the Higgs bosons the four gauge eigenstates represent complex fields, i.e. eight real degrees of freedom. This is due to the fact that *two* complex $SU(2)_L$ doublets are needed in order to obtain all the Yukawa couplings necessary to produce the SM masses. Through spontaneous symmetry breaking three degrees of freedom are absorbed into mass terms for the $W^{\pm}$ and Z^0 bosons, leaving five physical degrees of freedom. These are manifest as the three neutral scalars h^0, H^0 and A^0, and the charged scalar $H^{\pm}$. Although the rich parameter space of the MSSM will not be treated in detail, we note that the parameter $\tan\beta$ is defined as

$$\tan\beta \equiv \frac{v_u}{v_d} \tag{3.28}$$

Here v_u and v_d are the non-zero *vevs* of the two Higgs doublets $H_u = (H_u^+, H_u^0)$ and $H_d = (H_d^0, H_d^-)$, respectively. Further, v_u and v_d are related to the SM Higgs *vev* by $v = \sqrt{v_u^2 + v_d^2} \sim 246$ GeV. For the staus, which will be central in our further discussion, the amount of L-R mixing in the mass eigenstates depends on $\tan\beta$. For low $\tan\beta$ ($\lesssim 10$), $\widetilde{\tau}_1$ is predominantly $\widetilde{\tau}_R$, analogous to the two lighter slepton families which generally have $\widetilde{e}_1 \simeq \widetilde{e}_R$ and $\widetilde{\mu}_1 \simeq \widetilde{\mu}_R$ as the lighter mass states [5]. For larger $\tan\beta$ the amount of $\widetilde{\tau}_L$-$\widetilde{\tau}_R$ mixing in $\widetilde{\tau}_1$ is increased, with the additional effect that $\widetilde{\tau}_1$ becomes lighter.

The mass eigenstates of the neutral and charged gauginos are respectively named *neutralinos* and *charginos*. For our analysis the lighter two neutralinos are of importance. The phenomenology of the neutralinos is affected by the the amount of bino, wino and higgsino mixing in the various mass states. For example, in mSUGRA scenarios one often finds that $\widetilde{\chi}_1^0 \sim \widetilde{B}$ and $\widetilde{\chi}_2^0 \sim \widetilde{W}^0$, with the consequence that $\widetilde{\chi}_2^0$ predominantly couples to left-chiral states[1].

3.5 R-parity

In the SM there are no renormalisable terms that violate baryon number (B) or lepton number (L), and indeed no B or L violating processes have been seen experimentally.

[1] For the scalar sfermions, 'chirality' is simply a convenient label that refers to the chirality of their fermionic superpartner.

With only the general requirements of gauge and SUSY invariance the MSSM would allow several L- and B-violating interaction terms, leading to unacceptable predictions. For example, given unsuppressed couplings, the squark-mediated proton decays $p^+ \rightarrow e^+ \pi^0$ and $p^+ \rightarrow \mu^+ \pi^0$ would result in a far too low prediction for the proton lifetime. For these two processes experimental lower limits on the partial lifetime has been set to 8.2×10^{33} years for the e^+-mode and 6.6×10^{33} years for the μ^+-mode, at 90% confidence level [15].

In order to prevent such problematic predictions, all interactions of the MSSM are required to conserve the discrete and multiplicative R-parity, defined at the particle level as:

$$P_R \equiv (-1)^{3(B-L)+2s} \tag{3.29}$$

Here s denotes particle spin. From this definition it follows that all SM particles and the additional Higgs bosons of the MSSM have $P_R = +1$, while all sparticles have $P_R = -1$ (Table 3.1). The postulate that all interactions conserve R-parity has three important phenomenological consequences:

- When produced from SM particles, sparticles must be produced in even numbers.
- A sparticle decay must result in an odd number of lighter sparticles.
- The lightest sparticle (LSP) must be absolutely stable, implying that all sparticle decay chains end with the LSP.

One of the most attractive features of R-parity conservation (RPC) is that it promotes an electrically neutral LSP to a candidate for particle dark matter. The MSSM contains three such candidates, namely the lightest sneutrino, the lightest neutralino and the gravitino, with the neutralino and gravitino being the most popular candidates. For our analysis the lightest neutralino is assumed to be the LSP, or at least the 'effective LSP' at the scales of particle detectors[1].

[1] In GMSB models the gravitino is nearly always the LSP. However, if $\widetilde{\chi}_1^0$ is the next-to-lightest sparticle (NSLP) it can well be the effective LSP for collider experiments given that its decay length is greater than the detector radius.

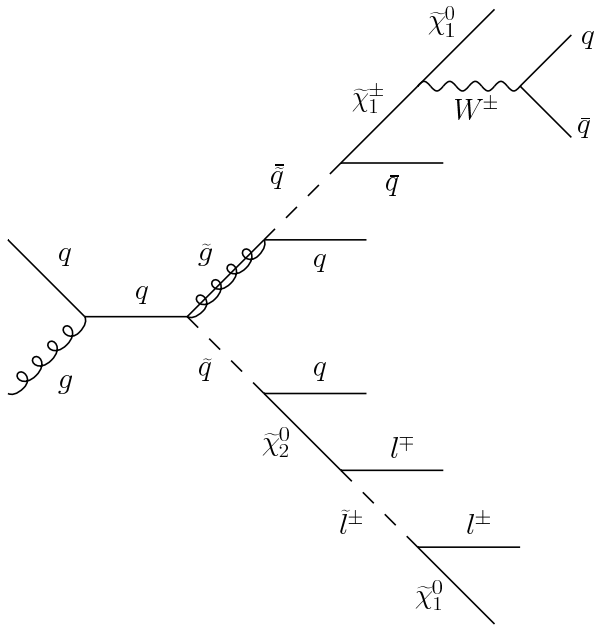

Figure 3.2: Example diagram of a complete SUSY event.

3.6 SUSY cascade decays

Due to R-parity conservation, a non-LSP sparticle will preferably decay through a kinematically allowed two-body decay into one lighter sparticle and one SM particle. Starting from a heavy sparticle produced in a collider experiment, one therefore expects a chain of sequential two-body decays, where each sub-decay results in one particle and one sparticle. Any such *cascade decay* (or simply *cascade*) must eventually terminate with the LSP. In the case where a given two-body decay is not kinematically allowed, the cascade can proceed by three-body decay through some off-shell sparticle or particle.

At the LHC, gluon-gluon and quark-gluon fusion to $\widetilde{g}\widetilde{g}$, $\widetilde{g}\widetilde{q}$ and $\widetilde{q}\overline{\widetilde{q}}$ pairs are expected to constitute the main SUSY production, given these sparticles are not heavier than ~ 1 TeV. The preferred decay modes of the squarks and gluinos depend on the mass hierarchy, couplings and mass state mixtures of the lighter sparticles. An example of a 'complete event' topology is given in Fig. 3.2.

With sparticles pair-produced due to RPC, there will consequently be two separate cascades taking place in the detector. In an experimental search for a specific cascade signal, the second cascade may constitute a significant SUSY background. The typical

detector signature of a SUSY event is large amounts of missing (transverse) energy combined with n jets and m leptons, where n or m can be zero. The missing energy is mainly due to the two escaping LSPs, but may also get contributions from neutrinos produced either in the cascade or in subsequent decays of SM taus and bosons. The main SM background comes from production of W and Z bosons combined with QCD jets. Upon decay, the gauge bosons produce final states with neutrinos that reproduce the missing energy signal.

3.7 Mass determination from cascade kinematics

If evidence for supersymmetry is found, the next challenge will be to determine the parameters of the underlying theory, including the masses of new particles. In addition to being interesting in itself, a well-measured mass spectrum can give important hints on the nature of SUSY breaking and dark matter. As the LSP escapes undetected, it is not possible to determine the sparticle masses from reconstructed invariant mass peaks. Instead, constraints on various sparticle masses can be obtained from kinematic features in the distributions of the detected SM particles[1]. One particular well-studied method is based on measuring distinct endpoints in observable invariant mass distributions [16, 17, 18, 19, 20]. As these endpoints correspond to extreme kinematic configurations, their position can be expressed solely in terms of the masses of the 'parent' sparticles. By measuring various such endpoints it is in principle possible to extract the values of the individual sparticles.

For a simple illustration of the above method, we consider the much-studied 'dilepton cascade'

$$\widetilde{\chi}_2^0 \;\rightarrow\; l_n^{\pm}\,\widetilde{l}^{\mp} \;\rightarrow\; l_n^{\pm}\,l_f^{\mp}\,\widetilde{\chi}_1^0\,, \qquad\qquad l = e, \mu \tag{3.30}$$

The two visible SM leptons are labelled n ('near') and f ('far') referring to their position in the cascade relative to $\widetilde{\chi}_2^0$. There is no spin correlation between the two leptons due to the intermediate scalar slepton. Consequently, the distribution of the dilepton invariant mass m_{ll} is determined by phase space alone. It can be shown to have a simple linear shape, often referred to as a 'triangle distribution' (Fig. 3.3, first column). The

[1] For an outline of how such observable distributions are related to the more abstract field theories, the reader is referred to Appendix C.

distinct endpoint should enable a quite clean experimental measurement, as have been demonstrated for various SUSY scenarios [19, 20] (among others).

The invariant mass value at the endpoint can be related to the sparticle masses by straightforward kinematics: If we take the leptons to be approximately massless, the squared dilepton invariant mass is given by

$$m_{ll}^2 \;=\; \big(P_{l_n} + P_{l_f}\big)^2 \;=\; 2\,\big(P_{l_n}\cdot P_{l_f}\big) \;=\; 2\,E_{l_n}E_{l_f}\big(1-\cos\theta\big) \tag{3.31}$$

Here θ is the angle between the three-momenta of the two leptons. For simplicity we now choose to work in the rest frame of the intermediate slepton. As we are only interested in the maximum invariant mass $(m_{ll})_{\max}$, we set $\cos\theta = -1$. This corresponds to the leptons going back-to-back. An expression for E_{l_n} is found by squaring the four-momentum conservation relation $P_{\widetilde{\chi}_2^0} = P_{\widetilde{l}} + P_{l_n}$:

$$\begin{aligned} m_{\widetilde{\chi}_2^0}^2 \;=\; P_{\widetilde{\chi}_2^0}^2 \;&=\; \big(P_{\widetilde{l}} + P_{l_f}\big)^2 \\ &=\; m_{\widetilde{l}}^2 \;+\; 2\,E_{l_n} m_{\widetilde{l}} \end{aligned} \tag{3.32}$$

Thus, we obtain

$$E_{l_n} \;=\; \frac{m_{\widetilde{\chi}_2^0}^2 - m_{\widetilde{l}}^2}{2\,m_{\widetilde{l}}} \tag{3.33}$$

Similarly, we find an expression for E_{l_f} from the four-momentum relation $P_{\widetilde{l}} \;=\; P_{\widetilde{\chi}_1^0} + P_{l_f}$:

$$E_{l_f} \;=\; \frac{m_{\widetilde{l}}^2 - m_{\widetilde{\chi}_1^0}^2}{2\,m_{\widetilde{l}}} \tag{3.34}$$

By combining the above results the invariant mass value at the endpoint is found to be

$$(m_{ll})_{\max} \;=\; \sqrt{\frac{\Big(m_{\widetilde{\chi}_2^0}^2 - m_{\widetilde{l}}^2\Big)\Big(m_{\widetilde{l}}^2 - m_{\widetilde{\chi}_1^0}^2\Big)}{m_{\widetilde{l}}^2}} \tag{3.35}$$

An experimental measurement of the endpoint position can therefore provide a relation between the masses of $\widetilde{\chi}_0^2$, $\widetilde{l}$ and $\widetilde{\chi}_0^2$.

In the above example there were three unknown masses but only one observable endpoint. The situation changes if we consider an 'extended' dilepton cascade where a parent squark decay is included (lower cascade in Fig. 3.2):

$$\widetilde{q} \;\to\; q\,\widetilde{\chi}_2^0 \;\to\; q\,l_n^{\pm}\,\widetilde{l}^{\mp} \;\to\; q\,l_n^{\pm}\,l_f^{\mp}\,\widetilde{\chi}_1^0\,, \qquad\qquad l = e,\mu \tag{3.36}$$

There are now four unknown sparticle masses ($m_{\tilde{q}}, m_{\tilde{\chi}_2^0}, m_{\tilde{l}}, m_{\tilde{\chi}_1^0}$) and four 'visible' invariant masses ($m_{ql_n}, m_{ql_f}, m_{ll}, m_{qll}$). Thus, by expressing the endpoints of the additional invariant mass distributions in terms of the sparticle masses, one can in principle obtain a system of equations that are exactly solvable for the unknown masses.

3.7.1 Complications

In the above example several complicating aspects were ignored: First, in a collider experiment it will not be possible to distinguish the 'near' from the 'far' lepton. This problem can be overcome by relating m_{ql_n} and m_{ql_f} to two invariant mass distributions that are experimentally unambiguous. One possible choice is to use the variables $m_{ql(\text{high})}$ and $m_{ql(\text{low})}$ defined on an event-by-event basis as [18]:

$$\begin{aligned} m_{ql(\text{high})} &\equiv \max\{m_{ql_n}, m_{ql_f}\} \\ m_{ql(\text{low})} &\equiv \min\{m_{ql_n}, m_{ql_f}\} \end{aligned} \tag{3.37}$$

Expressions for the various endpoints of in terms of sparticle masses (including the $m_{ql(\text{high})}$ and $m_{ql(\text{low})}$ distributions) are given in [18]. Inverted formulas expressing the sparticle masses in terms of endpoints can be found in [20].

A second complication arises due to the general form of the endpoint expressions. As is illustrated by (3.35), endpoint expressions depend strongly on mass *differences*, resulting in a more precise determination of these differences than the individual masses. A related difficulty is that of degenerate solutions: The inverted expressions for the sparticle masses are not necessarily single-valued functions, and there is a high probability that a given set of endpoint values is consistent with several sets of sparticle masses. This ambiguity is still present if one chooses to do a numerical fit of the masses to the endpoint values rather than using analytical inversion formulas. With an equal number of measured endpoints and masses there is in principle no way of discriminating two different solutions. If more endpoints are measured than there are unknown masses in the cascade, the system is overconstrained and the real solution would be preferred by a numerical fit. Nevertheless, with measurement uncertainties taken into account it is not given that a false solution can be safely rejected. A detailed discussion of such degenerate solutions can be found in [20].

Finally, we note that the shapes of the invariant mass distributions vary greatly with sparticle mass values (Fig. 3.3). (The exception is the simple triangle distribution

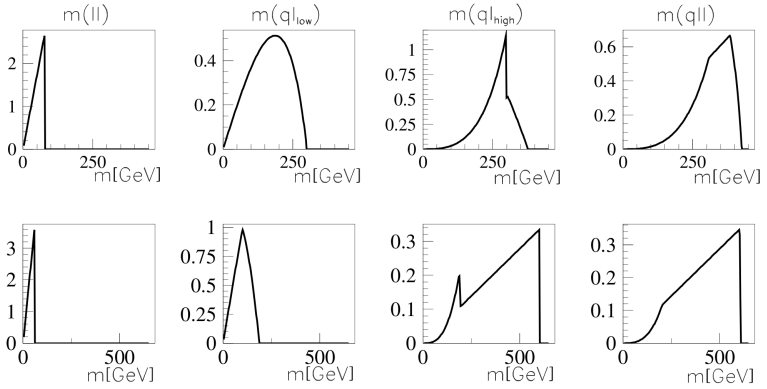

Figure 3.3: The theoretical distributions of m_{ll}, $m_{ql(\mathrm{low})}$, $m_{ql(\mathrm{high})}$ and m_{qll} for the extended dilepton cascade in (3.36). Each distribution is shown for two sets of benchmark masses. The figure is taken from [21].

of m_{ll}, whose intrinsic shape is the same for all on-shell mass configurations.) The variety of shapes may lead to additional difficulties when an endpoint, or some other distribution feature, is to be determined as precisely as possible from an experimental distribution. Specifically, for a given mass scenario the underlying distributions might exhibit structure close to the endpoint (like a sudden 'drop' or an extended 'foot') that is easily missed in an experimental study due to background.

The above mentioned complications are all on a rather conceptual level. When the endpoint method is applied to data there will be additional uncertainties related to backgrounds, statistics and correctly linking detector objects with cascade particles.

3.7.2 The need for analytical shape formulas

In order to measure an endpoint experimentally a fit must be performed to the endpoint region of the distribution. For such a fit to return an accurate endpoint value it is necessary have a realistic 'signal hypothesis', that is, choose a fit shape in good correspondence with the underlying distribution. This is especially important for scenarios in which the distribution exhibits some structure close to the endpoint that may become hidden by background. High accuracy in endpoint measurements is important as errors might get enlarged in the process of extracting sparticle mass values. Consequently, knowing the full analytical distribution shape would be a great advantage.

In addition to providing the correct signal shapes for endpoint determination, analytical shape formulas might help to solve some of the problems presented in the previous section. With the shape formulas expressed in terms of sparticle masses, performing fits to complete observed distributions would in principle return the mass values directly. Although such distributions can be obtained numerically for a given set of sparticle masses, this approach is computationally too expensive for use in fitting. Further, in scenarios where the endpoint method returns multiple solutions, a complete shape fit might provide the extra information needed to lift the degeneracy. These aspects are demonstrated in [22, 23].

3.7.3 The ditau cascade

For the extended dilepton cascade in (3.36) the leptons were assumed to be either electrons or muons. Shape formulas for this cascade have been derived in [24] and [25]. In our analysis we focus on the similar cascade where the leptons are taus. Due to their short lifetime of only $\tau_0 \simeq 2.9 \times 10^{-13}$ s [1], the taus will always decay before detection. This makes for a more complicated cascade topology, including neutrinos that escape detection. Assuming both taus decay as $\tau \to \nu\,\pi$ leaves us with the following cascade:

$$\widetilde{q} \;\to\; q\,\widetilde{\chi}_2^0 \;\to\; q\,\tau_n^{\pm}\,\widetilde{\tau}^{\mp} \;\to\; q\,(\pi_n^{\pm}\,\nu)\,(\tau_f^{\mp}\,\widetilde{\chi}_1^0) \;\to\; q\,\pi_n^{\pm}\,\nu\,\pi_f^{\mp}\,\nu\,\widetilde{\chi}_1^0 \tag{3.38}$$

The assumption of tau decay into pions will only be of direct importance for the analysis in Chapter 6. For the derivations presented in Chapters 4 and 5 any hadronic tau decay will be equally valid. Of course, at the LHC experiments the hadronically decaying taus will appear as tau jets.

A good understanding of the above cascade might be important for several reasons: First, it provides information on the mass of $\widetilde{\tau}_1$, which due to stau mixing may be quite different from the masses of the lightest selectron and smuon. Further, in scenarios with non-negligible stau mixing, the branching fraction for $\widetilde{\chi}_2^0$ into final states with taus is often larger than for final states with electrons or muons [5]. The tau cascade might therefore prove important also in the determination of neutralino and squark masses. Finally, due to their in-detector decays, the polarisation of the taus might result in observable effects in the invariant mass distributions of the visible particles. Although complicating mass measurements, these effects provide a possible way of measuring the

mixing parameters of the stau and gaugino sectors [26, 27]. We comment briefly on this topic in Section 6.5.

The above 'extended ditau cascade' will be studied in Chapter 5, while Chapters 4 and 6 will only treat the shorter 'ditau cascade':

$$\widetilde{\chi}_2^0 \;\rightarrow\; \tau_n^{\pm}\,\widetilde{\tau}^{\mp} \;\rightarrow\; (\pi_n^{\pm}\,\nu)\,(\tau_f^{\mp}\,\widetilde{\chi}_1^0) \;\rightarrow\; \pi_n^{\pm}\,\nu\,\pi_f^{\mp}\,\nu\,\widetilde{\chi}_1^0 \tag{3.39}$$

Chapter 4

The m_{ab} Distribution in the Spin-0 Approximation

4.1 General remarks and assumptions

We study the ditau cascade decay (Fig. 4.1)

$$C \to \tau_b\, B \to (b\,\nu)\,(\tau_a\, A) \to b\,\nu\,a\,\nu\,A \tag{4.1}$$

corresponding to the SUSY cascade

$$\widetilde{\chi}_2^0 \;\to\; \tau_n^{\pm}\,\widetilde{\tau}^{\mp} \;\to\; (\pi_n^{\pm}\,\nu)\,(\tau_f^{\mp}\,\widetilde{\chi}_1^0) \;\to\; \pi_n^{\pm}\,\nu\,\pi_f^{\mp}\,\nu\,\widetilde{\chi}_1^0 \tag{4.2}$$

In the following we will derive an analytical expression for the differential decay rate $\mathrm{d}\Gamma/\,\mathrm{d}m_{ab}$, where m_{ab} is the invariant mass of particles a and b. The derivation is based on a few simplifying assumptions:

- all particles are treated as spin-0
- particles a, b and ν are assumed massless
- all massive particles are taken to be on-shell and satisfying the hierarchy $m_\tau < m_A < m_B < m_C$

The spin-0 assumption ensures that a decay can be treated as isotropic in the decaying particle's rest frame. This is of course a considerable simplification as several of the particles involved clearly are not spin-0. However, as particle B is taken to be a scalar (stau) regardless of the spin-0 assumption, we know that there will be no spin dependent correlation between the two tau production vertices. With particles A and C not

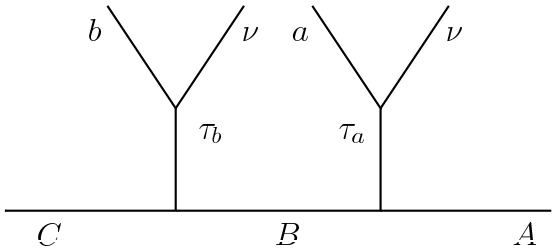

Figure 4.1: The ditau cascade decay

being observed, all we are leaving out with the spin-0 assumption are the effects of the tau spins on the energy spectra of a and b. Such effects will be included in Chapter 6, thus providing a more realistic result. The distribution derived here will only be strictly correct if right- and left-handed taus are produced with equal probability in the two vertices and all final states are summed, cancelling the spin effects. As these production probabilities depend on the $\widetilde{\tau}_L$-$\widetilde{\tau}_R$ mixture of the stau mass eigenstates and the $\widetilde{W}^0$-$\widetilde{B}^0$-$\widetilde{H}^0$ mixture of the neutralinos, the distributions derived here will consequently only be valid for certain values of the theoretical mixing parameters. Nevertheless, the following derivation will be valuable as an introduction to the general method used, as well as a clean way to illustrate the effects coming from kinematics alone.

The assumption of massless a and b is more accurate in the rest frames of B and C (masses of the order order $10^2 - 10^3$ GeV in most scenarios) than in the rest frames of τ_a and τ_b ($m_\tau = 1.78$ GeV), but for simplicity this assumption is used in all reference frames. It should also be noted that in taking all massive particles on-shell we neglect the effect of particle widths that generally will lead to a smearing of the distribution.

4.2 The derivation

We employ the same method as used in [24], adapted for the decay topology in Fig. 4.1. The derivation can be outlined as follows: From kinematical considerations we obtain an expression for m_{ab}^2 in terms of cosines for which the differential decay rate is flat. Then we perform a change of variables to a set that includes m_{ab}^2, before integrating over any extra variables. The resulting expression for $\mathrm{d}\Gamma / \mathrm{d}m_{ab}^2$ is related to the desired

m_{ab} distribution through the simple relation

$$\frac{\mathrm{d}\Gamma}{\mathrm{d}m_{ab}} \;=\; 2\,m_{ab}\frac{\mathrm{d}\Gamma}{\mathrm{d}m_{ab}^2} \tag{4.3}$$

4.2.1 Kinematics

We start by expressing m_{ab}^2 in terms of flat angular variables. Treating a and b as massless, the squared invariant mass is given by

$$m_{ab}^2 \;=\; (P_a + P_b)^2 \;=\; 2\,(P_a \cdot P_b) \;=\; 2\,E_a\,E_b\,(1 - \cos\theta_{ab}) \tag{4.4}$$

As $\cos\theta_{ab}$ will have a flat distribution in the rest frame of B, this frame is a suitable choice for the evaluation of m_{ab}^2. Introducing a notation where upper indices specify reference frames, we write

$$m_{ab}^2 \;=\; 2\,E_a^B\,E_b^B\,\left(1 - \cos\theta_{ab}^B\right) \tag{4.5}$$

To obtain an expression for E_b^B depending on flat angular variables we make use of the invariance relation

$$(P_b \cdot P_B)^B = \;(P_b \cdot P_B)^{\tau_b} \tag{4.6}$$

which for a massless b gives

$$\begin{aligned} E_b^B \;&=\; \frac{1}{m_B}\,E_b^{\tau_b}\,\left(E_B^{\tau_b} - p_B^{\tau_b}\cos\theta_{bB}^{\tau_b}\right) \\ &=\; \frac{1}{m_B}\left(\frac{m_\tau}{2}\right)\left(E_B^{\tau_b} - p_B^{\tau_b}\cos\theta_{bB}^{\tau_b}\right) \end{aligned} \tag{4.7}$$

Four-momentum conservation in the two-body decay $C \to B\;\tau_b$ can be expressed as

$$P_C \;=\; P_B + P_{\tau_b} \tag{4.8}$$

Squaring this relation and evaluating the cross term $2\,(P_B \cdot P_{\tau_b})$ in the rest frame of τ_b gives the following expression for $E_B^{\tau_b}$:

$$E_B^{\tau_b} \;=\; \frac{m_C^2 - m_B^2 - m_\tau^2}{2m_\tau} \tag{4.9}$$

Using (4.9) we can now express $p_B^{\tau_B}$ as

$$\begin{aligned} p_B^{\tau_b} &= \sqrt{(E_B^{\tau_b})^2 - m_B^2} \\ &= \frac{1}{2m_\tau}\sqrt{\left(m_C^2 - m_B^2 - m_\tau^2\right)^2 - 4\,m_B^2 m_\tau^2} \\ &= \frac{\sqrt{\lambda_{C\tau B}}}{2m_\tau} \end{aligned} \tag{4.10}$$

where we have introduced the Källen function λ defined by

$$\lambda_{XYZ} \equiv m_X^4 + m_Y^4 + m_Z^4 - 2\,m_X^2 m_Y^2 - 2\,m_X^2 m_Z^2 - 2\,m_Y^2 m_Z^2 \tag{4.11}$$

Inserting the results of (4.9) and (4.10) into (4.7) we get

$$E_b^B = \frac{1}{4m_B}\left((m_C^2 - m_B^2 - m_\tau^2) - \sqrt{\lambda_{C\tau B}}\cos\theta_{bB}^{\tau_b}\right) \tag{4.12}$$

where $\cos\theta_{bB}^{\tau_b}$ has a flat distribution by the spin-0 assumption.

In a completely analogous way we can express E_a^B in terms of the flat variable $\cos\theta_{aB}^{\tau_a}$: From the invariance relation

$$(P_a \cdot P_B)^B = (P_a \cdot P_B)^{\tau_a} \tag{4.13}$$

we obtain

$$\begin{aligned} E_a^B &= \frac{1}{m_B} E_a^{\tau_a}\left(E_B^{\tau_a} - p_B^{\tau_a}\cos\theta_{aB}^{\tau_a}\right) \\ &= \frac{1}{m_B}\left(\frac{m_\tau}{2}\right)\left(E_B^{\tau_a} - p_B^{\tau_a}\cos\theta_{aB}^{\tau_a}\right) \end{aligned} \tag{4.14}$$

An expression for $E_B^{\tau_a}$ can be found from the four-momentum relation

$$P_A = P_B - P_{\tau_a} \tag{4.15}$$

which by squaring and evaluating the cross term in the rest frame of τ_a gives

$$E_B^{\tau_a} = \frac{m_B^2 - m_A^2 + m_\tau^2}{2\,m_\tau} \tag{4.16}$$

From (4.16) it follows that

$$\begin{aligned} p_B^{\tau_a} &= \sqrt{(E_B^{\tau_a})^2 - m_B^2} \\ &= \frac{\sqrt{\lambda_{B\tau A}}}{2\,m_\tau} \end{aligned} \tag{4.17}$$

Combining (4.16) and (4.17) with (4.14) we find E_a^B given by

$$E_a^B \;=\; \frac{1}{4\,m_B}\left((m_B^2 - m_A^2 + m_\tau^2) - \sqrt{\lambda_{B\tau A}}\cos\theta_{aB}^{\tau_a}\right) \tag{4.18}$$

Finally, by inserting the results of (4.12) and (4.18) into (4.5) we arrive at the desired expression for m_{ab}^2:

$$\begin{aligned} m_{ab}^2 \;=\; \frac{1}{8\,m_B^2}&\left((m_C^2 - m_B^2 - m_\tau^2) - \sqrt{\lambda_{C\tau B}}\cos\theta_{bB}^{\tau_b}\right) \\ &\times\left((m_B^2 - m_A^2 + m_\tau^2) - \sqrt{\lambda_{B\tau A}}\cos\theta_{aB}^{\tau_a}\right)\left(1 - \cos\theta_{ab}^{B}\right) \end{aligned} \tag{4.19}$$

Treating all particles as spin-0 implies that $\cos\theta_{bB}^{\tau_b}$, $\cos\theta_{aB}^{\tau_a}$ and $\cos\theta_{ab}^{B}$ all have flat distributions. From these cosines we define three variables u, v and w:

$$\begin{aligned} u \;&\equiv\; \frac{1 - \cos\theta_{bB}^{\tau_b}}{2} \\ v \;&\equiv\; \frac{1 - \cos\theta_{aB}^{\tau_a}}{2} \\ w \;&\equiv\; \frac{1 - \cos\theta_{ab}^{B}}{2} \end{aligned} \tag{4.20}$$

To simplify notation we also define three parameters completely determined by the involved masses:

$$\begin{aligned} b_C \;&\equiv\; \frac{1}{2}\left(\frac{m_C^2 - m_B^2 - m_\tau^2}{\sqrt{\lambda_{C\tau B}}} \;-\; 1\right) \\ b_B \;&\equiv\; \frac{1}{2}\left(\frac{m_B^2 - m_A^2 + m_\tau^2}{\sqrt{\lambda_{B\tau A}}} \;-\; 1\right) \\ M^2 \;&\equiv\; \frac{\sqrt{\lambda_{C\tau B}}\sqrt{\lambda_{B\tau A}}}{m_B^2} \end{aligned} \tag{4.21}$$

We note that these parameters are positive for any choice of masses allowed by the on-shell kinematics ($m_C > m_B + m_\tau$ and $m_B > m_A + m_\tau$). Using the above definitions m_{ab}^2 can be expressed as

$$m_{ab}^2 \;=\; M^2\,(b_C + u)\,(b_B + v)\,w\;, \qquad 0 \;\leq\; (u, v, w) \;\leq\; 1 \tag{4.22}$$

4.2.2 Variable changes and integrations

Due to the flat distributions of $\cos\theta_{bB}^{\tau_b}$, $\cos\theta_{aB}^{\tau_a}$, $\cos\theta_{ab}^{B}$, the differential decay rate with respect to the variables u, v, w will be flat and non-zero in the range $0 \leq (u, v, w) \leq 1$.

This can be expressed using the step function $\theta(x)$:

$$\frac{1}{\Gamma}\frac{\mathrm{d}^3\Gamma}{\mathrm{d}u\,\mathrm{d}v\,\mathrm{d}w} = \theta(u)\,\theta(1-u)\,\theta(v)\,\theta(1-v)\,\theta(w)\theta(1-w) \tag{4.23}$$

Using (4.22) we now perform a change of variables from (u, v, w) to (u, v, m_{ab}^2)

$$\begin{aligned}\frac{1}{\Gamma}\frac{\mathrm{d}^3\Gamma}{\mathrm{d}u\,\mathrm{d}v\,\mathrm{d}m_{ab}^2} &= \left|\frac{\partial(u,v,w)}{\partial(u,v,m_{ab}^2)}\right|\frac{1}{\Gamma}\frac{\mathrm{d}^3\Gamma}{\mathrm{d}u\,\mathrm{d}v\,\mathrm{d}w} \\ &= \frac{\partial w}{\partial m_{ab}^2}\frac{1}{\Gamma}\frac{\mathrm{d}^3\Gamma}{\mathrm{d}u\,\mathrm{d}v\,\mathrm{d}w} \\ &= \frac{1}{M^2(b_C+u)(b_B+v)}\,\hat{\theta}(u)\,\hat{\theta}(v)\,\hat{\theta}\left(\frac{m_{ab}^2}{M^2(b_C+u)(b_B+v)}\right)\end{aligned} \tag{4.24}$$

where we have defined

$$\hat{\theta}(x) \equiv \theta(x)\,\theta(1-x) \tag{4.25}$$

To obtain $\mathrm{d}\Gamma/\,\mathrm{d}m_{ab}^2$ we must integrate over u and v. To keep expressions as simple as possible we make another change of variables:

$$x \equiv b_C + u \tag{4.26}$$

$$y \equiv b_B + v \tag{4.27}$$

In terms of these new variables we can write

$$\frac{1}{\Gamma}\frac{\mathrm{d}\Gamma}{\mathrm{d}m_{ab}^2} = \frac{1}{M^2}\int_{x_1}^{x_2}\int_{y_1}^{y_2}\frac{1}{x\,y}\,\hat{\theta}\left(\frac{m_{ab}^2}{M^2 x\,y}\right)\,\mathrm{d}y\,\mathrm{d}x \tag{4.28}$$

with the limits of integration

$$\begin{aligned} x_1 &= b_C & y_1 &= b_B \\ x_2 &= b_C + 1 & y_2 &= b_B + 1 \end{aligned}$$

obtained from the two step functions $\hat{\theta}(u)$ and $\hat{\theta}(v)$. The remaining step function provides a non-zero integrand as long as the following constraint is satisfied:

$$y \geq y_{\min}(x) \equiv \frac{m_{ab}^2}{M^2 x} \tag{4.29}$$

Depending on the relative size of $y_{\min}(x_1)$ to y_1 and y_2, and similarly for $y_{\min}(x_2)$, five different integration regions giving non-zero results can be constructed (Fig. 4.2).

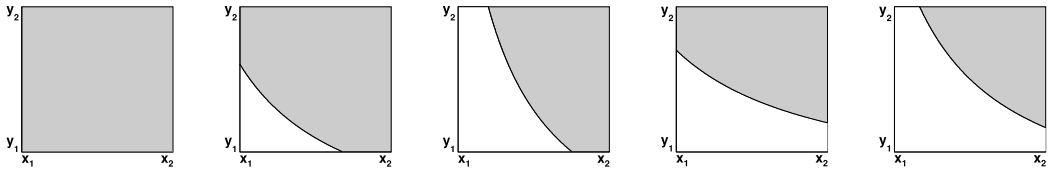

(a) (b) (c) (d) (e)

Figure 4.2: The five integration regions of the xy plane (grey).

Table 4.1: Integration regions and corresponding m_{ab}^2 ranges for mass scenario I

Integration region	Bounds on $y_{\min}(x)$	Range of m_{ab}^2
Region (a)	$y_{\min}(x_1) < y_1$ $y_{\min}(x_2) < y_1$	$0 < m_{ab}^2 < b_B b_C M^2$
Region (b)	$y_1 < y_{\min}(x_1) < y_2$ $y_{\min}(x_2) < y_1$	$b_B b_C M^2 < m_{ab}^2 < (b_B+1) b_C M^2$
Region (c)	$y_{\min}(x_1) > y_2$ $y_{\min}(x_2) < y_1$	$(b_B+1) b_C M^2 < m_{ab}^2 < b_B (b_C+1) M^2$
Region (e)	$y_{\min}(x_1) > y_2$ $y_1 < y_{\min}(x_2) < y_2$	$b_B (b_C+1) M^2 < m_{ab}^2 < (b_B+1)(b_C+1) M^2$

These regions correspond to different ranges for m_{ab}^2. Two separate mass scenarios must be considered:

$$b_C < b_B \qquad \text{Scenario I}$$
$$b_B < b_C \qquad \text{Scenario II}$$

The integration regions, with corresponding m_{ab}^2 ranges, for scenario I and II are given in Tables 4.1 and 4.2, respectively. All integrations are of the form

$$\iint\limits_{\text{region (x)}} \frac{1}{M^2 x\, y}\, \mathrm{d}y\, \mathrm{d}x$$

Performing all integrals and using the relation

$$\frac{\mathrm{d}\Gamma}{\mathrm{d}m_{ab}} = 2\, m_{ab} \frac{\mathrm{d}\Gamma}{\mathrm{d}m_{ab}^2} \tag{4.30}$$

we arrive at the final result for the differential decay rate.

Table 4.2: Integration regions and corresponding m_{ab}^2 ranges for mass scenario II

Integration region	Bounds on $y_{\min}(x)$	Range of m_{ab}^2
Region (a)	$y_{\min}(x_1) < y_1$ $y_{\min}(x_2) < y_1$	$0 < m_{ab}^2 < b_B b_C M^2$
Region (b)	$y_1 < y_{\min}(x_1) < y_2$ $y_{\min}(x_2) < y_1$	$b_B b_C M^2 < m_{ab}^2 < b_B(b_C+1)M^2$
Region (d)	$y_1 < y_{\min}(x_1) < y_2$ $y_1 < y_{\min}(x_2) < y_2$	$b_B(b_C+1)M^2 < m_{ab}^2 < (b_B+1)b_C M^2$
Region (e)	$y_{\min}(x_1) > y_2$ $y_1 < y_{\min}(x_2) < y_2$	$(b_B+1)b_C M^2 < m_{ab}^2 < (b_B+1)(b_C+1)M^2$

4.3 Results and discussion

Scenario I

$$\frac{1}{\Gamma}\frac{\mathrm{d}\Gamma}{\mathrm{d}m_{ab}} = \begin{cases} \frac{m_{ab}}{M^2}\left\{2\ln\left(\frac{b_B+1}{b_B}\right)\ln\left(\frac{b_C+1}{b_C}\right)\right\} & \text{for (1)} \\ \frac{m_{ab}}{M^2}\left\{\left[\ln\left(\frac{b_B+1}{b_B}\right)\right]^2 - \left[\ln\left(\frac{(b_B+1)b_C M^2}{m_{ab}^2}\right)\right]^2 + 2\ln\left(\frac{b_B+1}{b_B}\right)\ln\left(\frac{b_B(b_C+1)M^2}{m_{ab}^2}\right)\right\} & \text{for (2)} \\ \frac{m_{ab}}{M^2}\left\{\left[\ln\left(\frac{b_B+1}{b_B}\right)\right]^2 + 2\ln\left(\frac{b_B+1}{b_B}\right)\ln\left(\frac{b_B(b_C+1)M^2}{m_{ab}^2}\right)\right\} & \text{for (3)} \\ \frac{m_{ab}}{M^2}\left\{\left[\ln\left(\frac{(b_B+1)(b_C+1)M^2}{m_{ab}^2}\right)\right]^2\right\} & \text{for (4)} \end{cases}$$

with the ranges

$$\begin{aligned} (1) \quad & 0 < m_{ab} < \sqrt{b_B b_C M^2} \\ (2) \quad & \sqrt{b_B b_C M^2} < m_{ab} < \sqrt{(b_B+1)b_C M^2} \\ (3) \quad & \sqrt{(b_B+1)b_C M^2} < m_{ab} < \sqrt{b_B(b_C+1)M^2} \\ (4) \quad & \sqrt{b_B(b_C+1)M^2} < m_{ab} < \sqrt{(b_B+1)(b_C+1)M^2} \end{aligned}$$

Scenario II

$$\frac{1}{\Gamma}\frac{\mathrm{d}\Gamma}{\mathrm{d}m_{ab}} = \begin{cases} \frac{m_{ab}}{M^2}\left\{ 2\ln\left(\frac{b_B+1}{b_B}\right)\ln\left(\frac{b_C+1}{b_C}\right)\right\} & \text{for (1)} \\ \frac{m_{ab}}{M^2}\left\{\left[\ln\left(\frac{b_B+1}{b_B}\right)\right]^2 - \left[\ln\left(\frac{(b_B+1)b_C M^2}{m_{ab}^2}\right)\right]^2 \right. & \\ \qquad \left. + \; 2\ln\left(\frac{b_B+1}{b_B}\right)\ln\left(\frac{b_B(b_C+1)M^2}{m_{ab}^2}\right)\right\} & \text{for (2)} \\ \frac{m_{ab}}{M^2}\left\{\left[\ln\left(\frac{(b_B+1)(b_C+1)M^2}{m_{ab}^2}\right)\right]^2 - \left[\ln\left(\frac{(b_B+1)b_C M^2}{m_{ab}^2}\right)\right]^2\right\} & \text{for (3)} \\ \frac{m_{ab}}{M^2}\left\{\left[\ln\left(\frac{(b_B+1)(b_C+1)M^2}{m_{ab}^2}\right)\right]^2\right\} & \text{for (4)} \end{cases}$$

with the ranges

$$\begin{array}{lrcccl} (1) & 0 & < & m_{ab} & < & \sqrt{b_B b_C M^2} \\ (2) & \sqrt{b_B b_C M^2} & < & m_{ab} & < & \sqrt{b_B(b_C+1)M^2} \\ (3) & \sqrt{b_B(b_C+1)M^2} & < & m_{ab} & < & \sqrt{(b_B+1)b_C M^2} \\ (4) & \sqrt{(b_B+1)b_C M^2} & < & m_{ab} & < & \sqrt{(b_B+1)(b_C+1)M^2} \end{array}$$

We recall that

$$\begin{aligned} b_C &= \frac{1}{2}\left(\frac{m_C^2 - m_B^2 - m_\tau^2}{\sqrt{\lambda_{C\tau B}}} - 1\right) \\ b_B &= \frac{1}{2}\left(\frac{m_B^2 - m_A^2 + m_\tau^2}{\sqrt{\lambda_{B\tau A}}} - 1\right) \\ M^2 &= \frac{\sqrt{\lambda_{C\tau B}}\sqrt{\lambda_{B\tau A}}}{m_B^2} \\ \lambda_{XYZ} &= m_X^4 + m_Y^4 + m_Z^4 - 2\,m_X^2 m_Y^2 - 2\,m_X^2 m_Z^2 - 2\,m_Y^2 m_Z^2 \end{aligned}$$

Figure 4.3(b) depicts the distribution for a set of masses corresponding to the mSUGRA benchmark point SPS1a, while Figures 4.3(a) and 4.3(c) represent scenarios with $(m_B - m_A) \sim m_\tau$ and $(m_C - m_B) \sim m_\tau$, respectively. For Fig. 4.3(d) a set of masses where both these mass differences are small is chosen in order to illustrate the behaviour of all four parts of the analytical expression. The grey triangle represents the corresponding dilepton invariant mass distribution for the cascade in (3.30).

Due to the energy lost to the neutrinos, the m_{ab} distribution derived here is more rounded and shifted towards lower invariant masses compared to the dilepton distribution. In addition, as the dilepton distribution was derived assuming massless final state leptons while our result include massive taus, the m_{ab} endpoint is lower than the dilepton endpoint. This difference disappears if both $(m_C - m_B)$ and $(m_B - m_A)$ are large compared to m_τ, as will be shown in the next section.

4.4 The limit $m_\tau = 0$

In deriving the above results we made use of the fact that taus were massive by exploiting their rest frames. However, the same (invariant) expressions for $\mathrm{d}\Gamma / \mathrm{d}m_{ab}$ could in principle have been derived using any other set of reference frames, for which it would not be necessary to treat the taus as massive. Therefore we can be confident that taking the limit $m_\tau = 0$ in the above expressions will not cause any conflict with the fact that the taus' rest frames were used in the derivation.

From the definition of the Källen function in (4.11) we find that setting $m_\tau = 0$ corresponds to

$$\begin{aligned} \lambda_{C\tau B} &= \left(m_C^2 - m_B^2\right)^2 \\ \lambda_{B\tau A} &= \left(m_B^2 - m_A^2\right)^2 \end{aligned} \tag{4.31}$$

By (4.21) it then follows that

$$\begin{aligned} b_C &= 0 \\ b_B &= 0 \\ M^2 &= \frac{(m_C^2 - m_B^2)(m_B^2 - m_A^2)}{m_B^2} \end{aligned} \tag{4.32}$$

The above relations imply several simplifications: First, the distinction between mass scenarios I and II disappears as both b_B and b_C vanishes. Second, the contribution from integration region (e) of the xy plane now covers the entire m_{ab} range, given by

$$0 < m_{ab} < M \tag{4.33}$$

Third, the *shape* of the distribution is now independent of the masses m_A, m_B and m_C, as M only determines the upper limit for m_{ab}. Thus, in the limit of massless taus

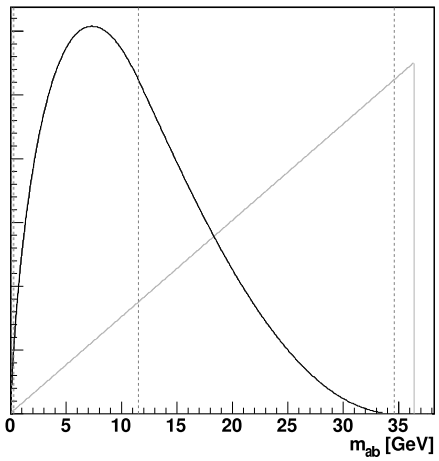

(a) $m_C = 180,\ m_B = 100,\ m_A = 97$ (GeV)
scenario I

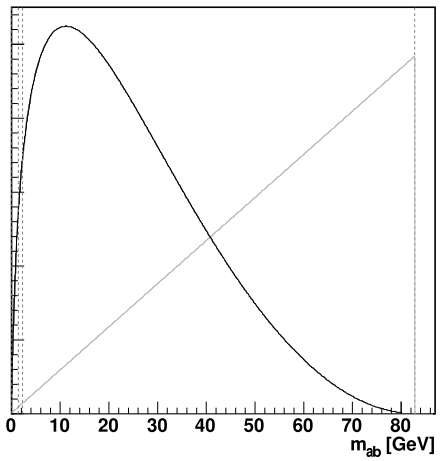

(b) $m_C = 180,\ m_B = 135,\ m_A = 97$ (GeV)
scenario I

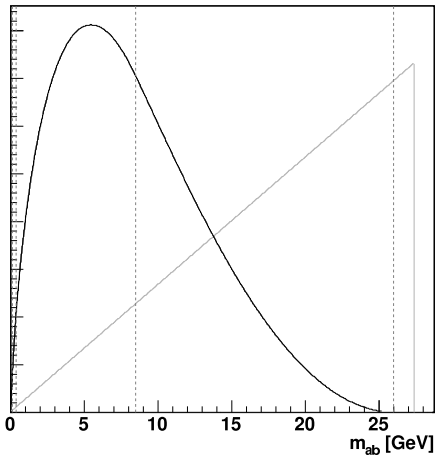

(c) $m_C = 180,\ m_B = 177,\ m_A = 97$ (GeV)
scenario II

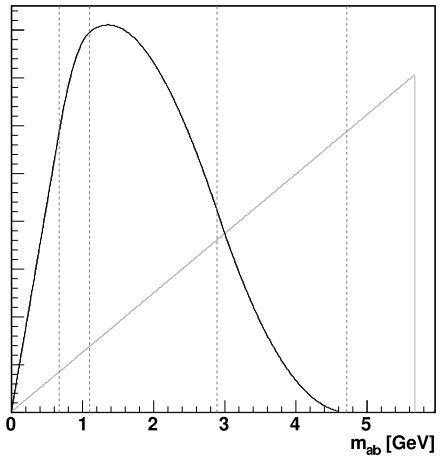

(d) $m_C = 180,\ m_B = 176,\ m_A = 174$ (GeV)
scenario I

Figure 4.3: $(1/\Gamma)(\,\mathrm{d}\Gamma/\,\mathrm{d}m_{ab})$ plotted for four different sets of masses. Dotted vertical lines mark the points where the functional form of the distribution changes. All plots use $m_\tau = 1.78$ GeV.

the m_{ab} distribution simplifies to

$$\frac{1}{\Gamma}\frac{\mathrm{d}\Gamma}{\mathrm{d}m_{ab}} \;=\; \frac{m_{ab}}{M^2}\left[\ln\!\left(\frac{m_{ab}^2}{M^2}\right)\right]^2 \qquad \text{for} \quad 0 \,<\, m_{ab} \,<\, M \tag{4.34}$$

As can be seen in Fig. 4.4 the non-zero tau mass only affects the distribution shape when $(m_C - m_B)$ and/or $(m_B - m_A)$ are close to m_τ. For a wide range of m_A, m_B and m_C values the limit $m_\tau = 0$ will thus be a very reasonable approximation. A point to notice is that with the distribution shape fixed, the position of the peak is given solely in terms of the endpoint M:

$$m_{ab}^{\text{peak}} \;=\; Me^{-2} \;\simeq\; 0.135\,M \tag{4.35}$$

In Fig. 4.4 we also note that the massless tau approximation leads to a broader distribution compared to the exact result. This can be understood by observing how the limit $m_\tau = 0$ affects the maximum and minimum allowed energies of particles a and b. In (4.12) we found the energy of b in the rest frame of B to be

$$E_b^B \;=\; \frac{1}{4\,m_B}\left(\left(m_C^2 - m_B^2 - m_\tau^2\right) - \sqrt{\lambda_{C\tau B}}\cos\theta_{bB}^{\tau_b}\right) \tag{4.36}$$

By taking $\cos\theta_{bB}^{\tau_b} = \pm 1$ and writing out $\lambda_{C\tau B}$ in terms of m_C, m_B and m_τ, we find the minimum and maximum energies of b:

$$\begin{aligned}(E_b^B)_{\min} \;&=\; \frac{1}{4\,m_B}\left(\left(m_C^2 - m_B^2 - m_\tau^2\right) - \sqrt{\left(m_C^2 - m_B^2 - m_\tau^2\right)^2 - \,4\,m_B^2 m_\tau^2}\right) \\ &=\; \frac{1}{4\,m_B}\left(m_C^2 - m_B^2 - m_\tau^2\right)\left(1 \,-\, \sqrt{1 - \frac{4\,m_B^2 m_\tau^2}{\left(m_C^2 - m_B^2 - m_\tau^2\right)^2}}\right)\end{aligned} \tag{4.37}$$

and similarly

$$(E_b^B)_{\max} \;=\; \frac{1}{4\,m_B}\left(m_C^2 - m_B^2 - m_\tau^2\right)\left(1 \,+\, \sqrt{1 - \frac{4\,m_B^2 m_\tau^2}{\left(m_C^2 - m_B^2 - m_\tau^2\right)^2}}\right) \tag{4.38}$$

Evidently, $(E_b^B)_{\min}$ decreases and $(E_b^B)_{\max}$ increases as we let m_τ go to zero. As similar behaviour holds for $(E_a^B)_{\min}$ and $(E_a^B)_{\max}$, minimal and maximal m_{ab} values are made more probable by the massless tau approximation.

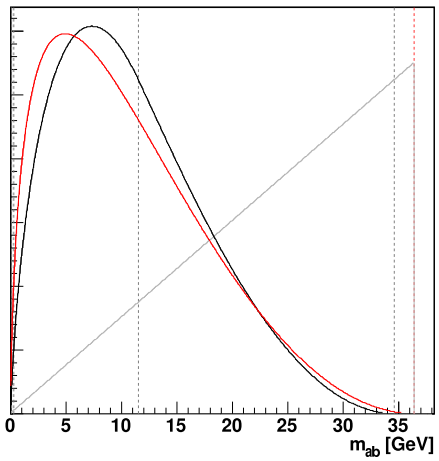

(a) $m_C = 180,\ m_B = 100,\ m_A = 97$ (GeV)
scenario I

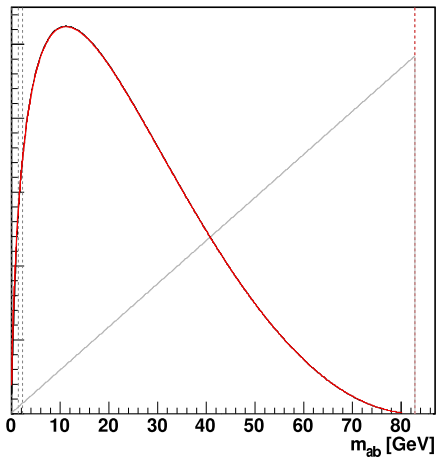

(b) $m_C = 180,\ m_B = 135,\ m_A = 97$ (GeV)
scenario I

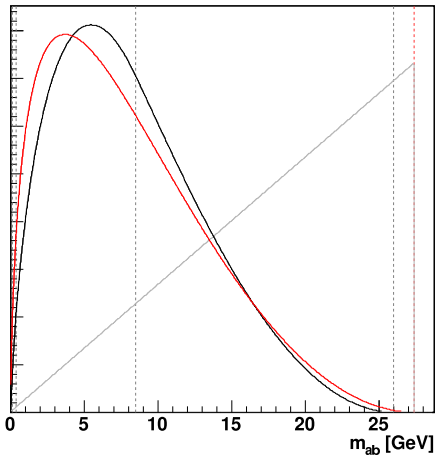

(c) $m_C = 180,\ m_B = 177,\ m_A = 97$ (GeV)
scenario II

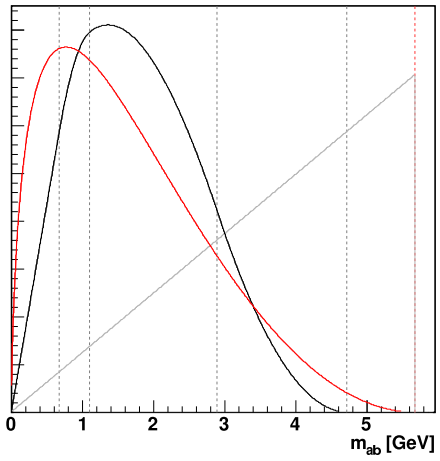

(d) $m_C = 180,\ m_B = 176,\ m_A = 174$ (GeV)
scenario I

Figure 4.4: $(1/\Gamma)(\,\mathrm{d}\Gamma/\,\mathrm{d}m_{ab})$ in the limit $m_\tau = 0$ (red) compared to the exact distribution (black). The shape of the red distribution is independent of the chosen masses for particles A, B and C.

Chapter 5

The m_{high} Distribution in the Spin-0 Approximation

5.1 General remarks and assumptions

Following the derivation of the m_{ab} distribution, we now go on to study the extended decay chain

$$D \to c\, C \to c\, \tau_b\, B \to c\, (b\, \nu)\, (\tau_a\, A) \to c\, b\, \nu\, a\, \nu\, A \tag{5.1}$$

In most SUSY studies the particles D and c are assumed to be a squark and a quark, respectively. In terms of particle and sparticle labels, the cascade is

$$\widetilde{q} \;\to\; q\, \widetilde{\chi}_2^0 \;\to\; q\, \tau_n^{\pm}\, \widetilde{\tau}^{\mp} \;\to\; q\, (\pi_n^{\pm}\, \nu)\, (\tau_f^{\mp}\, \widetilde{\chi}_1^0) \;\to\; q\, \pi_n^{\pm}\, \nu\, \pi_f^{\mp}\, \nu\, \widetilde{\chi}_1^0 \tag{5.2}$$

With c as an additional visible final state particle, we can combine particles into the invariant mass distributions m_{ac}, m_{bc} and m_{abc} in addition to the previously studied m_{ab} distribution. However, as noted in Section 3.7.1, it is not possible experimentally to determine which is the 'near' (b) and which is the 'far' (a) particle relative to c. To avoid this problem the m_{ac} and m_{bc} distributions must be replaced by two experimentally distinguishable distributions, the usual choice being $m_{\rm high}$ and $m_{\rm low}$:

$$m_{\rm high} \;\equiv\; \max\{m_{ac}\,,\; m_{bc}\} \tag{5.3}$$

$$m_{\rm low} \;\equiv\; \min\{m_{ac}\,,\; m_{bc}\} \tag{5.4}$$

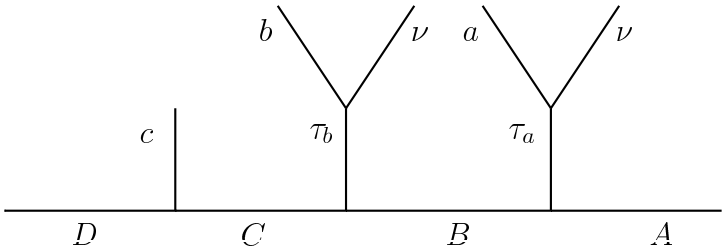

Figure 5.1: The extended ditau cascade decay

In the following we will derive an analytical expression for the distribution $\mathrm{d}\Gamma / \mathrm{d}m_{\text{high}}$. Derivations of the underlying m_{ac} and m_{bc} distributions follow in close analogy to the m_{ab} derivation, and the resulting expressions are given in Appendix A.

For the m_{high} distribution we will employ a similar set of assumptions as used in the previous chapter: treating all particles as spin-0, treating a, b, c, ν as massless, taking all massive particles on-shell and assuming the hierarchy $m_\tau < m_A < m_B < m_C < m_D$. Similar to the m_{ab} case, treating a, b and c as massless is more accurate in the rest frames of B, C, D than in the rest frames of τ_a and τ_b, and the on-shell assumption neglects a certain amount of smearing of the distribution. The spin-0 assumption requires some further comments as extending the cascade to include particles D and c allows for additional spin correlations.

As D is a scalar, the spins of c and C will be oppositely directed. This correlation may result in observable charge asymmetries in the invariant mass distributions, as discussed for dilepton cascades in [28, 29], among others. In order to illustrate this effect we consider the following scenario: First, $\widetilde{\chi}_2^0$ (C) is assumed to be mostly wino, implying that both the initial squark (D) and the resulting quark (c) are left-chiral. Second, we choose a scenario with low $\tan\beta$. This results in the lightest stau being almost purely 'right-chiral', that is, $B = \widetilde{\tau}_1 \sim \widetilde{\tau}_R$. ($\widetilde{\tau}_2 \sim \widetilde{\tau}_L$ is assumed to be heavier than $\widetilde{\chi}_2^0$.) Treating the taus as being approximately massless implies that τ_b is either a τ^- with right-helicity or a τ^+ with left-helicity. To conserve angular momentum in the rest frame of C, a right-helicity τ^- will prefer to go along the direction of c, while the opposite direction is preferred by a left-helicity τ^+. Therefore, as the invariant mass of two particles depend on their internal angle, there will be a clear asymmetry between the invariant mass distributions of $c\,\tau_b^-$ and $c\,\tau_b^+$.[1]

[1] Also, with B and τ_b going back-to-back in the rest frame of C, the boost of B relative to c will depend on the helicity, and thus the charge, of τ_b. This dependence will translate into a small asymmetry in the $c\,\tau_a^-$ and $c\,\tau_a^+$ invariant mass distributions.

As we study more closely in Chapter 6, a τ^- will in its rest frame preferably emit the scalar b along its spin direction. Consequently, for the decay of a boosted right-helicity τ^-, b will usually be emitted along the tau direction and carry the major fraction of the original tau energy. Due to CP invariance of tau decays, the same conclusion holds for the decay of a boosted left-helicity τ^+. With the original tau direction and energy being approximately 'inherited' by b, the charge asymmetry of the $c\,\tau_b$ invariant mass distribution can be expected to still be evident after being passed down to the $c\,b$ distribution.

A non-negligible amount of L-R stau mixing will diminish the above charge asymmetry, as the link between charge and helicity for the taus is weakened. Additionally, cascades starting with an anti-squark (decaying into an anti-quark) exhibit the opposite correlations. With the charge of a quark jet being very difficult to measure, an observed distribution would be a sum of contributions from both squark and anti-squark cascades, leading to a reduction of the observable asymmetry. (Still, detection of such charge asymmetries may be possible as more squarks than anti-squarks are expected from the proton-proton collisions at LHC.)

Nevertheless, the above considerations are based on observation of final state charges. If charges are summed, the asymmetries cancel and the invariant mass distributions of $c\,\tau_b$ and $c\,\tau_a$ are returned to the shapes determined by phase space alone [29]. Therefore, the only spin effects that are truly neglected by treating all particles as spin-0 are the effects on the directions and energies of particles a and b due to the handedness of τ_a and τ_b, respectively. In the special case where the L-R mixing of the staus is such that taus with left- and right-handed helicity are produced with equal probability, even these effects would cancel.

5.2 The derivation

We will follow the general steps of the m_{ab} derivation, expressing m_{ac}^2 and m_{bc}^2 in terms of cosines for which the differential decay rate is flat, then changing variables to a set that includes m_{high}^2 before integrating $\mathrm{d}\Gamma$ over the extra variables. As we will see, the main difficulty lies in keeping track of all the different integration regions that must be covered in order to obtain a complete result.

5.2.1 Kinematics

We start by obtaining expressions for m_{ac}^2 and m_{bc}^2 in terms of 'flat' cosines. To keep the number of extra variables at a minimum, we look for cosines that can be used in both expressions. As the following kinematical considerations closely resemble those for the m_{ab} distribution, we will go through them in a slightly less detailed manner here. For massless a and c, m_{ac}^2 can be expressed in the rest frame of τ_a as

$$\begin{aligned} m_{ac}^2 \;=\; (P_a \cdot P_c)^2 \;&=\; 2\, E_a^{\tau_a} E_c^{\tau_a} \,(1 - \cos\theta_{ac}^{\tau_a}) \\ &=\; 2\left(\frac{m_\tau}{2}\right) E_c^{\tau_a}\,(1 - \cos\theta_{ac}^{\tau_a}) \end{aligned} \tag{5.5}$$

Solving the invariance relation

$$(P_c \cdot P_{\tau_a})^{\tau_a} \;=\; (P_c \cdot P_{\tau_a})^B \tag{5.6}$$

for $E_c^{\tau_a}$ we find

$$\begin{aligned} E_c^{\tau_a} \;&=\; \frac{1}{m_{\tau_a}} E_c^B \left[E_{\tau_a}^B - \, p_{\tau_a}^B \cos\theta_{c\tau_a}^B\right] \\ &=\; \frac{1}{2\, m_B\, m_\tau} E_c^B \left[(m_B^2 + m_\tau^2 - m_A^2) - \sqrt{\lambda_{B\tau A}}\cos\theta_{c\tau_a}^B\right] \end{aligned} \tag{5.7}$$

where we recall that the Källen function λ is defined as

$$\lambda_{XYZ} \;\equiv\; m_X^4 + m_Y^4 + m_Z^4 - 2\, m_X^2 m_Y^2 - 2\, m_X^2 m_Z^2 - 2\, m_Y^2 m_Z^2 \tag{5.8}$$

An expression for E_c^B can be obtained from

$$P_D^2 \;=\; (P_c + P_{\tau_b} + P_B)^2 \tag{5.9}$$

by evaluating the cross terms as $(P_c \cdot P_{\tau_b})^C$, $(P_c \cdot P_B)^B$ and $(P_{\tau_b} \cdot P_B)^B$. Solving for E_c^B and using that

$$\begin{aligned} E_c^C \;&=\; \frac{m_D^2 - m_C^2}{2\, m_C} \\ E_{\tau_b}^C \;&=\; \frac{m_C^2 + m_\tau^2 - m_B^2}{2\, m_C} \\ E_{\tau_b}^B \;&=\; \frac{m_C^2 - m_\tau^2 - m_B^2}{2\, m_B} \end{aligned} \tag{5.10}$$

we find

$$E_c^B \;=\; \frac{m_D^2 - m_C^2}{2\, m_B}\left\{1 - \frac{1}{2\, m_C^2}\left[(m_C^2 + m_\tau^2 - m_B^2) - \sqrt{\lambda_{C\tau B}}\cos\theta_{c\tau_b}^C\right]\right\} \tag{5.11}$$

Combining the results from (5.7) and (5.11) with (5.5) we find that m_{ac}^2 can be expressed as

$$\begin{aligned} m_{ac}^2 \;=\; & \frac{(m_D^2 - m_C^2)\sqrt{\lambda_{C\tau B}}\sqrt{\lambda_{B\tau A}}}{m_B^2\, m_C^2} \\ & \times \left[\frac{m_C^2}{\sqrt{\lambda_{C\tau B}}} - \frac{1}{2}\left(\frac{m_C^2 + m_\tau^2 - m_B^2}{\sqrt{\lambda_{C\tau B}}} - \cos\theta^C_{c\tau_b}\right)\right] \\ & \times \frac{1}{2}\left(\frac{m_B^2 + m_\tau^2 - m_A^2}{\sqrt{\lambda_{B\tau A}}} - \cos\theta^B_{c\tau_a}\right) \\ & \times \frac{1}{2}\left(1 - \cos\theta^{\tau_a}_{ac}\right) \end{aligned} \tag{5.12}$$

Here all cosines have flat distributions under the spin-0 assumption. Using these cosines we define three variables u, v and w:

$$\begin{aligned} u \;&\equiv\; \frac{1}{2}\left(1 - \cos\theta^B_{c\tau_a}\right) \\ v \;&\equiv\; \frac{1}{2}\left(1 - \cos\theta^C_{c\tau_b}\right) \\ w \;&\equiv\; \frac{1}{2}\left(1 - \cos\theta^{\tau_a}_{ac}\right) \end{aligned} \tag{5.13}$$

In order to simplify notation we define a set of parameters completely determined by the involved masses:

$$\begin{aligned} a_B \;&\equiv\; \frac{m_B^2}{\sqrt{\lambda_{B\tau A}}} \\ a_C \;&\equiv\; \frac{m_C^2}{\sqrt{\lambda_{C\tau B}}} \\ b_B \;&\equiv\; \frac{1}{2}\left(\frac{m_B^2 + m_\tau^2 - m_A^2}{\sqrt{\lambda_{B\tau A}}} - 1\right) \\ b_C \;&\equiv\; \frac{1}{2}\left(\frac{m_C^2 + m_\tau^2 - m_B^2}{\sqrt{\lambda_{C\tau B}}} - 1\right) \\ M^2 \;&\equiv\; \frac{(m_D^2 - m_C^2)\sqrt{\lambda_{B\tau A}}\sqrt{\lambda_{C\tau B}}}{m_B^2\, m_C^2} \;=\; \frac{m_D^2 - m_C^2}{a_B\, a_C} \end{aligned} \tag{5.14}$$

Using the definitions above we can now write m_{ac}^2 as

$$m_{ac}^2 \;=\; \big[a_C - (b_C + v)\big](b_B + u)\, w\, M^2\,, \qquad 0 \;\leq\; (u, v, w) \;\leq\; 1 \tag{5.15}$$

Having obtained the desired expression for m_{ac}^2 we must now find a corresponding expression for m_{bc}^2. This task is somewhat simpler due to the fact that b and c are closer to each other in the decay chain compared to a and c. We must however keep in

mind that we would like to reuse cosines used for m_{ac}^2 if possible. In the rest frame of τ_b we know that m_{bc}^2 is given by

$$\begin{aligned} m_{bc}^2 &= 2\,E_b^{\tau_b} E_c^{\tau_b}\left(1-\cos\theta_{bc}^{\tau_b}\right) \\ &= 2\left(\frac{m_\tau}{2}\right) E_c^{\tau_b}\left(1-\cos\theta_{bc}^{\tau_b}\right) \end{aligned} \tag{5.16}$$

An expression for $E_c^{\tau_b}$ can be found by expanding the invariance relation

$$(P_c\cdot P_{\tau_b})^{\tau_b} = (P_c\cdot P_{\tau_b})^C \tag{5.17}$$

noting that

$$\begin{aligned} E_c^C &= \frac{m_D^2-m_C^2}{2\,m_C} \\ E_{\tau_b}^C &= \frac{m_C^2+m_\tau^2-m_B^2}{2\,m_C} \\ p_{\tau_b}^C &= \frac{\sqrt{\lambda_{C\tau B}}}{2\,m_C} \end{aligned} \tag{5.18}$$

This way we obtain

$$E_c^{\tau_b} = \frac{m_D^2-m_C^2}{4\,m_C^2\,m_\tau}\left[(m_C^2+m_\tau^2-m_B^2)-\sqrt{\lambda_{C\tau B}}\cos\theta_{c\tau_b}^C\right] \tag{5.19}$$

Combining (5.19) with (5.16) we find that m_{bc}^2 can be written as

$$\begin{aligned} m_{bc}^2 = \;& \frac{(m_D^2-m_C^2)\sqrt{\lambda_{C\tau B}}}{m_C^2} \\ &\times \frac{1}{2}\left(\frac{m_C^2+m_\tau^2-m_B^2}{\sqrt{\lambda_{C\tau B}}}-\cos\theta_{c\tau_b}^C\right) \\ &\times \frac{1}{2}\left(1-\cos\theta_{bc}^{\tau_b}\right) \end{aligned} \tag{5.20}$$

where we note that $\cos\theta_{c\tau_b}^C$ now has been used in expressing both m_{ac}^2 and m_{bc}^2. For $\cos\theta_{bc}^{\tau_b}$ we define yet another variable t as

$$t \equiv \frac{1}{2}\left(1-\cos\theta_{bc}^{\tau_b}\right) \tag{5.21}$$

Using the definitions in (5.13) and (5.14) we can now express m_{bc}^2 in the simple form

$$m_{bc}^2 = a_B\,(b_C+v)\,t\,M^2\,, \qquad 0 \le (t,v) \le 1 \tag{5.22}$$

5.2.2 Variable changes

Equations (5.15) and (5.22) express m_{ac}^2 and m_{bc}^2 in terms of the variables t, u, v and w. As these variables are linearly dependent on the cosines the differential decay rate will be a flat distribution in the range $0 \leq (t, u, v, w) \leq 1$. This can be expressed as

$$\frac{1}{\Gamma}\frac{\mathrm{d}^4\Gamma}{\mathrm{d}t\,\mathrm{d}u\,\mathrm{d}v\,\mathrm{d}w} \;=\; \hat{\theta}(t)\,\hat{\theta}(u)\,\hat{\theta}(v)\,\hat{\theta}(w) \tag{5.23}$$

where we have used the notation

$$\hat{\theta}(x) \;\equiv\; \theta(x)\,\theta(1-x) \tag{5.24}$$

Our next task is to perform a change of variables from (t, u, v, w) to a set that includes m_{high}^2. In order to do this we must first relate the expressions for m_{ac}^2 and m_{bc}^2 to m_{high}^2. We recall that

$$m_{\mathrm{high}} \;\equiv\; \max\{m_{ac}\,,\; m_{bc}\} \tag{5.25}$$

and introduce a new variable x defined by

$$\begin{aligned} x \;&\equiv\; m_{bc}^2 - m_{ac}^2 \\ &=\; \Big\{a_B\,(b_C+v)\,t\,M^2\Big\} \\ &\quad -\Big\{\big[a_C-(b_C+v)\big](b_B+u)\,w\,M^2\Big\} \end{aligned} \tag{5.26}$$

As the sign of x is determined by which of m_{ac} and m_{bc} is greater, this enables us to combine m_{ac}^2, m_{bc}^2 and m_{high}^2 in a single expression using the step function $\theta(x)$:

$$\begin{aligned} m_{\mathrm{high}}^2 \;&=\; \theta(x)\,m_{bc}^2 \,+\, \theta(-x)\,m_{ac}^2 \\ &=\; \theta(x)\Big\{a_B\,(b_C+v)\,t\,M^2\Big\} \\ &\quad +\,\theta(-x)\Big\{\big[a_C-(b_C+v)\big](b_B+u)\,w\,M^2\Big\} \end{aligned} \tag{5.27}$$

Now a possible change of variables is to go from (t, u, v, w) to $(u, v, x, m_{\mathrm{high}}^2)$. Solving (5.26) and (5.27) for t and w and using that

$$\theta(x) \,+\, \theta(-x) \;=\; 1 \tag{5.28}$$

$$x \,-\, \theta(x)\,x \;=\; \theta(-x)\,x \tag{5.29}$$

we obtain

$$t = \frac{m_{\text{high}}^2 + \theta(-x)\, x}{a_B\,(b_C + v)M^2} \tag{5.30}$$

$$w = \frac{m_{\text{high}}^2 - \theta(x)\, x}{\big[a_C - (b_C + v)\big](b_B + u)M^2} \tag{5.31}$$

From these relations we can specify the Jacobian for the variable change:

$$\begin{aligned}\frac{\partial(u,v,w,t)}{\partial(u,v,x,m_{\text{high}}^2)} &= \frac{\partial w}{\partial x}\frac{\partial t}{\partial m_{\text{high}}^2} - \frac{\partial w}{\partial m_{\text{high}}^2}\frac{\partial t}{\partial x} \\ &= -\frac{1}{a_B(b_B+u)(b_C+v)\big[a_C-(b_C+v)\big]M^4}\end{aligned} \tag{5.32}$$

It should be noted that $a_C > b_C + v$ for all values of v given the assumed mass hierarchy. We can now write out the variable change

$$\frac{1}{\Gamma}\frac{\mathrm{d}^4\Gamma}{\mathrm{d}u\,\mathrm{d}v\,\mathrm{d}x\,\mathrm{d}m_{\text{high}}^2} = \left|\frac{\partial(u,v,w,t)}{\partial(u,v,x,m_{\text{high}}^2)}\right| \frac{1}{\Gamma}\frac{\mathrm{d}^4\Gamma}{\mathrm{d}t\,\mathrm{d}u\,\mathrm{d}v\,\mathrm{d}w} \tag{5.33}$$

which by using (5.23) and (5.32) becomes

$$\begin{aligned}\frac{1}{\Gamma}\frac{\mathrm{d}^4\Gamma}{\mathrm{d}u\,\mathrm{d}v\,\mathrm{d}x\,\mathrm{d}m_{\text{high}}^2} &= \frac{1}{a_B(b_B+u)(b_C+v)\big[a_C-(b_C+v)\big]M^4} \\ &\quad\times \hat{\theta}(u)\,\hat{\theta}(v)\,\hat{\theta}\left(\frac{m_{\text{high}}^2 + \theta(-x)\,x}{a_B(b_C+v)M^2}\right) \\ &\quad\times \hat{\theta}\left(\frac{m_{\text{high}}^2 - \theta(x)\,x}{\big[a_C-(b_C+v)\big](b_B+u)M^2}\right)\end{aligned} \tag{5.34}$$

To further simplify notation we perform yet another variable change, introducing the variables y and z defined by

$$\begin{aligned} y &\equiv b_B + u \\ z &\equiv b_C + v \end{aligned} \tag{5.35}$$

The differential decay rate in terms of the variables $(x, y, z, m_{\text{high}}^2)$ is thus

$$\begin{aligned}\frac{1}{\Gamma}\frac{\mathrm{d}^4\Gamma}{\mathrm{d}x\,\mathrm{d}y\,\mathrm{d}z\,\mathrm{d}m_{\text{high}}^2} &= \frac{1}{a_B\,y\,z\,(a_C-z)M^4} \\ &\quad\times \hat{\theta}(y-b_B)\,\hat{\theta}(z-b_C)\,\hat{\theta}\left(\frac{m_{\text{high}}^2 + \theta(-x)\,x}{a_B\,z\,M^2}\right) \\ &\quad\times \hat{\theta}\left(\frac{m_{\text{high}}^2 - \theta(x)\,x}{y\,(a_C-z)M^2}\right)\end{aligned} \tag{5.36}$$

5.2.3 Integrations

To obtain the m^2_{high} distribution we must integrate (5.36) over all regions of x, y and z giving non-zero contributions. As m_{high} is the only invariant mass involved in the rest of the derivation we set $m_{\text{high}} \equiv m$ to keep notation as simple as possible. We start by integrating over x. Splitting the integral into two parts, one for $x > 0$ and one for $x < 0$, we can write

$$\frac{1}{\Gamma}\frac{\mathrm{d}^3\Gamma}{\mathrm{d}y\,\mathrm{d}z\,\mathrm{d}m^2} \;=\; I_{x+} + \; I_{x-} \tag{5.37}$$

where

$$I_{x+} \;=\; \int_0^\infty \mathrm{d}x \; \frac{\hat{\theta}(y-b_B)\,\hat{\theta}(z-b_C)}{a_B\,y\,z\,(a_C-z)M^4}\;\hat{\theta}\Big(\frac{m^2}{a_B\,z\,M^2}\Big)\,\hat{\theta}\Big(\frac{m^2-x}{y\,(a_C-z)M^2}\Big) \tag{5.38}$$

$$I_{x-} \;=\; \int_{-\infty}^0 \mathrm{d}x \; \frac{\hat{\theta}(y-b_B)\,\hat{\theta}(z-b_C)}{a_B\,y\,z\,(a_C-z)M^4}\;\hat{\theta}\Big(\frac{m^2+x}{a_B\,z\,M^2}\Big)\,\hat{\theta}\Big(\frac{m^2}{y\,(a_C-z)M^2}\Big) \tag{5.39}$$

Solving I_{x+} first we note that the only x dependence of the integrand is through the last step function. In order for I_{x+} to give a non-zero result the following two constraints on x must be satisfied:

$$0 \;<\; x \;<\; \infty \tag{5.40}$$

$$m^2 - \; y\,(a_C-z)M^2 \;<\; x \;<\; m^2 \tag{5.41}$$

From these constraints we obtain the limits of integration

$$\begin{aligned} x_1 \;&=\; \max\big\{0\;,\; m^2 - \; y\,(a_C-z)M^2\big\} \\ x_2 \;&=\; m^2 \end{aligned} \tag{5.42}$$

where the two possible values for x_1 correspond to two different constraints on the remaining variables y, z and m^2. The solution of I_{x+} can be expressed as

$$\begin{aligned} I_{x+} \;=\;& \quad \theta\big(y\,(a_C-z)M^2 - m^2\big) \int_0^{m^2} f\,\big(y,z,m^2\big)\;\mathrm{d}x \\ &+\; \theta\big(m^2 - y\,(a_C-z)M^2\big) \int_{m^2-y\,(a_C-z)M^2}^{m^2} f\,\big(y,z,m^2\big)\;\mathrm{d}x \end{aligned} \tag{5.43}$$

where

$$f\left(y,z,m^2\right) \;=\; \frac{\hat{\theta}(y-b_B)\,\hat{\theta}(z-b_C)}{a_B\,y\,z\,(a_C-z)M^4}\;\hat{\theta}\Big(\frac{m^2}{a_B\,z\,M^2}\Big) \tag{5.44}$$

and the step functions in front of the integrals enforce the constraints on y, z and m^2 corresponding to the limits of integration. As $f\left(y,z,m^2\right)$ is independent of x, writing out the final expression for I_{x+} is straightforward:

$$\begin{aligned} I_{x+} \;=\;& \theta\big(y\,(a_C-z)M^2-m^2\big)\,\hat{\theta}\Big(\frac{m^2}{a_B\,z\,M^2}\Big)\,\hat{\theta}(y-b_B)\,\hat{\theta}(z-b_C) \\ & \times\;\frac{m^2}{a_B\,y\,z\,(a_C-z)M^4} \\ +\;& \theta\big(m^2-y\,(a_C-z)M^2\big)\,\hat{\theta}\Big(\frac{m^2}{a_B\,z\,M^2}\Big)\,\hat{\theta}(y-b_B)\,\hat{\theta}(z-b_C) \\ & \times\;\frac{1}{a_B\,z\,M^2} \end{aligned} \tag{5.45}$$

Doing the integration over negative x values (I_{x-}) in a completely analogous way, we obtain the result

$$\begin{aligned} I_{x-} \;=\;& \theta\big(a_B\,z\,M^2-m^2\big)\,\hat{\theta}\Big(\frac{m^2}{y\,(a_C-z)M^2}\Big)\,\hat{\theta}(y-b_B)\,\hat{\theta}(z-b_C) \\ & \times\;\frac{m^2}{a_B\,y\,z\,(a_C-z)M^4} \\ +\;& \theta\big(m^2-a_B\,z\,M^2\big)\,\hat{\theta}\Big(\frac{m^2}{y\,(a_C-z)M^2}\Big)\,\hat{\theta}(y-b_B)\,\hat{\theta}(z-b_C) \\ & \times\;\frac{1}{y\,(a_C-z)M^2} \end{aligned} \tag{5.46}$$

Before combining I_{x+} and I_{x-} into a single expression, we comment on the equivalence of some of the step functions involved: In order for $\hat{\theta}\Big(\frac{m^2}{a_B\,z\,M^2}\Big)$ to be non-zero we must have

$$0 \;\leq\; \frac{m^2}{a_B\,z\,M^2} \;\leq\; 1 \tag{5.47}$$

Keeping in mind that m^2 and all constant parameters are positive, this reduces to the constraint

$$m^2 \;\leq\; a_B\,z\,M^2 \tag{5.48}$$

which can be expressed by the step function $\theta\big(a_B\, z\, M^2 - m^2\big)$. A similar equivalence relates $\hat{\theta}\Big(\frac{m^2}{y\,(a_C - z)M^2}\Big)$ to $\theta\big(y\,(a_C - z)M^2 - m^2\big)$. Performing the substitutions

$$\begin{aligned} \hat{\theta}\left(\frac{m^2}{a_B\, z\, M^2}\right) \;&\Rightarrow\; \theta\big(a_B\, z\, M^2 - m^2\big) \\ \hat{\theta}\left(\frac{m^2}{y\,(a_C - z)M^2}\right) \;&\Rightarrow\; \theta\big(y\,(a_C - z)M^2 - m^2\big) \end{aligned}$$

in (5.45) and (5.46) we note that the first terms in the two equations become identical. We can now write out the final result of the x integration:

$$\begin{aligned} \frac{1}{\Gamma}\frac{\mathrm{d}^3\Gamma}{\mathrm{d}y\,\mathrm{d}z\,\mathrm{d}m^2} \;&=\; I_{x+} \;+\; I_{x-} \\ &= \;\; \theta\big(y\,(a_C - z)M^2 - m^2\big)\;\theta\big(a_B\, z\, M^2 - m^2\big) \\ &\quad\;\times\; \hat{\theta}(y - b_B)\;\hat{\theta}(z - b_C)\;\frac{2m^2}{a_B\, y\, z\,(a_C - z)M^4} \\ &\quad+\; \theta\big(m^2 - y\,(a_C - z)M^2\big)\;\theta\big(a_B\, z\, M^2 - m^2\big) \\ &\quad\;\times\; \hat{\theta}(y - b_B)\;\hat{\theta}(z - b_C)\;\frac{1}{a_B\, z\, M^2} \\ &\quad+\; \theta\big(y\,(a_C - z)M^2 - m^2\big)\;\theta\big(m^2 - a_B\, z\, M^2\big) \\ &\quad\;\times\; \hat{\theta}(y - b_B)\;\hat{\theta}(z - b_C)\;\frac{1}{y\,(a_C - z)M^2} \end{aligned} \tag{5.49}$$

In performing the integration over x the differential decay rate split into three terms, each with its own set of step functions that determine for what ranges of y, z, and m^2 the term is non-vanishing. This general pattern repeats as we integrate over y and z. It turns out the final expression for $\mathrm{d}\Gamma/\,\mathrm{d}m^2$ consists of 28 terms in total, where each term comes with a set of step functions limiting it to a certain range of m^2. Due to this large number of terms and the fact that all derivations follow a similar pattern, we will in the following only give a detailed derivation of the first few terms. The complete result with all terms included will then be discussed at the end.

We continue by integrating (5.49) over y. This can be expressed as

$$\frac{1}{\Gamma}\frac{\mathrm{d}^2\Gamma}{\mathrm{d}z\,\mathrm{d}m^2} \;=\; I_A \;+\; I_B \;+\; I_C \tag{5.50}$$

where I_A is the y integral of the first term of (5.49)

$$\begin{aligned} I_A \;=\; & \theta\big(a_B\, z\, M^2 - m^2\big)\; \hat{\theta}(z - b_C) \\ & \times \int_{y_1}^{y_2} \theta\big(y\,(a_C - z)M^2 - m^2\big)\; \hat{\theta}(y - b_B)\; \frac{2m^2}{a_B\, y\, z\,(a_C - z)M^4}\; \mathrm{d}y \end{aligned} \tag{5.51}$$

and I_B and I_C are similar integrals with the second and third term of (5.49) as their respective integrands. From the two y-depending step functions we see that the following constraints must be satisfied for I_A to be non-zero:

$$b_B \;<\; y \;<\; b_B + 1 \tag{5.52}$$

$$\frac{m^2}{(a_C - z)M^2} \;<\; y \tag{5.53}$$

These constraints also imply that

$$m^2 \;<\; (a_C - z)(b_B + 1)M^2 \tag{5.54}$$

As for the integration over x this leaves us with two sets of integration limits:

$$\begin{aligned} y_1 \;&=\; \max\left\{b_B\;,\; \frac{m^2}{(a_C - z)M^2}\right\} \\ y_2 \;&=\; b_B + 1 \end{aligned} \tag{5.55}$$

Analogously to (5.43) for I_{x+}, we can now express I_A as

$$\begin{aligned} I_A \;=\; & \theta\big((a_C - z)\,(b_B + 1)M^2 - m^2\big)\; \theta\big((a_C - z)\, b_B\, M^2 - m^2\big) \\ & \times \int_{b_B}^{b_B+1} g\left(y, z, m^2\right)\; \mathrm{d}y \\ & + \;\theta\big((a_C - z)\,(b_B + 1)M^2 - m^2\big)\; \theta\big(m^2 - (a_C - z)\, b_B\, M^2\big) \\ & \times \int_{\frac{m^2}{(a_C - z)M^2}}^{b_B+1} g\left(y, z, m^2\right)\; \mathrm{d}y \end{aligned} \tag{5.56}$$

with $g\left(y, z, m^2\right)$ given by

$$g\left(y, z, m^2\right) \;=\; \theta\big(a_B\, z\, M^2 - m^2\big)\, \hat{\theta}(z - b_C)\, \frac{2m^2}{a_B\, y\, z\,(a_C - z)M^4} \tag{5.57}$$

In each term of (5.56) two new step functions have been introduced to enforce the additional constraints on z and m^2 coming from (5.54) and the integration limits. Looking at the first term we see that the step function $\theta\big((a_C - z)\,(b_B + 1)M^2 - m^2\big)$ is redundant due to the stronger constraint of the second step function. Nevertheless we include both step functions in what follows as this will illustrate the origin of some restrictions on m^2 that are important for the final terms not derived in detail here. On performing the integration over y we can write

$$I_A \;=\; A_1(z, m^2) \;+\; A_2(z, m^2) \tag{5.58}$$

where A_1 and A_2 correspond to the first and second term of (5.56), respectively. As integrating $g\left(y, z, m^2\right)$ over y only gives a logarithmic factor, A_1 is given by

$$\begin{aligned} A_1(z, m^2) \;\;=\;\; & \theta\big((a_C - z)\,(b_B + 1)M^2 - m^2\big)\;\theta\big((a_C - z)\,b_B\,M^2 - m^2\big) \\ & \times \theta\big(a_B\,z\,M^2 - m^2\big)\;\hat{\theta}(z - b_C) \\ & \times \frac{2m^2}{a_B\,z\,(a_C - z)M^4}\;\ln\!\left(\frac{b_B + 1}{b_B}\right) \end{aligned} \tag{5.59}$$

In the following we will derive all the final terms originating from $A_1(z, m^2)$, while terms from $A_2(z, m^2)$ as well as from I_B and I_C are left out.

We are now left with the task of integrating $A_1(z, m^2)$ over z. From the four step functions in (5.59) we find that z must satisfy

$$b_C \;<\; z \;<\; b_C + 1 \tag{5.60}$$

$$z \;<\; a_C - \frac{m^2}{b_B\,M^2} \tag{5.61}$$

$$\frac{m^2}{a_B\,M^2} \;<\; z \tag{5.62}$$

$$z \;<\; a_C - \frac{m^2}{(b_B + 1)M^2} \tag{5.63}$$

We note that the constraint in (5.63) will have no impact as (5.61) obviously is more restrictive. Satisfying (5.60) – (5.63) all at once implies that the following relations

must hold:

$$m^2 \;<\; a_B\,(b_C+1)M^2 \tag{5.64}$$

$$m^2 \;<\; (a_C-b_C)\,(b_B+1)M^2 \tag{5.65}$$

$$m^2 \;<\; (a_C-b_C)\,b_B\,M^2 \tag{5.66}$$

$$m^2 \;<\; \frac{a_B\,a_C\,(b_B+1)}{a_B+(b_B+1)}\,M^2 \tag{5.67}$$

$$m^2 \;<\; \frac{a_B\,a_C\,b_B}{a_B+b_B}\,M^2 \tag{5.68}$$

Thus, the final terms being derived here will contribute only to the lower end of the invariant mass distribution. Inequalities (5.65) and (5.67) originate from the redundant step function in (5.56) and are clearly rendered unnecessary by the more restrictive constraints (5.66) and (5.68). However, for final terms derived from $A_2(z,m^2)$, I_B and I_C the constraints (5.65) and (5.67) come about in the same way as above but will in these cases put important restrictions on the allowed invariant mass values. The requirements of (5.60), (5.61) and (5.62) leaves us with four possible sets of integration limits, given by

$$\begin{aligned} z_1 \;&=\; \max\left\{b_C\;,\;\frac{m^2}{a_B\,M^2}\right\} \\ z_2 \;&=\; \min\left\{b_C+1\;,\;a_C-\frac{m^2}{b_B\,M^2}\right\} \end{aligned} \tag{5.69}$$

The integration of $A_1(z,m^2)$ over z can thus be expressed as

$$\begin{aligned} &\int_0^\infty A_1(z,m^2)\;\mathrm{d}z \\ &\quad= \quad \theta\Big(a_B\,(b_C+1)M^2-m^2\Big)\;\theta\Big((a_C-b_C)\,b_B\,M^2-m^2\Big)\;\theta\left(\frac{a_B\,a_C\,b_B}{a_B+b_B}-m^2\right) \\ &\qquad\times\Bigg\{\quad \theta(\alpha)\;\theta(\beta)\int_{b_C}^{b_C+1} h\left(z,m^2\right)\,\mathrm{d}z \;\;+\;\; \theta(\alpha)\;\theta(-\beta)\int_{b_C}^{a_C-\frac{m^2}{b_B\,M^2}} h\left(z,m^2\right)\,\mathrm{d}z \\ &\qquad\quad+\theta(-\alpha)\;\theta(\beta)\int_{\frac{m^2}{a_B\,M^2}}^{b_C+1} h\left(z,m^2\right)\,\mathrm{d}z \;\;+\;\; \theta(-\alpha)\;\theta(-\beta)\int_{\frac{m^2}{a_B\,M^2}}^{a_C-\frac{m^2}{b_B\,M^2}} h\left(z,m^2\right)\,\mathrm{d}z \quad\Bigg\} \end{aligned} \tag{5.70}$$

where the integrand $h\left(z, m^2\right)$ and the step functions $\theta(\alpha)$, $\theta(\beta)$ are given by

$$h\left(z, m^2\right) = \frac{2m^2}{a_B\, z\,(a_C - z) M^4} \ln\!\left(\frac{b_B + 1}{b_B}\right) \tag{5.71}$$

$$\theta(\alpha) = \theta\Big(a_B\, b_C\, M^2 - m^2\Big) \tag{5.72}$$

$$\theta(\beta) = \theta\Big(\big(a_C - (b_C + 1)\big)\, b_B\, M^2 - m^2\Big) \tag{5.73}$$

The first three step functions of (5.70) enforce the constraints from (5.64), (5.66) and (5.68) common for all terms derived from $A_1(z, m^2)$. As the integration of $h\left(z, m^2\right)$ has the general solution

$$\int_{z_1}^{z_2} h\left(z, m^2\right)\, \mathrm{d}z = \frac{2m^2}{a_B\, a_C\, M^4} \ln\!\left(\frac{b_B + 1}{b_B}\right) \ln\!\left(\frac{z_2\,(a_C - z_1)}{z_1\,(a_C - z_2)}\right) \tag{5.74}$$

writing out the four terms of (5.70) is just a matter of substituting the correct integration limits. Referring to the these terms as $A_{11}\left(m^2\right)$, $A_{12}\left(m^2\right)$, $A_{13}\left(m^2\right)$ and $A_{14}\left(m^2\right)$, we have found that the four first terms of $(1/\Gamma)(\,\mathrm{d}\Gamma/\,\mathrm{d}m^2)$ are:

$$A_{11}(m^2) = \frac{2m^2}{a_B\, a_C\, M^4} \ln\!\left(\frac{b_B + 1}{b_B}\right) \ln\!\left(\frac{(b_C + 1)\,(a_C - b_C)}{b_C\ (a_C - (b_C + 1))}\right)$$

$$\text{for} \begin{cases} m^2 < a_B\, b_C\, M^2 \\ m^2 < \big(a_C - (b_C + 1)\big)\, b_B\, M^2 \\ m^2 < \dfrac{a_B\, a_C\, b_B}{a_B + b_B}\, M^2 \end{cases}$$

$$A_{12}(m^2) = \frac{2m^2}{a_B\, a_C\, M^4} \ln\!\left(\frac{b_B + 1}{b_B}\right) \ln\!\left(\frac{(a_C\, b_B\, M^2 - m^2)\,(a_C - b_C)}{b_C\, m^2}\right)$$

$$\text{for} \begin{cases} m^2 < a_B\, b_C\, M^2 \\ m^2 > \big(a_C - (b_C + 1)\big)\, b_B\, M^2 \\ m^2 < (a_C - b_C)\, b_B\, M^2 \\ m^2 < \dfrac{a_B\, a_C\, b_B}{a_B + b_B}\, M^2 \end{cases}$$

$$A_{13}(m^2) \;=\; \frac{2m^2}{a_B\,a_C\,M^4}\,\ln\!\left(\frac{b_B+1}{b_B}\right)\ln\!\left(\frac{(b_C+1)\,(a_B\,a_C\,M^2-m^2)}{(a_C-(b_C+1))\,m^2}\right)$$

$$\text{for}\;\begin{cases} m^2 > a_B\,b_C\,M^2 \\ m^2 < (a_C-(b_C+1))\,b_B\,M^2 \\ m^2 < a_B\,(b_C+1)M^2 \\ m^2 < \dfrac{a_B\,a_C\,b_B}{a_B+b_B}\,M^2 \end{cases}$$

$$A_{14}(m^2) \;=\; \frac{2m^2}{a_B\,a_C\,M^4}\,\ln\!\left(\frac{b_B+1}{b_B}\right)\ln\!\left(\frac{(a_C\,b_B\,M^2-m^2)\,(a_B\,a_C\,M^2-m^2)}{m^4}\right)$$

$$\text{for}\;\begin{cases} m^2 > a_B\,b_C\,M^2 \\ m^2 > (a_C-(b_C+1))\,b_B\,M^2 \\ m^2 < a_B\,(b_C+1)M^2 \\ m^2 < (a_C-b_C)\,b_B\,M^2 \\ m^2 < \frac{a_B\,a_C\,b_B}{a_B+b_B}\,M^2 \end{cases}$$

For clarity we have replaced the step functions with inequalities, keeping in mind that a term vanishes unless all constraints on m^2 are satisfied.

5.3 Results and discussion

Summarizing the derivation so far we have found that

$$\frac{1}{\Gamma}\frac{\mathrm{d}\Gamma}{\mathrm{d}m^2} \;=\; A_{11} \;+\; A_{12} \;+\; A_{13} \;+\; A_{14} \;+\; (\ldots) \tag{5.75}$$

where $(\ldots)$ denotes the 24 terms originating from $A_2\left(z,m^2\right)$, I_B and I_C. A complete list of all terms is given at the end of this derivation. Studying the constraints on m^2 for all these terms, we find that the functional form of $\mathrm{d}\Gamma/\,\mathrm{d}m^2$ changes at the following eight points (normalised to M^2):

$$\begin{aligned}\frac{m^2}{M^2} \;=\; \Bigg\{ & a_B b_C \;,\; (a_C-(b_C+1))\,b_B \;,\; (a_C-(b_C+1))\,(b_B+1) \;, \\ & \frac{a_B\,a_C\,b_B}{a_B+b_B} \;,\; \frac{a_B\,a_C\,(b_B+1)}{a_B+(b_B+1)} \;,\; (a_C-b_C)b_B \;, \\ & (a_C-b_C)(b_B+1) \;,\; a_B(b_C+1) \Bigg\}\end{aligned} \tag{5.76}$$

Apart from some obvious relations like $a_B\, b_C < a_B\, (b_C + 1)$, the order in which these points appear along the m^2-axis depends on the relative sizes of the parameters a_B, a_C, b_B and b_C. As can be seen from (5.14) these parameters are completely determined by the masses m_A, m_B, m_C and m_τ. By varying m_B within the kinematically allowed range $(m_A + m_\tau\,,\, m_C - m_\tau)$ we find that the 'split points' of (5.76) can be arranged in six different orders. We refer to these orders as 'mass scenarios' one to six, covering the range of allowed m_B values from lowest to highest, respectively. The correct order of split points for each scenario is written out in Tables 5.1 and 5.2.

Due to m_τ being very small compared to any viable choice of values for m_A, m_B and m_C, mass scenarios 1, 2 and 3 cover only a very narrow range of m_B values close to the kinematical limit $m_B = m_A + m_\tau$. In Fig. 5.2 we illustrate this behaviour by taking $m_C = 180$ GeV and $m_A = 97$ GeV, and plot the eight split points as functions of m_B in the range $(m_A + m_\tau\,,\, m_C - m_\tau)$. Vertical lines mark the borders between 'neighbouring' mass scenarios. In Fig. 5.2(a), where the entire allowed m_B range is shown, only the four largest split points are clearly visible. In order to illustrate the evolution of the smaller split points Fig. 5.2(b) depicts the region close to $m_B = m_A + m_\tau$. For the chosen mass values $m_C = 180$ GeV, $m_A = 97$ GeV and $m_\tau = 1.78$ GeV the m_B ranges of the different mass scenarios are:

$$\begin{aligned}
&\text{Scenario 1:} \quad m_B \in (\ 98.7800\,,\ 98.7801\ ) \ \text{(GeV)} \\
&\text{Scenario 2:} \quad m_B \in (\ 98.7801\,,\ 99.1073\ ) \ \text{(GeV)} \\
&\text{Scenario 3:} \quad m_B \in (\ 99.1073\,,\ 99.1128\ ) \ \text{(GeV)} \\
&\text{Scenario 4:} \quad m_B \in (\ 99.1128\,, 132.1483\ ) \ \text{(GeV)} \\
&\text{Scenario 5:} \quad m_B \in (\ 132.1483\,, 144.5729\ ) \ \text{(GeV)} \\
&\text{Scenario 6:} \quad m_B \in (\ 144.5729\,, 178.2200\ ) \ \text{(GeV)}
\end{aligned}$$

In Tables 5.3 – 5.8 the final results for $(1/\Gamma)(\,\mathrm{d}\Gamma/\,\mathrm{d}m^2)$ are given for the six mass scenarios. As can been seen in these tables, for a given scenario about half of the 28 terms do not contribute. (In fact, due to the constraints set by the assumed mass hierarchy and on-shell kinematics, the terms A_{24}, B_{11}, B_{22}, C_{11} and A_{24} vanish everywhere for all six mass scenarios.)

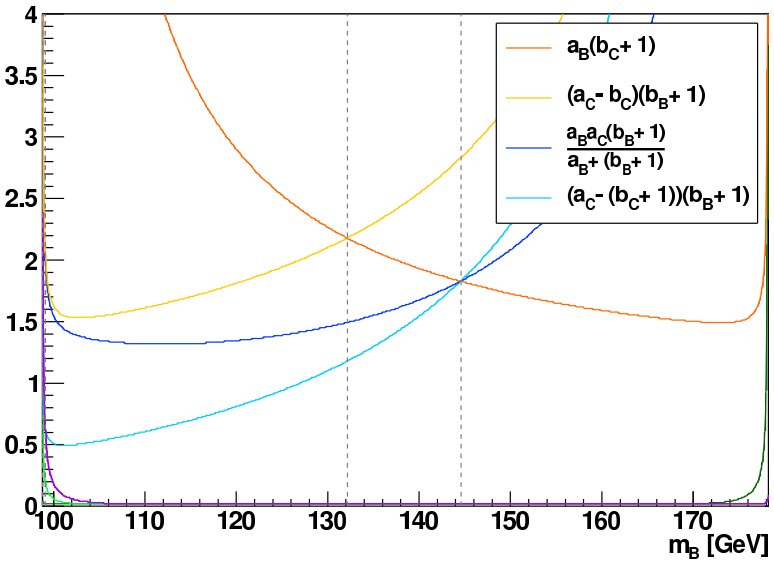

(a) The larger m^2_{high} split points shown for the entire allowed m_B range.

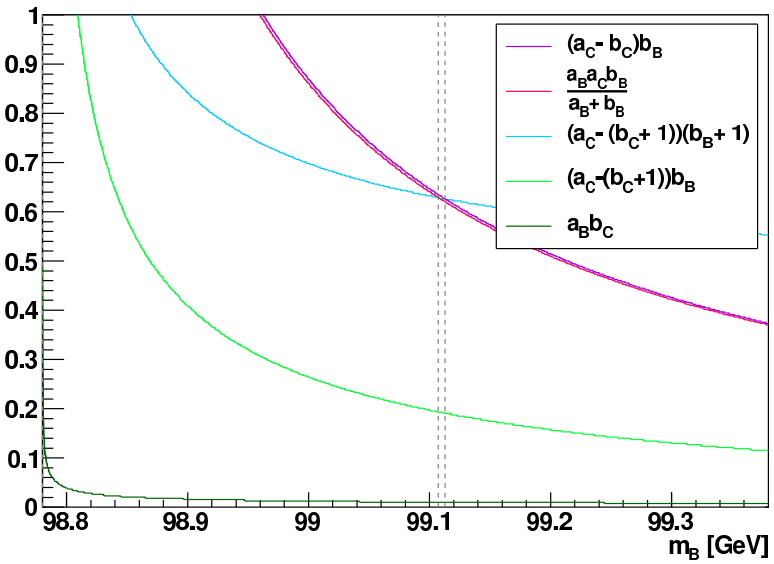

(b) The smaller m^2_{high} split points shown near the lower limit $m_B = m_A + m_\tau = 98.78$ GeV. The range of scenario 1 is too narrow to be seen in this figure.

Figure 5.2: The m^2_{high} split points as functions of m_B, with $m_C = 180$, $m_A = 97$ and $m_\tau = 1.78$ (GeV)

Table 5.1: Order of split points for mass scenarios 1 – 3 (normalised to M^2)

scenario 1	scenario 2	scenario 3
$a_B b_C$	$a_B b_C$	$a_B b_C$
$(a_C - (b_C + 1))\, b_B$	$(a_C - (b_C + 1))\, b_B$	$(a_C - (b_C + 1))\, b_B$
$(a_C - (b_C + 1))\, (b_B + 1)$	$(a_C - (b_C + 1))\, (b_B + 1)$	$\frac{a_B\, a_C\, b_B}{a_B + b_B}$
$\frac{a_B\, a_C\, b_B}{a_B + b_B}$	$\frac{a_B\, a_C\, b_B}{a_B + b_B}$	$(a_C - (b_C + 1))\, (b_B + 1)$
$\frac{a_B\, a_C\, (b_B+1)}{a_B + (b_B+1)}$	$(a_C - b_C) b_B$	$(a_C - b_C) b_B$
$(a_C - b_C) b_B$	$\frac{a_B\, a_C\, (b_B+1)}{a_B + (b_B+1)}$	$\frac{a_B\, a_C\, (b_B+1)}{a_B + (b_B+1)}$
$(a_C - b_C)(b_B + 1)$	$(a_C - b_C)(b_B + 1)$	$(a_C - b_C)(b_B + 1)$
$a_B(b_C + 1)$	$a_B(b_C + 1)$	$a_B(b_C + 1)$

Table 5.2: Order of split points for mass scenarios 4 – 6 (normalised to M^2)

scenario 4	scenario 5	scenario 6
$a_B b_C$	$(a_C - (b_C + 1))\, b_B$	$(a_C - (b_C + 1))\, b_B$
$(a_C - (b_C + 1))\, b_B$	$a_B b_C$	$(a_C - b_C) b_B$
$\frac{a_B\, a_C\, b_B}{a_B + b_B}$	$\frac{a_B\, a_C\, b_B}{a_B + b_B}$	$\frac{a_B\, a_C\, b_B}{a_B + b_B}$
$(a_C - b_C) b_B$	$(a_C - b_C) b_B$	$a_B b_C$
$(a_C - (b_C + 1))\, (b_B + 1)$	$(a_C - (b_C + 1))\, (b_B + 1)$	$a_B(b_C + 1)$
$\frac{a_B\, a_C\, (b_B+1)}{a_B + (b_B+1)}$	$\frac{a_B\, a_C\, (b_B+1)}{a_B + (b_B+1)}$	$\frac{a_B\, a_C\, (b_B+1)}{a_B + (b_B+1)}$
$(a_C - b_C)(b_B + 1)$	$a_B(b_C + 1)$	$(a_C - (b_C + 1))\, (b_B + 1)$
$a_B(b_C + 1)$	$(a_C - b_C)(b_B + 1)$	$(a_C - b_C)(b_B + 1)$

In Figure 5.3 the resulting distribution is plotted (black) along with the corresponding distribution for a dilepton cascade (grey) [24]. For Figures 5.3(a) – 5.3(e) the values of m_A, m_C and m_D are kept fixed while different m_B values are chosen to sample mass scenarios 4, 5 and 6. In Fig. 5.3(f) a set of masses with both $(m_C - m_B)$ and $(m_B - m_A)$ close to m_τ is chosen. While the values of m_A, m_B and m_C determine the shape of the distribution, the value of m_D has no other effect than setting the overall energy scale through the factor $(m_D^2 - m_C^2)$ in the definition of M^2. As the tables give the expressions for $\mathrm{d}\Gamma/\,\mathrm{d}m^2_{\text{high}}$ while the plots depict $\mathrm{d}\Gamma/\,\mathrm{d}m_{\text{high}}$, we recall that the two distributions are related through

$$\frac{1}{\Gamma}\frac{\mathrm{d}\Gamma}{\mathrm{d}m_{\text{high}}} \;=\; 2\,m_{\text{high}}\,\frac{1}{\Gamma}\frac{\mathrm{d}\Gamma}{\mathrm{d}m^2_{\text{high}}} \tag{5.77}$$

As for the m_{ab} distribution, the escaping neutrinos leave the m_{high} distribution rounded and shifted towards lower invariant masses compared to the dilepton distribution. The shape of the m_{high} distribution can be further explained by comparison with the underlying m_{ac} and m_{bc} distributions (Fig. 5.4). As m_{high} is defined to prefer high invariant masses, whichever of the two distributions $\mathrm{d}\Gamma/\,\mathrm{d}m_{ac}$ and $\mathrm{d}\Gamma/\,\mathrm{d}m_{bc}$ is larger at high mass values will also have the greatest impact on the shape of $\mathrm{d}\Gamma/\,\mathrm{d}m_{\text{high}}$. For invariant masses above the endpoint of either $\mathrm{d}\Gamma/\,\mathrm{d}m_{ac}$ or $\mathrm{d}\Gamma/\,\mathrm{d}m_{bc}$, the m_{high} distribution will by definition be identical to the remaining one. (Analytical expressions for the m_{ac} and m_{bc} distributions are given in Appendix A.)

We also note the appearance of extended 'feet' near the endpoints of the distributions in Figs. 5.3(c), 5.3(d) and 5.3(e) (barely visible). The foot appears as m_B enters mass scenario 5. The length of the foot increases with higher m_B values, before decreasing again once m_B is within the range of mass scenario 6. This behaviour can be understood from Fig. 5.2(a) showing the evolution of the upper split points as m_B is increased. From the lower limit of scenario 5 and upwards, the length of the distribution foot is determined by the difference between the endpoint $(a_C - b_C)(b_B + 1)$ and the closest split point. From Fig. 5.4 it can be seen that the foot is a feature of the m_{ac} distribution.

Below we list all the 28 terms resulting from the integration of (5.36) over x, y and z. The terms A_{11}, A_{12}, A_{13} and A_{14} have already been given, and the terms A_{24}, B_{11}, B_{22}, C_{11} and C_{24} do not contribute to the m_{high} distribution in any of the six mass scenarios, yet for completeness they are all included here. We recall that the simplified

notation $m_{\rm high} \equiv m$ is used, and note that $\mathrm{Li}_2(x)$ is the dilogarithm function, defined for real arguments x by

$$\mathrm{Li}_2(x) \;\equiv\; \sum_{n=1}^{\infty} \frac{x^n}{n^2} \;=\; -\int_0^x \frac{\ln(1-u)}{u}\,\mathrm{d}u\,, \qquad |x| \;\leq\; 1 \tag{5.78}$$

Table 5.3: $\frac{1}{\Gamma}\frac{\mathrm{d}\Gamma}{\mathrm{d}m^2_{\mathrm{high}}}$ for mass scenario 1

$\frac{m^2_{\mathrm{high}}}{M^2}$ range			$\frac{1}{\mathrm{d}\Gamma}\frac{\mathrm{d}\Gamma}{\mathrm{d}m^2_{\mathrm{high}}} =$
0	$<\frac{m^2_{\mathrm{high}}}{M^2}<$	$a_B b_C$	A_{11}
$a_B b_C$	$<\frac{m^2_{\mathrm{high}}}{M^2}<$	$(a_C-(b_C+1))\,b_B$	$A_{13}+C_{12}$
$(a_C-(b_C+1))\,b_B$	$<\frac{m^2_{\mathrm{high}}}{M^2}<$	$(a_C-(b_C+1))\,(b_B+1)$	$A_{14}+A_{23}+B_{25}+C_{12}$
$(a_C-(b_C+1))\,(b_B+1)$	$<\frac{m^2_{\mathrm{high}}}{M^2}<$	$\frac{a_B\,a_C\,b_B}{a_B+b_B}$	$A_{14}+A_{26}+B_{13}+B_{26}+C_{12}$
$\frac{a_B\,a_C\,b_B}{a_B+b_B}$	$<\frac{m^2_{\mathrm{high}}}{M^2}<$	$\frac{a_B\,a_C\,(b_B+1)}{a_B+(b_B+1)}$	$A_{25}+B_{13}+B_{24}+C_{13}+C_{25}$
$\frac{a_B\,a_C\,(b_B+1)}{a_B+(b_B+1)}$	$<\frac{m^2_{\mathrm{high}}}{M^2}<$	$(a_C-b_C)b_B$	$B_{12}+C_{13}+C_{26}$
$(a_C-b_C)b_B$	$<\frac{m^2_{\mathrm{high}}}{M^2}<$	$(a_C-b_C)(b_B+1)$	$B_{12}+C_{23}$
$(a_C-b_C)(b_B+1)$	$<\frac{m^2_{\mathrm{high}}}{M^2}<$	$a_B(b_C+1)$	B_{12}

Table 5.4: $\frac{1}{\Gamma}\frac{\mathrm{d}\Gamma}{\mathrm{d}m^2_{\mathrm{high}}}$ for mass scenario 2

$\frac{m^2_{\mathrm{high}}}{M^2}$ range			$\frac{1}{\mathrm{d}\Gamma}\frac{\mathrm{d}\Gamma}{\mathrm{d}m^2_{\mathrm{high}}} =$
0	$<\frac{m^2_{\mathrm{high}}}{M^2}<$	$a_B b_C$	A_{11}
$a_B b_C$	$<\frac{m^2_{\mathrm{high}}}{M^2}<$	$(a_C-(b_C+1))\,b_B$	$A_{13}+C_{12}$
$(a_C-(b_C+1))\,b_B$	$<\frac{m^2_{\mathrm{high}}}{M^2}<$	$(a_C-(b_C+1))\,(b_B+1)$	$A_{14}+A_{23}+B_{25}+C_{12}$
$(a_C-(b_C+1))\,(b_B+1)$	$<\frac{m^2_{\mathrm{high}}}{M^2}<$	$\frac{a_B\,a_C\,b_B}{a_B+b_B}$	$A_{14}+A_{26}+B_{13}+B_{26}+C_{12}$
$\frac{a_B\,a_C\,b_B}{a_B+b_B}$	$<\frac{m^2_{\mathrm{high}}}{M^2}<$	$(a_C-b_C)b_B$	$A_{25}+B_{13}+B_{24}+C_{13}+C_{25}$
$(a_C-b_C)b_B$	$<\frac{m^2_{\mathrm{high}}}{M^2}<$	$\frac{a_B\,a_C\,(b_B+1)}{a_B+(b_B+1)}$	$A_{25}+B_{13}+B_{24}+C_{22}$
$\frac{a_B\,a_C\,(b_B+1)}{a_B+(b_B+1)}$	$<\frac{m^2_{\mathrm{high}}}{M^2}<$	$(a_C-b_C)(b_B+1)$	$B_{12}+C_{23}$
$(a_C-b_C)(b_B+1)$	$<\frac{m^2_{\mathrm{high}}}{M^2}<$	$a_B(b_C+1)$	B_{12}

Table 5.5: $\frac{1}{\Gamma}\frac{\mathrm{d}\Gamma}{\mathrm{d}m^2_{\mathrm{high}}}$ for mass scenario 3

$\frac{m^2_{\mathrm{high}}}{M^2}$ range			$\frac{1}{\mathrm{d}\Gamma}\frac{\mathrm{d}\Gamma}{\mathrm{d}m^2_{\mathrm{high}}} =$
0	$< \frac{m^2_{\mathrm{high}}}{M^2} <$	$a_B b_C$	A_{11}
$a_B b_C$	$< \frac{m^2_{\mathrm{high}}}{M^2} <$	$(a_C - (b_C+1))\, b_B$	$A_{13} + C_{12}$
$(a_C - (b_C+1))\, b_B$	$< \frac{m^2_{\mathrm{high}}}{M^2} <$	$\frac{a_B\, a_C\, b_B}{a_B + b_B}$	$A_{14} + A_{23} + B_{25} + C_{12}$
$\frac{a_B\, a_C\, b_B}{a_B + b_B}$	$< \frac{m^2_{\mathrm{high}}}{M^2} <$	$(a_C - (b_C+1))\,(b_B+1)$	$A_{22} + B_{23} + C_{13} + C_{25}$
$(a_C - (b_C+1))\,(b_B+1)$	$< \frac{m^2_{\mathrm{high}}}{M^2} <$	$(a_C - b_C) b_B$	$A_{25} + B_{13} + B_{24} + C_{13} + C_{25}$
$(a_C - b_C) b_B$	$< \frac{m^2_{\mathrm{high}}}{M^2} <$	$\frac{a_B\, a_C\, (b_B+1)}{a_B + (b_B+1)}$	$A_{25} + B_{13} + B_{24} + C_{22}$
$\frac{a_B\, a_C\, (b_B+1)}{a_B + (b_B+1)}$	$< \frac{m^2_{\mathrm{high}}}{M^2} <$	$(a_C - b_C)(b_B+1)$	$B_{12} + C_{23}$
$(a_C - b_C)(b_B+1)$	$< \frac{m^2_{\mathrm{high}}}{M^2} <$	$a_B(b_C+1)$	B_{12}

Table 5.6: $\frac{1}{\Gamma}\frac{\mathrm{d}\Gamma}{\mathrm{d}m^2_{\mathrm{high}}}$ for mass scenario 4

$\frac{m^2_{\mathrm{high}}}{M^2}$ range			$\frac{1}{\mathrm{d}\Gamma}\frac{\mathrm{d}\Gamma}{\mathrm{d}m^2_{\mathrm{high}}} =$
0	$< \frac{m^2_{\mathrm{high}}}{M^2} <$	$a_B b_C$	A_{11}
$a_B b_C$	$< \frac{m^2_{\mathrm{high}}}{M^2} <$	$(a_C - (b_C+1))\, b_B$	$A_{13} + C_{12}$
$(a_C - (b_C+1))\, b_B$	$< \frac{m^2_{\mathrm{high}}}{M^2} <$	$\frac{a_B\, a_C\, b_B}{a_B + b_B}$	$A_{14} + A_{23} + B_{25} + C_{12}$
$\frac{a_B\, a_C\, b_B}{a_B + b_B}$	$< \frac{m^2_{\mathrm{high}}}{M^2} <$	$(a_C - b_C) b_B$	$A_{22} + B_{23} + C_{13} + C_{25}$
$(a_C - b_C) b_B$	$< \frac{m^2_{\mathrm{high}}}{M^2} <$	$(a_C - (b_C+1))\,(b_B+1)$	$A_{22} + B_{23} + C_{22}$
$(a_C - (b_C+1))\,(b_B+1)$	$< \frac{m^2_{\mathrm{high}}}{M^2} <$	$\frac{a_B\, a_C\, (b_B+1)}{a_B + (b_B+1)}$	$A_{25} + B_{13} + B_{24} + C_{22}$
$\frac{a_B\, a_C\, (b_B+1)}{a_B + (b_B+1)}$	$< \frac{m^2_{\mathrm{high}}}{M^2} <$	$(a_C - b_C)(b_B+1)$	$B_{12} + C_{23}$
$(a_C - b_C)(b_B+1)$	$< \frac{m^2_{\mathrm{high}}}{M^2} <$	$a_B(b_C+1)$	B_{12}

Table 5.7: $\frac{1}{\Gamma}\frac{\mathrm{d}\Gamma}{\mathrm{d}m^2_{\mathrm{high}}}$ for mass scenario 5

$\frac{m^2_{\mathrm{high}}}{M^2}$ range			$\frac{1}{\mathrm{d}\Gamma}\frac{\mathrm{d}\Gamma}{\mathrm{d}m^2_{\mathrm{high}}} =$
0	$<\frac{m^2_{\mathrm{high}}}{M^2}<$	$(a_C-(b_C+1))\,b_B$	A_{11}
$(a_C-(b_C+1))\,b_B$	$<\frac{m^2_{\mathrm{high}}}{M^2}<$	$a_B b_C$	$A_{12}+A_{23}+B_{25}$
$a_B b_C$	$<\frac{m^2_{\mathrm{high}}}{M^2}<$	$\frac{a_B\,a_C\,b_B}{a_B+b_B}$	$A_{14}+A_{23}+B_{25}+C_{12}$
$\frac{a_B\,a_C\,b_B}{a_B+b_B}$	$<\frac{m^2_{\mathrm{high}}}{M^2}<$	$(a_C-b_C)b_B$	$A_{22}+B_{23}+C_{13}+C_{25}$
$(a_C-b_C)b_B$	$<\frac{m^2_{\mathrm{high}}}{M^2}<$	$(a_C-(b_C+1))\,(b_B+1)$	$A_{22}+B_{23}+C_{22}$
$(a_C-(b_C+1))\,(b_B+1)$	$<\frac{m^2_{\mathrm{high}}}{M^2}<$	$\frac{a_B\,a_C\,(b_B+1)}{a_B+(b_B+1)}$	$A_{25}+B_{13}+B_{24}+C_{22}$
$\frac{a_B\,a_C\,(b_B+1)}{a_B+(b_B+1)}$	$<\frac{m^2_{\mathrm{high}}}{M^2}<$	$a_B(b_C+1)$	$B_{12}+C_{23}$
$a_B(b_C+1)$	$<\frac{m^2_{\mathrm{high}}}{M^2}<$	$(a_C-b_C)(b_B+1)$	C_{23}

Table 5.8: $\frac{1}{\Gamma}\frac{\mathrm{d}\Gamma}{\mathrm{d}m^2_{\mathrm{high}}}$ for mass scenario 6

$\frac{m^2_{\mathrm{high}}}{M^2}$ range			$\frac{1}{\mathrm{d}\Gamma}\frac{\mathrm{d}\Gamma}{\mathrm{d}m^2_{\mathrm{high}}} =$
0	$<\frac{m^2_{\mathrm{high}}}{M^2}<$	$(a_C-(b_C+1))\,b_B$	A_{11}
$(a_C-(b_C+1))\,b_B$	$<\frac{m^2_{\mathrm{high}}}{M^2}<$	$(a_C-b_C)b_B$	$A_{12}+A_{23}+B_{25}$
$(a_C-b_C)b_B$	$<\frac{m^2_{\mathrm{high}}}{M^2}<$	$\frac{a_B\,a_C\,b_B}{a_B+b_B}$	$A_{21}+B_{21}$
$\frac{a_B\,a_C\,b_B}{a_B+b_B}$	$<\frac{m^2_{\mathrm{high}}}{M^2}<$	$a_B b_C$	$A_{21}+B_{21}$
$a_B b_C$	$<\frac{m^2_{\mathrm{high}}}{M^2}<$	$a_B(b_C+1)$	$A_{22}+B_{23}+C_{22}$
$a_B(b_C+1)$	$<\frac{m^2_{\mathrm{high}}}{M^2}<$	$\frac{a_B\,a_C\,(b_B+1)}{a_B+(b_B+1)}$	C_{21}
$\frac{a_B\,a_C\,(b_B+1)}{a_B+(b_B+1)}$	$<\frac{m^2_{\mathrm{high}}}{M^2}<$	$(a_C-(b_C+1))\,(b_B+1)$	C_{21}
$(a_C-(b_C+1))\,(b_B+1)$	$<\frac{m^2_{\mathrm{high}}}{M^2}<$	$(a_C-b_C)(b_B+1)$	C_{23}

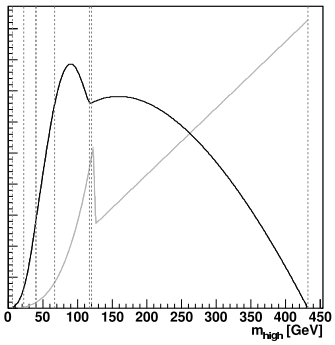

(a) $m_D = 550,\ m_C = 180,$
$m_B = 100,\ m_A = 97$ (GeV)
scenario 4

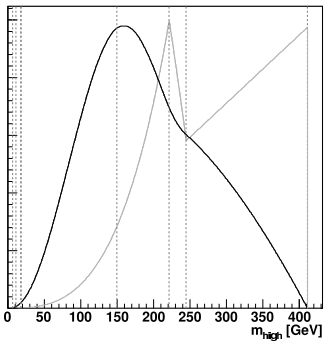

(b) $m_D = 550,\ m_C = 180,$
$m_B = 110,\ m_A = 97$ (GeV)
scenario 4

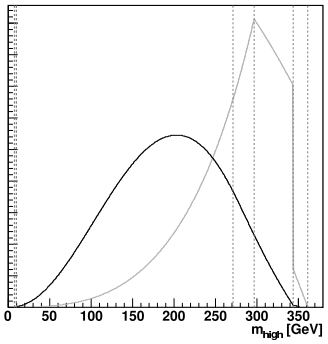

(c) $m_D = 550,\ m_C = 180,$
$m_B = 135,\ m_A = 97$ (GeV)
scenario 5

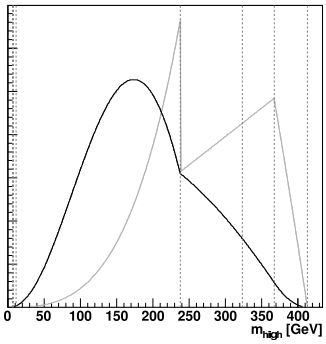

(d) $m_D = 550,\ m_C = 180,$
$m_B = 160,\ m_A = 97$ (GeV)
scenario 6

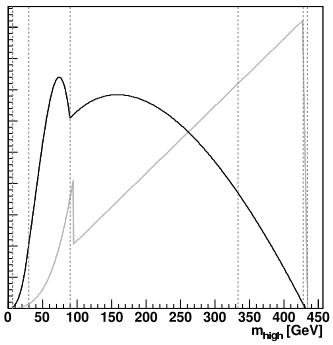

(e) $m_D = 550,\ m_C = 180,$
$m_B = 177,\ m_A = 97$ (GeV)
scenario 6

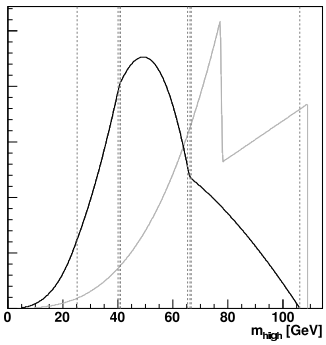

(f) $m_D = 550,\ m_C = 180,$
$m_B = 176,\ m_A = 174$ (GeV)
scenario 4

Figure 5.3: $(1/\Gamma)(\,\mathrm{d}\Gamma/\,\mathrm{d}m_{\mathrm{high}})$ (black) for six different sets of masses. Dotted vertical lines mark the split points where the functional form of the distribution changes. The corresponding distribution for a dilepton cascade is shown in grey.

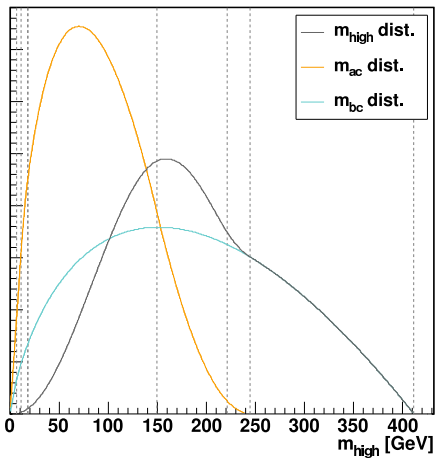

(a) $m_D = 550,\ m_C = 180,\ m_B = 110,$ $m_A = 97$ (GeV), scenario 4

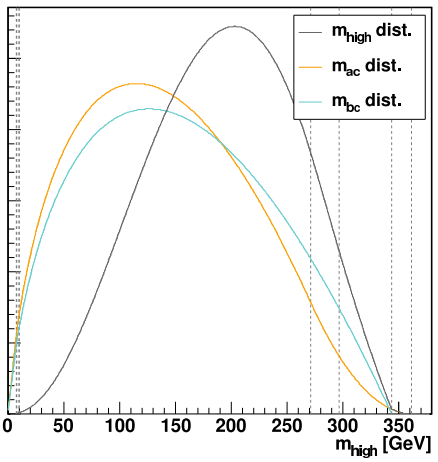

(b) $m_D = 550,\ m_C = 180,\ m_B = 135,$ $m_A = 97$ (GeV), scenario 5

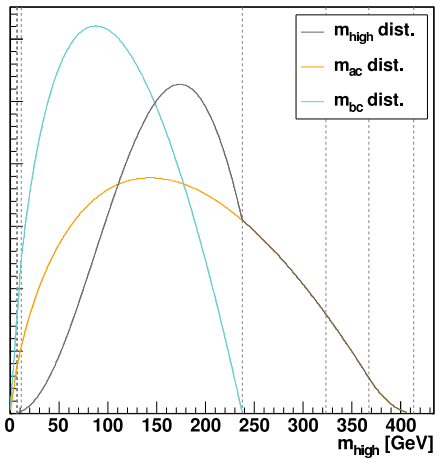

(c) $m_D = 550,\ m_C = 180,\ m_B = 160,$ $m_A = 97$ (GeV), scenario 6

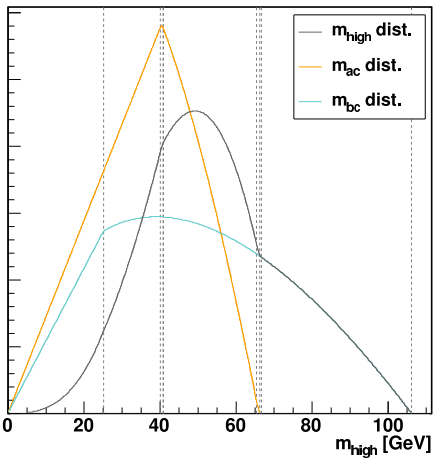

(d) $m_D = 550,\ m_C = 180,\ m_B = 176,$ $m_A = 174$ (GeV), scenario 4

Figure 5.4: $(1/\Gamma)(\,\mathrm{d}\Gamma/\,\mathrm{d}m_{\mathrm{high}})$ (dark grey) compared to $(1/\Gamma)(\,\mathrm{d}\Gamma/\,\mathrm{d}m_{ac})$ (orange) and $(1/\Gamma)(\,\mathrm{d}\Gamma/\,\mathrm{d}m_{bc})$ (blue) for four different sets of masses.

$$A_{11}(m^2) = \frac{2m^2}{a_B\, a_C\, M^4} \ln\!\left(\frac{b_B+1}{b_B}\right) \ln\!\left(\frac{(b_C+1)\,(a_C-b_C)}{b_C\,(a_C-(b_C+1))}\right)$$

$$\text{for} \begin{cases} m^2 < a_B\, b_C\, M^2 \\ m^2 < (a_C-(b_C+1))\, b_B\, M^2 \\ m^2 < \frac{a_B\, a_C\, b_B}{a_B+b_B}\, M^2 \end{cases}$$

$$A_{12}(m^2) = \frac{2m^2}{a_B\, a_C\, M^4} \ln\!\left(\frac{b_B+1}{b_B}\right) \ln\!\left(\frac{(a_C\, b_B\, M^2-m^2)\,(a_C-b_C)}{b_C\, m^2}\right)$$

$$\text{for} \begin{cases} m^2 < a_B\, b_C\, M^2 \\ m^2 > (a_C-(b_C+1))\, b_B\, M^2 \\ m^2 < (a_C-b_C)\, b_B\, M^2 \\ m^2 < \frac{a_B\, a_C\, b_B}{a_B+b_B}\, M^2 \end{cases}$$

$$A_{13}(m^2) = \frac{2m^2}{a_B\, a_C\, M^4} \ln\!\left(\frac{b_B+1}{b_B}\right) \ln\!\left(\frac{(b_C+1)\,(a_B\, a_C\, M^2-m^2)}{(a_C-(b_C+1))\, m^2}\right)$$

$$\text{for} \begin{cases} m^2 > a_B\, b_C\, M^2 \\ m^2 < (a_C-(b_C+1))\, b_B\, M^2 \\ m^2 < a_B\,(b_C+1) M^2 \\ m^2 < \frac{a_B\, a_C\, b_B}{a_B+b_B}\, M^2 \end{cases}$$

$$A_{14}(m^2) = \frac{2m^2}{a_B\, a_C\, M^4} \ln\!\left(\frac{b_B+1}{b_B}\right) \ln\!\left(\frac{(a_C\, b_B\, M^2-m^2)\,(a_B\, a_C\, M^2-m^2)}{m^4}\right)$$

$$\text{for} \begin{cases} m^2 > a_B\, b_C\, M^2 \\ m^2 > (a_C-(b_C+1))\, b_B\, M^2 \\ m^2 < a_B\,(b_C+1) M^2 \\ m^2 < (a_C-b_C)\, b_B\, M^2 \\ m^2 < \frac{a_B\, a_C\, b_B}{a_B+b_B}\, M^2 \end{cases}$$

$$
\begin{aligned}
A_{21}(m^2) \;=\; \frac{2m^2}{a_B\, a_C\, M^4} \Bigg\{ & \;\; \frac{1}{2}\left[\ln\!\left(\frac{(a_C - b_C)\,(b_B+1)M^2}{m^2}\right)\right]^2 \\
& - \frac{1}{2}\left[\ln\!\left(\frac{(a_C - (b_C+1))\,(b_B+1)M^2}{m^2}\right)\right]^2 \\
& + \ln\!\left(\frac{a_C\,(b_B+1)M^2}{m^2}\right)\ln\!\left(\frac{b_C+1}{b_C}\right) \\
& + \mathrm{Li}_2\!\left(\frac{b_C}{a_C}\right) \;-\; \mathrm{Li}_2\!\left(\frac{b_C+1}{a_C}\right) \;\; \Bigg\}
\end{aligned}
$$

$$
\text{for} \begin{cases}
m^2 \;<\; a_B\, b_C\, M^2 \\
m^2 \;>\; (a_C - b_C)\, b_B\, M^2 \\
m^2 \;<\; (a_C - (b_C+1))\,(b_B+1)M^2 \\
m^2 \;<\; (a_C - b_C)\,(b_B+1)M^2 \\
m^2 \;<\; \frac{a_B\, a_C\,(b_B+1)}{a_B + (b_B+1)}\, M^2
\end{cases}
$$

$$
\begin{aligned}
A_{22}(m^2) \;=\; \frac{2m^2}{a_B\, a_C\, M^4} \Bigg\{ & \;\; \frac{1}{2}\left[\ln\!\left(\frac{(a_B\, a_C\, M^2 - m^2)\,(b_B+1)}{a_B\, m^2}\right)\right]^2 \\
& - \frac{1}{2}\left[\ln\!\left(\frac{(a_C - (b_C+1))\,(b_B+1)M^2}{m^2}\right)\right]^2 \\
& + \ln\!\left(\frac{a_C\,(b_B+1)M^2}{m^2}\right)\ln\!\left(\frac{a_B\,(b_C+1)M^2}{m^2}\right) \\
& + \mathrm{Li}_2\!\left(\frac{m^2}{a_B\, a_C\, M^2}\right) \;-\; \mathrm{Li}_2\!\left(\frac{b_C+1}{a_C}\right) \;\; \Bigg\}
\end{aligned}
$$

$$
\text{for} \begin{cases}
m^2 \;>\; a_B\, b_C\, M^2 \\
m^2 \;>\; \frac{a_B\, a_C\, b_B}{a_B + b_B}\, M^2 \\
m^2 \;<\; (a_C - (b_C+1))\,(b_B+1)M^2 \\
m^2 \;<\; (a_C - b_C)\,(b_B+1)M^2 \\
m^2 \;<\; \frac{a_B\, a_C\,(b_B+1)}{a_B + (b_B+1)}\, M^2 \\
m^2 \;<\; a_B\,(b_C+1)M^2 \\
m^2 \;>\; (a_C - (b_C+1))\, b_B\, M^2
\end{cases}
$$

$$
\begin{aligned}
A_{23}(m^2) \;=\; \frac{2m^2}{a_B\, a_C\, M^4} \Bigg\{ \quad & \frac{1}{2}\left[\ln\!\left(\frac{b_B+1}{b_B}\right)\right]^2 \\
& - \frac{1}{2}\left[\ln\!\left(\frac{(a_C-(b_C+1))\,(b_B+1)M^2}{m^2}\right)\right]^2 \\
& + \ln\!\left(\frac{a_C\,(b_B+1)M^2}{m^2}\right)\ln\!\left(\frac{(b_C+1)\,b_B\,M^2}{a_C\,b_B\,M^2-m^2}\right) \\
& + \mathrm{Li}_2\!\left(\frac{a_C\,b_B\,M^2-m^2}{a_C\,b_B\,M^2}\right) \;-\; \mathrm{Li}_2\!\left(\frac{b_C+1}{a_C}\right) \quad \Bigg\}
\end{aligned}
$$

$$
\text{for} \begin{cases}
m^2 \;<\; (a_C-b_C)\,b_B\,M^2 \\
m^2 \;<\; \frac{a_B\,a_C\,b_B}{a_B+b_B}\,M^2 \\
m^2 \;<\; (a_C-(b_C+1))\,(b_B+1)M^2 \\
m^2 \;<\; a_B\,(b_C+1)M^2 \\
m^2 \;>\; (a_C-(b_C+1))\,b_B\,M^2
\end{cases}
$$

$$
\begin{aligned}
A_{24}(m^2) \;=\; \frac{2m^2}{a_B\, a_C\, M^4} \Bigg\{ \quad & \frac{1}{2}\left[\ln\!\left(\frac{(a_C-b_C)\,(b_B+1)M^2)}{m^2}\right)\right]^2 \\
& + \ln\!\left(\frac{a_C\,(b_B+1)M^2}{m^2}\right)\ln\!\left(\frac{a_C\,(b_B+1)M^2-m^2}{b_C\,(b_B+1)M^2}\right) \\
& + \mathrm{Li}_2\!\left(\frac{b_C}{a_C}\right) \;-\; \mathrm{Li}_2\!\left(\frac{a_C\,(b_B+1)M^2-m^2}{a_C\,(b_B+1)M^2}\right) \quad \Bigg\}
\end{aligned}
$$

$$
\text{for} \begin{cases}
m^2 \;<\; a_B\,b_C\,M^2 \\
m^2 \;>\; (a_C-b_C)\,b_B\,M^2 \\
m^2 \;>\; (a_C-(b_C+1))\,(b_B+1)M^2 \\
m^2 \;<\; \frac{a_B\,a_C\,(b_B+1)}{a_B+(b_B+1)}\,M^2 \\
m^2 \;<\; (a_C-b_C)\,(b_B+1)M^2
\end{cases}
$$

$$
\begin{aligned}
A_{25}(m^2) \;=\; \frac{2m^2}{a_B\, a_C\, M^4} \Bigg\{ & \;\; \frac{1}{2}\left[\ln\!\left(\frac{(a_B\, a_C\, M^2 - m^2)\,(b_B+1)}{a_B\, m^2}\right)\right]^2 \\
& + \ln\!\left(\frac{a_C\,(b_B+1)M^2}{m^2}\right)\ln\!\left(\frac{a_B\,\left(a_C\,(b_B+1)M^2 - m^2\right)}{(b_B+1)\,m^2}\right) \\
& + \mathrm{Li}_2\!\left(\frac{m^2}{a_B\, a_C\, M^2}\right) \;-\; \mathrm{Li}_2\!\left(\frac{a_C\,(b_B+1)M^2 - m^2}{a_C\,(b_B+1)M^2}\right) \;\; \Bigg\}
\end{aligned}
$$

$$
\text{for} \begin{cases}
m^2 \;>\; a_B\, b_C\, M^2 \\
m^2 \;>\; \frac{a_B\, a_C\, b_B}{a_B + b_B}\, M^2 \\
m^2 \;>\; (a_C - (b_C+1))\,(b_B+1)M^2 \\
m^2 \;<\; \frac{a_B\, a_C\,(b_B+1)}{a_B + (b_B+1)}\, M^2 \\
m^2 \;<\; a_B\,(b_C+1)M^2 \\
m^2 \;<\; (a_C - b_C)\,(b_B+1)M^2
\end{cases}
$$

$$
\begin{aligned}
A_{26}(m^2) \;=\; \frac{2m^2}{a_B\, a_C\, M^4} \Bigg\{ & \;\; \frac{1}{2}\left[\ln\!\left(\frac{b_B+1}{b_B}\right)\right]^2 \\
& + \ln\!\left(\frac{a_C\,(b_B+1)M^2}{m^2}\right)\ln\!\left(\frac{\left(a_C\,(b_B+1)M^2 - m^2\right)b_B}{(a_C\, b_B\, M^2 - m^2)\,(b_B+1)}\right) \\
& + \mathrm{Li}_2\!\left(\frac{a_C\, b_B\, M^2 - m^2}{a_C\, b_B\, M^2}\right) \;-\; \mathrm{Li}_2\!\left(\frac{a_C\,(b_B+1)M^2 - m^2}{a_C\,(b_B+1)M^2}\right) \;\; \Bigg\}
\end{aligned}
$$

$$
\text{for} \begin{cases}
m^2 \;<\; (a_C - b_C)\, b_B\, M^2 \\
m^2 \;<\; \frac{a_B\, a_C\, b_B}{a_B + b_B}\, M^2 \\
m^2 \;>\; (a_C - (b_C+1))\,(b_B+1)M^2 \\
m^2 \;<\; a_B\,(b_C+1)M^2
\end{cases}
$$

$$B_{11}(m^2) \;=\; \frac{1}{a_B\,M^2}\;\ln\!\left(\frac{b_C+1}{b_C}\right)$$

$$\text{for}\;\begin{cases} m^2 \;<\; a_B\,b_C\,M^2 \\ m^2 \;>\; (a_C-b_C)\,(b_B+1)M^2 \end{cases}$$

$$B_{12}(m^2) \;=\; \frac{1}{a_B\,M^2}\;\ln\!\left(\frac{a_B\,(b_C+1)M^2}{m^2}\right)$$

$$\text{for}\;\begin{cases} m^2 \;>\; a_B\,b_C\,M^2 \\ m^2 \;>\; \frac{a_B\,a_C\,(b_B+1)}{a_B+(b_B+1)}\,M^2 \\ m^2 \;>\; (a_C-(b_C+1))\,b_B\,M^2 \\ m^2 \;<\; a_B\,(b_C+1)M^2 \\ m^2 \;>\; (a_C-(b_C+1))\,(b_B+1)M^2 \end{cases}$$

$$B_{13}(m^2) \;=\; \frac{1}{a_B\,M^2}\;\ln\!\left(\frac{(b_C+1)\,(b_B+1)M^2}{a_C\,(b_B+1)M^2-m^2}\right)$$

$$\text{for}\;\begin{cases} m^2 \;<\; (a_C-b_C)\,(b_B+1)M^2 \\ m^2 \;<\; \frac{a_B\,a_C\,(b_B+1)}{a_B+(b_B+1)}\,M^2 \\ m^2 \;>\; (a_C-(b_C+1))\,b_B\,M^2 \\ m^2 \;<\; a_B\,(b_C+1)M^2 \\ m^2 \;>\; (a_C-(b_C+1))\,(b_B+1)M^2 \end{cases}$$

$$B_{21}(m^2) \;=\; \frac{m^2}{a_B\,a_C\,M^4}\left\{\quad \left(1-\frac{a_C\,b_B\,M^2}{m^2}\right)\ln\!\left(\frac{b_C+1}{b_C}\right) \right.$$
$$\left. +\;\ln\!\left(\frac{a_C-b_C}{a_C-(b_C+1)}\right)\quad\right\}$$
$$\text{for}\;\begin{cases} m^2 \;<\; a_B\,b_C\,M^2 \\ m^2 \;>\; (a_C-b_C)\,b_B\,M^2 \\ m^2 \;<\; (a_C-(b_C+1))\,(b_B+1)M^2 \\ m^2 \;<\; \frac{a_B\,a_C\,(b_B+1)}{a_B+(b_B+1)}\,M^2 \end{cases}$$

$$B_{22}(m^2) \;=\; \frac{m^2}{a_B\,a_C\,M^4}\left\{\quad \left(1-\frac{a_C\,b_B\,M^2}{m^2}\right)\,\ln\!\left(\frac{a_C\,(b_B+1)M^2-m^2}{b_C\,(b_B+1)M^2}\right) \right.$$
$$\left. +\;\ln\!\left(\frac{(a_C-b_C)\,(b_B+1)M^2}{m^2}\right)\quad\right\}$$
$$\text{for}\;\begin{cases} m^2 \;<\; a_B\,b_C\,M^2 \\ m^2 \;>\; (a_C-b_C)\,b_B\,M^2 \\ m^2 \;>\; (a_C-(b_C+1))\,(b_B+1)M^2 \\ m^2 \;<\; \frac{a_B\,a_C\,(b_B+1)}{a_B+(b_B+1)}\,M^2 \\ m^2 \;<\; (a_C-b_C)\,(b_B+1)M^2 \end{cases}$$

$$B_{23}(m^2) \;=\; \frac{m^2}{a_B\,a_C\,M^4}\left\{\quad \left(1-\frac{a_C\,b_B\,M^2}{m^2}\right)\,\ln\!\left(\frac{a_B\,(b_C+1)M^2}{m^2}\right) \right.$$
$$\left. +\;\ln\!\left(\frac{a_B\,a_C\,M^2-m^2}{a_B\,(a_C-(b_C+1))M^2}\right)\quad\right\}$$
$$\text{for}\;\begin{cases} m^2 \;>\; a_B\,b_C\,M^2 \\ m^2 \;>\; \frac{a_B\,a_C\,b_B}{a_B+b_B}\,M^2 \\ m^2 \;<\; (a_C-(b_C+1))\,(b_B+1)M^2 \\ m^2 \;>\; (a_C-(b_C+1))\,b_B\,M^2 \\ m^2 \;<\; a_B\,(b_C+1)M^2 \\ m^2 \;<\; \frac{a_B\,a_C\,(b_B+1)}{a_B+(b_B+1)}\,M^2 \end{cases}$$

$$B_{24}(m^2) \;=\; \frac{m^2}{a_B\,a_C\,M^4}\left\{\quad \left(1-\frac{a_C\,b_B\,M^2}{m^2}\right)\,\ln\!\left(\frac{a_B\,\left(a_C\,(b_B+1)M^2-m^2\right)}{(b_B+1)\,m^2}\right)\right.$$
$$\left. +\;\ln\!\left(\frac{(b_B+1)\,(a_B\,a_C\,M^2-m^2)}{a_B\,m^2}\right)\quad\right\}$$
$$\text{for}\begin{cases} m^2 \;>\; a_B\,b_C\,M^2 \\ m^2 \;>\; \frac{a_B\,a_C\,b_B}{a_B+b_B}\,M^2 \\ m^2 \;>\; (a_C-(b_C+1))\,(b_B+1)M^2 \\ m^2 \;<\; a_B\,(b_C+1)M^2 \\ m^2 \;<\; \frac{a_B\,a_C\,(b_B+1)}{a_B+(b_B+1)}\,M^2 \\ m^2 \;<\; (a_C-b_C)\,(b_B+1)M^2 \end{cases}$$

$$B_{25}(m^2) \;=\; \frac{m^2}{a_B\,a_C\,M^4}\left\{\quad \left(1-\frac{a_C\,b_B\,M^2}{m^2}\right)\,\ln\!\left(\frac{(b_C+1)\,b_B\,M^2}{a_C\,b_B\,M^2-m^2}\right)\right.$$
$$\left. +\;\ln\!\left(\frac{m^2}{(a_C-(b_C+1))\,b_B\,M^2}\right)\quad\right\}$$
$$\text{for}\begin{cases} m^2 \;<\; (a_C-b_C)\,b_B\,M^2 \\ m^2 \;<\; \frac{a_B\,a_C\,b_B}{a_B+b_B}\,M^2 \\ m^2 \;<\; (a_C-(b_C+1))\,(b_B+1)M^2 \\ m^2 \;>\; (a_C-(b_C+1))\,b_B\,M^2 \\ m^2 \;<\; a_B\,(b_C+1)M^2 \end{cases}$$

$$B_{26}(m^2) \;=\; \frac{m^2}{a_B\,a_C\,M^4}\left\{\quad \left(1-\frac{a_C\,b_B\,M^2}{m^2}\right)\,\ln\!\left(\frac{\left(a_C\,(b_B+1)M^2-m^2\right)\,b_B}{(a_C\,b_B\,M^2-m^2)\,(b_B+1)}\right)\right.$$
$$\left. +\;\ln\!\left(\frac{b_B+1}{b_B}\right)\quad\right\}$$
$$\text{for}\begin{cases} m^2 \;<\; (a_C-b_C)\,b_B\,M^2 \\ m^2 \;<\; \frac{a_B\,a_C\,b_B}{a_B+b_B}\,M^2 \\ m^2 \;>\; (a_C-(b_C+1))\,(b_B+1)M^2 \\ m^2 \;<\; a_B\,(b_C+1)M^2 \end{cases}$$

$$C_{11}(m^2) \;=\; \frac{1}{M^2}\,\ln\!\left(\frac{b_B+1}{b_B}\right)\,\ln\!\left(\frac{a_C-b_C}{a_C-(b_C+1)}\right)$$

$$\text{for}\;\begin{cases} m^2 \;>\; a_B\,(b_C+1)M^2 \\ m^2 \;<\; (a_C-(b_C+1))\,b_B\,M^2 \end{cases}$$

$$C_{12}(m^2) \;=\; \frac{1}{M^2}\,\ln\!\left(\frac{b_B+1}{b_B}\right)\,\ln\!\left(\frac{a_B\,(a_C-b_C)M^2}{a_B\,a_C\,M^2-m^2}\right)$$

$$\text{for}\;\begin{cases} m^2 \;<\; a_B\,(b_C+1)M^2 \\ m^2 \;<\; \frac{a_B\,a_C\,b_B}{a_B+b_B}\,M^2 \\ m^2 \;>\; a_B\,b_C\,M^2 \\ m^2 \;<\; (a_C-b_C)\,b_B\,M^2 \end{cases}$$

$$C_{13}(m^2) \;=\; \frac{1}{M^2}\,\ln\!\left(\frac{b_B+1}{b_B}\right)\,\ln\!\left(\frac{(a_C-b_C)\,b_B\,M^2}{m^2}\right)$$

$$\text{for}\;\begin{cases} m^2 \;>\; (a_C-(b_C+1))\,b_B\,M^2 \\ m^2 \;>\; \frac{a_B\,a_C\,b_B}{a_B+b_B}\,M^2 \\ m^2 \;>\; a_B\,b_C\,M^2 \\ m^2 \;<\; (a_C-b_C)\,b_B\,M^2 \end{cases}$$

$$C_{21}(m^2) \;=\; \frac{1}{2\,M^2}\left\{ \quad \left[\ln\!\left(\frac{(a_C-b_C)\,(b_B+1)M^2}{m^2}\right)\right]^2 - \left[\ln\!\left(\frac{(a_C-(b_C+1))\,(b_B+1)M^2}{m^2}\right)\right]^2 \quad \right\}$$

$$\text{for} \begin{cases} m^2 \;>\; (a_C-b_C)\,b_B\,M^2 \\ m^2 \;>\; a_B\,(b_C+1)M^2 \\ m^2 \;<\; (a_C-(b_C+1))\,(b_B+1)M^2 \\ m^2 \;>\; \frac{a_B\,a_C\,b_B}{a_B+b_B}\,M^2 \end{cases}$$

$$C_{22}(m^2) \;=\; \frac{1}{2\,M^2}\left\{ \quad \left[\ln\!\left(\frac{(a_C-b_C)\,(b_B+1)M^2}{m^2}\right)\right]^2 - \left[\ln\!\left(\frac{(a_B\,a_C\,M^2-m^2)\,(b_B+1)}{a_B\,m^2}\right)\right]^2 \quad \right\}$$

$$\text{for} \begin{cases} m^2 \;>\; (a_C-b_C)\,b_B\,M^2 \\ m^2 \;<\; a_B\,(b_C+1)M^2 \\ m^2 \;<\; \frac{a_B\,a_C\,(b_B+1)}{a_B+(b_B+1)}\,M^2 \\ m^2 \;<\; (a_C-b_C)\,(b_B+1)M^2 \\ m^2 \;>\; a_B\,b_C\,M^2 \\ m^2 \;>\; \frac{a_B\,a_C\,b_B}{a_B+b_B}\,M^2 \end{cases}$$

$$C_{23}(m^2) \;=\; \frac{1}{2\,M^2}\left\{ \quad \left[\ln\!\left(\frac{(a_C-b_C)\,(b_B+1)M^2}{m^2}\right)\right]^2 \quad \right\}$$

$$\text{for} \begin{cases} m^2 \;>\; (a_C-b_C)\,b_B\,M^2 \\ m^2 \;>\; (a_C-(b_C+1))\,(b_B+1)M^2 \\ m^2 \;>\; \frac{a_B\,a_C\,(b_B+1)}{a_B+(b_B+1)}\,M^2 \\ m^2 \;<\; (a_C-b_C)\,(b_B+1)M^2 \\ m^2 \;>\; a_B\,b_C\,M^2 \end{cases}$$

$$C_{24}(m^2) \;=\; \frac{1}{2\,M^2}\left\{ \quad \left[\ln\!\left(\frac{b_B+1}{b_B}\right)\right]^2 - \left[\ln\!\left(\frac{(a_C-(b_C+1))\,(b_B+1)M^2}{m^2}\right)\right]^2 \quad \right\}$$

$$\text{for} \begin{cases} m^2 \;<\; (a_C-b_C)\,b_B\,M^2 \\ m^2 \;>\; a_B\,(b_C+1)M^2 \\ m^2 \;<\; (a_C-(b_C+1))\,(b_B+1)M^2 \\ m^2 \;>\; \frac{a_B\,a_C\,b_B}{a_B+b_B}\,M^2 \\ m^2 \;>\; (a_C-(b_C+1))\,b_B\,M^2 \end{cases}$$

$$C_{25}(m^2) \;=\; \frac{1}{2\,M^2}\left\{ \quad \left[\ln\!\left(\frac{b_B+1}{b_B}\right)\right]^2 - \left[\ln\!\left(\frac{(a_B\,a_C\,M^2-m^2)\,(b_B+1)}{a_B\,m^2}\right)\right]^2 \quad \right\}$$

$$\text{for} \begin{cases} m^2 \;<\; (a_C-b_C)\,b_B\,M^2 \\ m^2 \;<\; a_B\,(b_C+1)M^2 \\ m^2 \;<\; \frac{a_B\,a_C\,(b_B+1)}{a_B+(b_B+1)}\,M^2 \\ m^2 \;>\; a_B\,b_C\,M^2 \\ m^2 \;>\; \frac{a_B\,a_C\,b_B}{a_B+b_B}\,M^2 \\ m^2 \;>\; (a_C-(b_C+1))\,b_B\,M^2 \end{cases}$$

$$C_{26}(m^2) \;=\; \frac{1}{2\,M^2}\left\{ \quad \left[\ln\!\left(\frac{b_B+1}{b_B}\right)\right]^2 \quad \right\}$$

$$\text{for} \begin{cases} m^2 \;<\; (a_C-b_C)\,b_B\,M^2 \\ m^2 \;>\; (a_C-(b_C+1))\,(b_B+1)M^2 \\ m^2 \;>\; \frac{a_B\,a_C\,(b_B+1)}{a_B+(b_B+1)}\,M^2 \\ m^2 \;>\; a_B\,b_C\,M^2 \end{cases}$$

5.4 The limit $m_\tau = 0$

Taking $m_\tau = 0$ corresponds to

$$\begin{aligned} \lambda_{C\tau B} &= \left(m_C^2 - m_B^2\right)^2 \\ \lambda_{B\tau A} &= \left(m_B^2 - m_A^2\right)^2 \end{aligned} \tag{5.79}$$

which has the following implications for the mass parameters defined in (5.14):

$$\begin{aligned} a_B &= \frac{m_B^2}{m_B^2 - m_A^2} & b_B &= 0 \\ a_C &= \frac{m_C^2}{m_C^2 - m_B^2} & b_C &= 0 \\ M^2 &= \frac{(m_D^2 - m_C^2)(m_C^2 - m_B^2)(m_B^2 - m_A^2)}{m_B^2\, m_C^2} \end{aligned} \tag{5.80}$$

Analogous to what we found for the m_{ab} distribution, the above relations imply a much simplified result: First, four of the eight split points vanish along with b_B and b_C, leaving the non-zero split points at

$$\frac{m_{\text{high}}^2}{M^2} = \left\{ (a_C - 1)\,,\ \frac{a_B\, a_C}{a_B + 1}\,,\ a_C\,,\ a_B \right\} \tag{5.81}$$

This means we are left only with mass scenarios 4, 5 and 6 which correspond to the following orders of split points:

$$\begin{aligned} \text{Scenario 4:} \quad & (a_C - 1) < \frac{a_B\, a_C}{a_B + 1} < a_C < a_B \\ \text{Scenario 5:} \quad & (a_C - 1) < \frac{a_B\, a_C}{a_B + 1} < a_B < a_C \\ \text{Scenario 6:} \quad & a_B < \frac{a_B\, a_C}{a_B + 1} < (a_C - 1) < a_C \end{aligned}$$

Second, only nine of the final terms now contribute to the m_{high} distribution, and several of these terms are greatly simplified due to the vanishing of parameters b_B and b_C. Taking the above results into account, we can now write out $\mathrm{d}\Gamma / \mathrm{d}m_{\text{high}}$ for mass scenarios 4–6 in the limit of massless taus. A list of the nine contributing terms is given at the end of this section.

Scenario 4

$$\frac{1}{\Gamma}\frac{\mathrm{d}\Gamma}{\mathrm{d}m_{\mathrm{high}}}\bigg|_{m_\tau=0} = \begin{cases} 2\,m_{\mathrm{high}}\big[A_{22}+B_{23}+C_{22}\big]_{m_\tau=0} & \text{for (1)} \\ 2\,m_{\mathrm{high}}\big[A_{25}+B_{13}+B_{24}+C_{22}\big]_{m_\tau=0} & \text{for (2)} \\ 2\,m_{\mathrm{high}}\big[B_{12}+C_{23}\big]_{m_\tau=0} & \text{for (3)} \\ 2\,m_{\mathrm{high}}\big[B_{12}\big]_{m_\tau=0} & \text{for (4)} \end{cases}$$

$$\begin{aligned} &(1) && 0 && < && m_{\mathrm{high}} && < && \sqrt{(a_C-1)M^2} \\ &(2) && \sqrt{(a_C-1)M^2} && < && m_{\mathrm{high}} && < && \sqrt{\frac{a_B\,a_C}{a_B+1}M^2} \\ &(3) && \sqrt{\frac{a_B\,a_C}{a_B+1}M^2} && < && m_{\mathrm{high}} && < && \sqrt{a_C M^2} \\ &(4) && \sqrt{a_C M^2} && < && m_{\mathrm{high}} && < && \sqrt{a_B M^2} \end{aligned}$$

Scenario 5

$$\frac{1}{\Gamma}\frac{\mathrm{d}\Gamma}{\mathrm{d}m_{\mathrm{high}}}\bigg|_{m_\tau=0} = \begin{cases} 2\,m_{\mathrm{high}}\big[A_{22}+B_{23}+C_{22}\big]_{m_\tau=0} & \text{for (1)} \\ 2\,m_{\mathrm{high}}\big[A_{25}+B_{13}+B_{24}+C_{22}\big]_{m_\tau=0} & \text{for (2)} \\ 2\,m_{\mathrm{high}}\big[B_{12}+C_{23}\big]_{m_\tau=0} & \text{for (3)} \\ 2\,m_{\mathrm{high}}\big[C_{23}\big]_{m_\tau=0} & \text{for (4)} \end{cases}$$

$$\begin{aligned} &(1) && 0 && < && m_{\mathrm{high}} && < && \sqrt{(a_C-1)M^2} \\ &(2) && \sqrt{(a_C-1)M^2} && < && m_{\mathrm{high}} && < && \sqrt{\frac{a_B\,a_C}{a_B+1}M^2} \\ &(3) && \sqrt{\frac{a_B\,a_C}{a_B+1}M^2} && < && m_{\mathrm{high}} && < && \sqrt{a_B M^2} \\ &(4) && \sqrt{a_B M^2} && < && m_{\mathrm{high}} && < && \sqrt{a_C M^2} \end{aligned}$$

Scenario 6

$$\frac{1}{\Gamma}\frac{\mathrm{d}\Gamma}{\mathrm{d}m_{\mathrm{high}}}\bigg|_{m_\tau=0} = \begin{cases} 2\,m_{\mathrm{high}}\big[A_{22}+B_{23}+C_{22}\big]_{m_\tau=0} & \text{for (1)} \\ 2\,m_{\mathrm{high}}\big[C_{21}\big]_{m_\tau=0} & \text{for (2)} \\ 2\,m_{\mathrm{high}}\big[C_{21}\big]_{m_\tau=0} & \text{for (3)} \\ 2\,m_{\mathrm{high}}\big[C_{23}\big]_{m_\tau=0} & \text{for (4)} \end{cases}$$

$$\begin{aligned} &(1) && 0 && < && m_{\mathrm{high}} && < && \sqrt{a_B M^2} \\ &(2) && \sqrt{a_B M^2} && < && m_{\mathrm{high}} && < && \sqrt{\frac{a_B\,a_C}{a_B+1}M^2} \\ &(3) && \sqrt{\frac{a_B\,a_C}{a_B+1}M^2} && < && m_{\mathrm{high}} && < && \sqrt{(a_C-1)M^2} \\ &(4) && \sqrt{(a_C-1)M^2} && < && m_{\mathrm{high}} && < && \sqrt{a_C M^2} \end{aligned}$$

In Figure 5.5 these approximate distributions (red) are compared to the complete results of Section 5.3 (black). Not surprisingly there is very good agreement between the distributions as long as the mass differences $(m_C - m_B)$ and $(m_B - m_A)$ are not close to m_τ. The deviations can be understood by considering how the underlying m_{bc} and m_{ac} distributions are affected by taking $m_\tau = 0$, which is shown in Appendix A (Figures A.1 and A.2). The general picture, however, is the same as for the m_{ab} distribution: taking $m_\tau = 0$ leads to a broader distribution as the ranges of allowed energies for particles a and b are expanded in both directions. As the m_{ac} distribution deviates from the $m_\tau = 0$ approximation when m_B is close to m_A, while this only happens for the m_{bc} distribution if m_B is close to m_C, the approximate m_{high} distribution shows relatively good agreement even with one of these mass differences being small.

Below we list all terms contributing to $\mathrm{d}\Gamma/\,\mathrm{d}m_{\mathrm{high}}$ in the limit of massless taus. Once again the simplified notation $m_{\mathrm{high}} \equiv m$ is used.

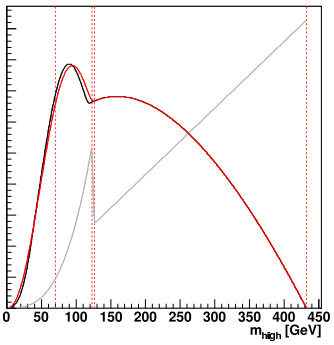

(a) $m_D = 550,\ m_C = 180,$
$m_B = 100,\ m_A = 97$ (GeV)
scenario 4

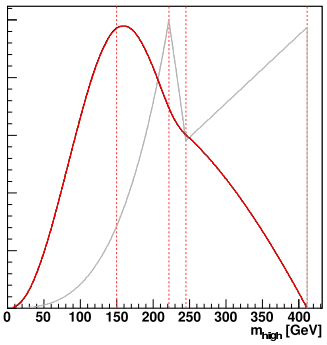

(b) $m_D = 550,\ m_C = 180,$
$m_B = 110,\ m_A = 97$ (GeV)
scenario 4

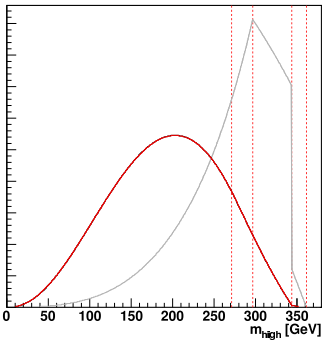

(c) $m_D = 550,\ m_C = 180,$
$m_B = 135,\ m_A = 97$ (GeV)
scenario 5

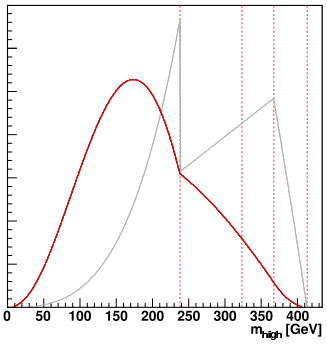

(d) $m_D = 550,\ m_C = 180,$
$m_B = 160,\ m_A = 97$ (GeV)
scenario 6

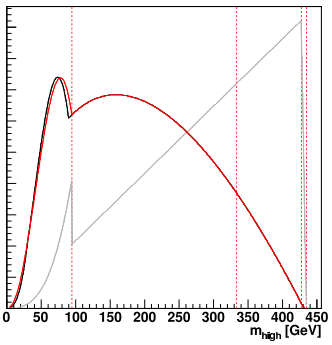

(e) $m_D = 550,\ m_C = 180,$
$m_B = 177,\ m_A = 97$ (GeV)
scenario 6

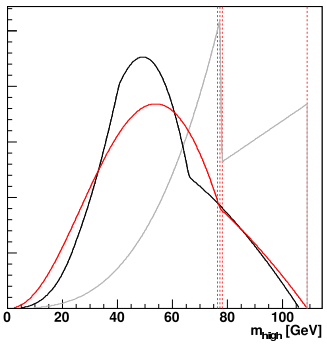

(f) $m_D = 550,\ m_C = 180,$
$m_B = 176,\ m_A = 174$ (GeV)
scenario 4

Figure 5.5: $(1/\Gamma)(\,\mathrm{d}\Gamma/\,\mathrm{d}m_{\mathrm{high}})$ in the limit $m_\tau = 0$ (red) compared to the exact distribution (black).

$$
\begin{aligned}
A_{22}(m^2)\Big|_{m_\tau=0} = \; & \frac{2\,m^2}{a_B\,a_C\,M^4}\left\{ \right. \\
& \frac{1}{2}\left[\ln\!\left(\frac{(a_B\,a_C\,M^2-m^2}{a_B\,m^2}\right)\right]^2 \\
& -\frac{1}{2}\left[\ln\!\left(\frac{(a_C-1)M^2}{m^2}\right)\right]^2 \\
& +\ln\!\left(\frac{a_C\,M^2}{m^2}\right)\ln\!\left(\frac{a_B\,M^2}{m^2}\right) \\
& +\mathrm{Li}_2\!\left(\frac{m^2}{a_B\,a_C\,M^2}\right) - \mathrm{Li}_2\!\left(\frac{1}{a_C}\right) \left.\right\} \\
& \text{for} \begin{cases} m^2 < (a_C-1)\,M^2 \\ m^2 < \frac{a_B\,a_C}{a_B+1}\,M^2 \\ m^2 < a_B\,M^2 \end{cases}
\end{aligned}
$$

$$
\begin{aligned}
A_{25}(m^2)\Big|_{m_\tau=0} = \; & \frac{2\,m^2}{a_B\,a_C\,M^4}\left\{ \right. \\
& \frac{1}{2}\left[\ln\!\left(\frac{a_B\,a_C\,M^2-m^2}{a_B\,m^2}\right)\right]^2 \\
& +\ln\!\left(\frac{a_C\,M^2}{m^2}\right)\ln\!\left(\frac{a_B\,(a_C\,M^2-m^2)}{m^2}\right) \\
& +\mathrm{Li}_2\!\left(\frac{m^2}{a_B\,a_C\,M^2}\right) - \mathrm{Li}_2\!\left(\frac{a_C\,M^2-m^2}{a_C\,M^2}\right) \left.\right\} \\
& \text{for} \begin{cases} m^2 > (a_C-1)\,M^2 \\ m^2 < \frac{a_B\,a_C}{a_B+1}\,M^2 \\ m^2 < a_B\,M^2 \end{cases}
\end{aligned}
$$

$$B_{12}(m^2)\Big|_{m_\tau=0} = \frac{1}{a_B\,M^2}\left\{\ln\left(\frac{a_B\,M^2}{m^2}\right)\right\} \quad \text{for} \begin{cases} m^2 > (a_C-1)\,M^2 \\ m^2 > \frac{a_B\,a_C}{a_B+1}\,M^2 \\ m^2 < a_B\,M^2 \end{cases}$$

$$B_{13}(m^2)\Big|_{m_\tau=0} = \frac{1}{a_B\,M^2}\left\{\ln\left(\frac{M^2}{a_C\,M^2-m^2}\right)\right\} \quad \text{for} \begin{cases} m^2 > (a_C-1)\,M^2 \\ m^2 < \frac{a_B\,a_C}{a_B+1}\,M^2 \\ m^2 < a_B\,M^2 \end{cases}$$

$$B_{23}(m^2)\Big|_{m_\tau=0} = \frac{m^2}{a_B\,a_C\,M^4}\left\{\ln\left(\frac{a_B\,a_C\,M^2-m^2}{(a_C-1)\,m^2}\right)\right\} \quad \text{for} \begin{cases} m^2 < (a_C-1)\,M^2 \\ m^2 < \frac{a_B\,a_C}{a_B+1}\,M^2 \\ m^2 < a_B\,M^2 \end{cases}$$

$$B_{24}(m^2)\Big|_{m_\tau=0} = \frac{m^2}{a_B\,a_C\,M^4}\left\{\ln\left(\frac{a_B\,(a_C\,M^2-m^2)}{m^2}\right) + \ln\left(\frac{a_B\,a_C\,M^2-m^2}{a_B\,m^2}\right)\right\} \quad \text{for} \begin{cases} m^2 > (a_C-1)\,M^2 \\ m^2 < \frac{a_B\,a_C}{a_B+1}\,M^2 \\ m^2 < a_B\,M^2 \end{cases}$$

$$C_{21}(m^2)\Big|_{m_\tau=0} = \frac{1}{2\,M^2}\left\{ \left[\ln\left(\frac{a_C\,M^2}{m^2}\right)\right]^2 - \left[\ln\left(\frac{(a_C-1)M^2}{m^2}\right)\right]^2 \right\}$$

$$\text{for} \begin{cases} m^2 < (a_C-1)\,M^2 \\ m^2 > a_B\,M^2 \end{cases}$$

$$C_{22}(m^2)\Big|_{m_\tau=0} = \frac{1}{2\,M^2}\left\{ \left[\ln\left(\frac{a_C\,M^2}{m^2}\right)\right]^2 - \left[\ln\left(\frac{a_B\,a_C\,M^2-m^2}{a_B\,m^2}\right)\right]^2 \right\}$$

$$\text{for} \begin{cases} m^2 < \frac{a_B\,a_C}{a_B+1}\,M^2 \\ m^2 < a_B\,M^2 \end{cases}$$

$$C_{23}(m^2)\Big|_{m_\tau=0} = \frac{1}{2\,M^2}\left\{ \left[\ln\left(\frac{a_C\,M^2}{m^2}\right)\right]^2 \right\}$$

$$\text{for} \begin{cases} m^2 > (a_C-1)\,M^2 \\ m^2 > \frac{a_B\,a_C}{a_B+1}\,M^2 \\ m^2 < a_C\,M^2 \end{cases}$$

Chapter 6

The Spin Dependent m_{ab} Distribution

6.1 General remarks and assumptions

Here we expand on the result for the m_{ab} distribution of the ditau decay

$$C \;\rightarrow\; \tau_b\, B \;\rightarrow\; (b\,\nu)\,(\tau_a\, A) \;\rightarrow\; b\,\nu\,a\,\nu\,A \tag{6.1}$$

by incorporating the effects of particle spins. The results so far have been derived under the assumption of all particles being spin-0. This has resulted in distributions that are strictly valid only when summing all final states and assuming that positive and negative helicity taus are produced with equal probability at the two vertices. In a SUSY scenario this would only be true for a specific set of mixing parameters determining the $\widetilde{\tau}_L$-$\widetilde{\tau}_R$ mixture of the stau mass eigenstates and the $\widetilde{W}^0$-$\widetilde{B}^0$-$\widetilde{H}^0$ mixture of the neutralinos. Therefore, the spin dependent distributions will not only reveal the underlying structure of the m_{ab} distribution we found in the spin-0 approximation, but also allow us to study much more general scenarios with arbitrary mixing for staus and neutralinos. The prospects of probing these mixing effects using such spin dependent distributions from tau cascades have been studied in [26, 27]. We will return to this topic in Section 6.5.

In the lab frame τ_a and τ_b will generally be highly boosted. For this reason one can make use of the 'collinear approximation' in which the visible decay products a and b are assumed to move in the same directions as their parent taus. A derivation of the

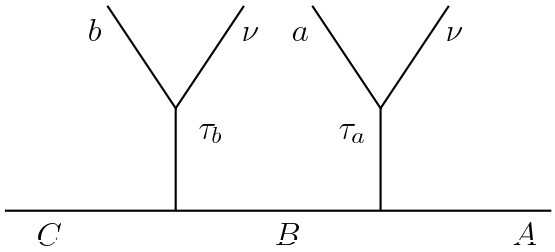

Figure 6.1: The ditau cascade decay

desired m_{ab}-distributions making use of this approximation is given in Appendix B. As it turns out, the different combinations of τ_a and τ_b chiralities give rise to three different m_{ab} distributions.

The following derivation is kept slightly more general as the collinear approximation is not employed. This implies that the various tau helicities, rather than chiralities, must be be differentiated. The final result will consist of four different distributions corresponding to the four possible combinations of τ_a and τ_b helicities. As expected, when taking the limit $m_\tau = 0$ we find that two of the helicity dependent distributions merge and the results from the collinear approximation are reproduced. The reason why we choose not to invoke the collinear approximation right away is twofold: First, it ensures that most of the derivation follows in close analogy with the previous derivations, thus illustrating how spin effects can be included in this framework. Second, it allows us to better understand the distributions found in the collinear limit and the possible effects missed by this approximation.

In correspondence with the SUSY cascade

$$\widetilde{\chi}_2^0 \;\rightarrow\; \tau_n^\pm\, \widetilde{\tau}^\mp \;\rightarrow\; (\pi_n^\pm\, \nu)\, (\tau_f^\mp\, \widetilde{\chi}_1^0) \;\rightarrow\; \pi_n^\pm\, \nu\, \pi_f^\mp\, \nu\, \widetilde{\chi}_1^0 \tag{6.2}$$

spins are assigned in the following way:

$$\begin{aligned} \text{fermions:} &\quad C,\, A,\, \tau,\, \nu \\ \text{scalars:} &\quad B,\, b,\, a \end{aligned}$$

We will still assume that particles a, b and ν are massless, and all massive particles are taken to be on-shell and satisfying the hierarchy $m_\tau < m_A < m_B < m_C$. In the following all L/R indices and statements about particle 'handedness' refer to helicity, not chirality, unless otherwise noted.

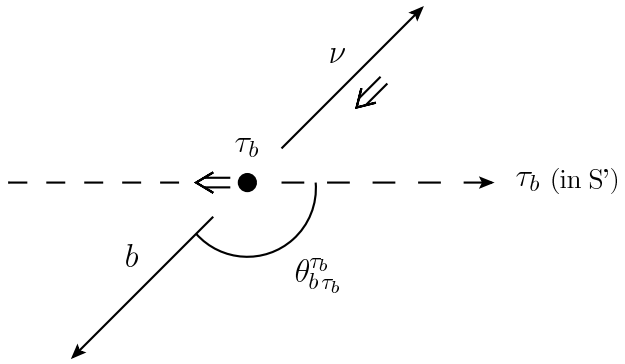

Figure 6.2: The angle $\theta^{\tau_b}_{b\,\tau_b}$ as defined in the rest frame of the decaying τ_b. Double arrows indicate spin/helicity direction, while the dashed axis represents the direction of τ_b as seen from the frame S'.

The invariant mass of particles a and b depends on their energies and the angle between their three-momenta. As any angular correlation between a and b due to spin is erased by the intermediate scalar B, only spin effects in the particles' energy spectra will alter the m_{ab} distribution relative to the distribution found in the spin-0 approximation.

6.2 The derivation

The derivation of $\mathrm{d}\Gamma/\,\mathrm{d}m_{ab}$ can be outlined as follows: We begin by studying the angular distribution for the decay $\tau_b \to b\,\nu$ (the decay of τ_a is identical). Then we express m_{ab} in terms of the angular variables that we now know the distributions of. The rest of the derivation then follows the familiar pattern of variable changes and integrations.

6.2.1 Angular distributions in tau decays

In the weak decay $\tau_b^- \to b^-\,\nu$ we can define an angle $\theta^{\tau_b}_{b\,\tau_b}$ in the rest frame of τ_b as the angle between the τ spin quantization axis and the momentum of the outgoing scalar b. This spin axis can be chosen to coincide with the τ momentum direction in some other reference frame S'. Thus, $\theta^{\tau_b}_{b\,\tau_b}$ is the angle between the direction of τ_b in S' and the direction of b in the τ_b rest frame, as shown in Fig. 6.2. In S' the two spin states of τ_b are interpreted in terms of positive and negative helicity.

The matrix element for $\tau_b^- \to b^- \nu$ depends on the polarisation of the decaying τ_b. For positive polarisation we have [27]

$$\mathcal{M}_+ \propto \cos \frac{\theta_{b\,\tau_b}^{\tau_b}}{2} \tag{6.3}$$

while negative polarisation gives

$$\mathcal{M}_- \propto \sin \frac{\theta_{b\,\tau_b}^{\tau_b}}{2} \tag{6.4}$$

Squaring the matrix element and integrating over all phase space variables except $\cos \theta_{b\,\tau_b}^{\tau_b}$, we find the normalised differential decay rate to be

$$\frac{1}{\Gamma} \frac{\mathrm{d}\Gamma}{\mathrm{d}\cos \theta_{b\,\tau_b}^{\tau_b}}\bigg|_{\tau^-} = \frac{1}{2}\left(1 + \mathcal{P}_\beta \cos \theta_{b\,\tau_b}^{\tau_b}\right) \tag{6.5}$$

where $\mathcal{P}_\beta = \pm$ correspond to positive and negative tau polarisation, respectively. This distribution can qualitatively be understood by considering angular momentum conservation: As b is a scalar, the neutrino must carry the total angular momentum after the decay. Since the massless neutrino is always left-handed it will preferably be emitted in direction opposite to the tau spin. Conservation of momentum in the tau rest frame thus implies that b will be emitted along the tau spin direction.

A CP transformation of this process corresponds to the decay $\tau_b^+ \to b^+ \bar{\nu}$ with all three-momenta inverted and all spin directions unchanged, relative to Fig. 6.2. As tau decays are CP invariant we immediately find that decays of positively polarised τ^+ and negatively polarised τ^- give rise to identical angular distributions. Similarly it must hold that decays of negatively polarised τ^+ and positively polarised τ^- have identical distributions. Thus, we can describe the $\tau_b^\pm$ decays with the distribution

$$\frac{1}{\Gamma} \frac{\mathrm{d}\Gamma}{\mathrm{d}\cos \theta_{b\,\tau_b}^{\tau_b}} = \frac{1}{2}\left(1 - \beta\,\mathcal{P}_\beta \cos \theta_{b\,\tau_b}^{\tau_b}\right) \tag{6.6}$$

where $\beta = \pm$ denotes the charge and $\mathcal{P}_\beta = \pm$ the polarisation of τ_b. Similarly, the decay $\tau_a \to a\,\nu$ is described by the distribution

$$\frac{1}{\Gamma} \frac{\mathrm{d}\Gamma}{\mathrm{d}\cos \theta_{a\,\tau_a}^{\tau_a}} = \frac{1}{2}\left(1 - \alpha\,\mathcal{P}_\alpha \cos \theta_{a\,\tau_a}^{\tau_a}\right) \tag{6.7}$$

with $\alpha = \pm$ and $\mathcal{P}_\alpha = \pm$ specifying the τ_a charge and polarisation, respectively.

6.2.2 Kinematics

We now turn to the problem of expressing m_{ab}^2 by a set of variables including $\cos\theta_{b\,\tau_b}^{\tau_b}$ and $\cos\theta_{a\,\tau_a}^{\tau_a}$. When deriving the spin-0 m_{ab}-distribution in Chapter 4 we found through kinematical considerations that m_{ab}^2 can be expressed as (Equation 4.19)

$$\begin{aligned} m_{ab}^2 \;=\; & \frac{1}{8m_B^2}\left((m_C^2 - m_B^2 - m_\tau^2) - \sqrt{\lambda_{C\tau B}}\cos\theta_{bB}^{\tau_b}\right) \\ & \times\left((m_B^2 - m_A^2 + m_\tau^2) - \sqrt{\lambda_{B\tau A}}\cos\theta_{aB}^{\tau_a}\right)\left(1 - \cos\theta_{ab}^{B}\right) \end{aligned} \tag{6.8}$$

The angles $\theta_{b\,\tau_b}^{\tau_b}$ and $\theta_{a\,\tau_a}^{\tau_a}$ used for the tau decay distributions (6.6) and (6.7) were defined based on the taus' directions in some reference frame S', which we now choose to be the rest frame of B. Since the direction of τ_b (τ_a) in the rest frame of B is opposite to the direction of B in the rest frame of τ_b (τ_a), we obtain

$$\cos\,\theta_{b\,\tau_b}^{\tau_b} \;=\; -\cos\theta_{bB}^{\tau_b} \tag{6.9}$$

$$\cos\,\theta_{a\,\tau_a}^{\tau_a} \;=\; -\cos\theta_{aB}^{\tau_a} \tag{6.10}$$

Thus, m_{ab}^2 in terms of $\cos\theta_{b\,\tau_b}^{\tau_b}$ and $\cos\theta_{a\,\tau_a}^{\tau_a}$ simply becomes

$$\begin{aligned} m_{ab}^2 \;=\; & \frac{1}{8m_B^2}\left((m_C^2 - m_B^2 - m_\tau^2) + \sqrt{\lambda_{C\tau B}}\cos\,\theta_{b\,\tau_b}^{\tau_b}\right) \\ & \times\left((m_B^2 - m_A^2 + m_\tau^2) + \sqrt{\lambda_{B\tau A}}\cos\,\theta_{a\,\tau_a}^{\tau_a}\right)\left(1 - \cos\theta_{ab}^{B}\right) \end{aligned} \tag{6.11}$$

As B is a scalar, $\cos\theta_{ab}^{B}$ will still have a flat distribution when spins are taken into account. The non-flat distributions of $\cos\theta_{b\,\tau_b}^{\tau_b}$ and $\cos\theta_{a\,\tau_a}^{\tau_a}$ are given by (6.6) and (6.7), respectively.

It is important to note that choosing S' as the rest frame of B implies that tau helicities are defined relative to this frame. As helicity is a frame dependent quantity, an observer in the rest frame of B might disagree with an observer in the lab frame as to what helicity distribution an observed event belongs to. (They will, of course, always agree on the invariant mass value.) However, assuming that the distribution of B directions in the lab frame is symmetric under reflection through the origin, any such 'helicity disagreement' should cancel statistically, making the distributions derived here valid also in the lab frame. In the limit $m_\tau = 0$ the derived distributions are valid in all frames as tau helicity corresponds to chirality, which is frame independent.

The rest of the $\mathrm{d}\Gamma/\,\mathrm{d}m_{ab}$ derivation follows in close analogy with the spin-0 derivation. To keep notation simple we define the variables

$$\begin{aligned} u &\equiv \frac{1+\cos\theta^{\tau_b}_{b\tau_b}}{2} \\ v &\equiv \frac{1+\cos\theta^{\tau_a}_{a\tau_a}}{2} \\ w &\equiv \frac{1-\cos\theta^{B}_{ab}}{2} \end{aligned} \tag{6.12}$$

along with the mass dependent parameters

$$\begin{aligned} b_C &\equiv \frac{1}{2}\left(\frac{m_C^2-m_B^2-m_\tau^2}{\sqrt{\lambda_{C\tau B}}}-1\right) \\ b_B &\equiv \frac{1}{2}\left(\frac{m_B^2-m_A^2+m_\tau^2}{\sqrt{\lambda_{B\tau A}}}-1\right) \\ M^2 &\equiv \frac{\sqrt{\lambda_{C\tau B}}\sqrt{\lambda_{B\tau A}}}{m_B^2} \end{aligned} \tag{6.13}$$

We note that the variables defined in (6.12) are different from the variables defined in (4.20), while the mass parameters of (6.13) are identical to those defined in (4.21). These parameters are positive for any choice of masses allowed by on-shell kinematics ($m_C > m_B + m_\tau$ and $m_B > m_A + m_\tau$). In terms of the variables and parameters defined above, m_{ab}^2 can be expressed as

$$m_{ab}^2 = M^2\,(b_C+u)\,(b_B+v)\,w\,, \qquad 0 \le (u,v,w) \le 1 \tag{6.14}$$

6.2.3 Variable changes and integrations

While the spin-0 approximation ensured that all of the variables u, v and w had flat distributions, this is now only true for w. By change of variables in (6.6) and (6.7) we find the distributions for u and v to be

$$\frac{1}{\Gamma}\frac{\mathrm{d}\Gamma}{\mathrm{d}u} = 1-\beta\,\mathcal{P}_\beta(2u-1) \equiv f_{\beta\,\mathcal{P}_\beta}(u) \tag{6.15}$$

$$\frac{1}{\Gamma}\frac{\mathrm{d}\Gamma}{\mathrm{d}v} = 1-\alpha\,\mathcal{P}_\alpha(2v-1) \equiv g_{\alpha\,\mathcal{P}_\alpha}(v) \tag{6.16}$$

Using indices $\beta, \alpha = \pm$ and $\mathcal{P}_\beta, \mathcal{P}_\alpha = R/L$, and keeping in mind that $f_{\beta\,\mathcal{P}_\beta}(u)$ and $g_{\alpha\,\mathcal{P}_\alpha}(v)$ describe the decays of τ_b and τ_a respectively, we write out the explicit distributions

$$\tau_b = \begin{cases} \tau_L^-, \tau_R^+ & \Rightarrow \quad f_{-L}(u) \;=\; f_{+R}(u) \;=\; 2(1-u) \\ \tau_R^-, \tau_L^+ & \Rightarrow \quad f_{-R}(u) \;=\; f_{+L}(u) \;=\; 2u \end{cases} \tag{6.17}$$

$$\tau_a = \begin{cases} \tau_L^-, \tau_R^+ & \Rightarrow \quad g_{-L}(v) \;=\; g_{+R}(v) \;=\; 2(1-v) \\ \tau_R^-, \tau_L^+ & \Rightarrow \quad g_{-R}(v) \;=\; g_{+L}(v) \;=\; 2v \end{cases} \tag{6.18}$$

For a given choice of charges and helicities for τ_a and τ_b the differential decay rate w.r.t. the variables (u, v, w) can now be expressed as

$$\frac{1}{\Gamma}\frac{\mathrm{d}^3\Gamma}{\mathrm{d}u\,\mathrm{d}v\,\mathrm{d}w} \;=\; \hat{\theta}(u)\,\hat{\theta}(v)\,\hat{\theta}(w)\,f_{\beta\,\mathcal{P}_\beta}(u)\,g_{\alpha\,\mathcal{P}_\alpha}(v) \tag{6.19}$$

Here we once again make use of the simplified step function notation

$$\hat{\theta}(x) \;\equiv\; \theta(x)\theta(1-x) \tag{6.20}$$

By (6.14) we now perform the variable change from (u, v, w) to (u, v, m_{ab}^2), resulting in the distribution

$$\frac{1}{\Gamma}\frac{\mathrm{d}^3\Gamma}{\mathrm{d}u\,\mathrm{d}v\,\mathrm{d}m_{ab}^2} \;=\; \hat{\theta}(u)\,\hat{\theta}(v)\,\hat{\theta}\!\left(\frac{m_{ab}^2}{(b_C+u)(b_B+v)M^2}\right)\,\frac{f_{\beta\,\mathcal{P}_\beta}(u)\;g_{\alpha\,\mathcal{P}_\alpha}(v)}{(b_C+u)(b_B+v)M^2} \tag{6.21}$$

Finally, by defining the variables x and y as

$$x \;\equiv\; b_C + u \tag{6.22}$$

$$y \;\equiv\; b_B + v \tag{6.23}$$

and performing yet another variable change, we end up with the expression

$$\frac{1}{\Gamma}\frac{\mathrm{d}^3\Gamma}{\mathrm{d}x\,\mathrm{d}y\,\mathrm{d}m_{ab}^2} \;=\; \hat{\theta}(x-b_C)\,\hat{\theta}(y-b_B)\,\hat{\theta}\!\left(\frac{m_{ab}^2}{xyM^2}\right)\,\frac{f_{\beta\,\mathcal{P}_\beta}(x-b_C)\;g_{\alpha\,\mathcal{P}_\alpha}(y-b_B)}{xyM^2} \tag{6.24}$$

To obtain the m_{ab} distribution for a specific choice of tau charges (β, α) and helicities $(\mathcal{P}_\beta, \mathcal{P}_\alpha)$ we must integrate (6.24) over x and y. Just as for the spin-0 derivation, the step functions impose the following constraints on the ranges of x and y:

$$b_C \;<\; x \;<\; b_C + 1 \tag{6.25}$$

$$b_B \;<\; y \;<\; b_B + 1 \tag{6.26}$$

$$\frac{m_{ab}^2}{xM^2} \;<\; y \tag{6.27}$$

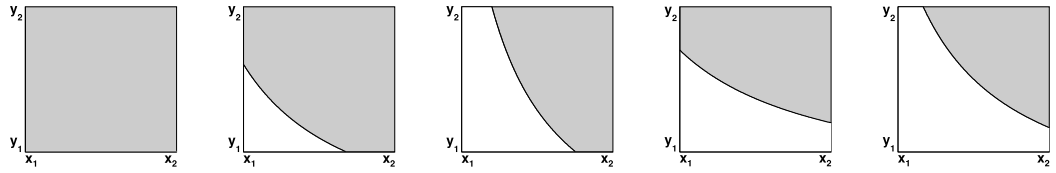

(a) (b) (c) (d) (e)

Figure 6.3: The five integration regions of the xy plane (grey).

In other words, when including spin in the derivation the integrand changes relative to the spin-0 case while the integration limits remain the same. The integration regions of the xy plane are illustrated in fig 6.3, where

$$\begin{aligned} x_1 &= b_C & y_1 &= b_B \\ x_2 &= b_C + 1 & y_2 &= b_B + 1 \end{aligned}$$

and they grey areas represent the regions satisfying (6.27). As before we must consider the two mass scenarios

$$\begin{aligned} b_C &< b_B \qquad \text{Scenario I} \\ b_B &< b_C \qquad \text{Scenario II} \end{aligned}$$

The correspondence between different integration regions and m_{ab}^2 ranges for the resulting $\mathrm{d}\Gamma/\,\mathrm{d}m_{ab}^2$ expressions can be found in Tables 4.1 and 4.2 for scenarios I and II, respectively. All integrations take the general form

$$\iint\limits_{\text{region (x)}} \frac{f_{\beta\,\mathcal{P}_\beta}(x - b_C)\; g_{\alpha\,\mathcal{P}_\alpha}(y - b_B)}{x\,y\,M^2}\,\mathrm{d}y\,\mathrm{d}x \tag{6.28}$$

As particles C and A are taken to be neutral (corresponding to (6.2)), charge conservation implies that τ_a and τ_b are oppositely charged. We therefore only solve (6.28) for choices of $f_{\beta\,\mathcal{P}_\beta}$ and $g_{\alpha\,\mathcal{P}_\alpha}$ that satisfy $\alpha = -\beta$. Performing all necessary integrations is straightforward but somewhat tedious, so further details will be omitted. The resulting m_{ab}^2 distributions for the two mass scenarios are given in Tables 6.1 and 6.2. All terms referred to in the tables are collected in a list following the discussion of the results. The terms' lower-case indices refer back to what xy integration region they result from. Since each term is zero outside the m_{ab} range dictated by its integration region, for any m_{ab} value only one of the four terms will contribute to $\mathrm{d}\Gamma/\,\mathrm{d}m_{ab}^2$.

Table 6.1: $\frac{1}{\Gamma}\frac{\mathrm{d}\Gamma}{\mathrm{d}m_{ab}^2}$ for mass scenario I ($b_C < b_B$)

$(\tau_b\ ,\ \tau_a)$	$f_{\beta\,\mathcal{P}_\beta}(u)$	$g_{\alpha\,\mathcal{P}_\alpha}(v)$	$\frac{1}{\Gamma}\frac{\mathrm{d}\Gamma}{\mathrm{d}m_{ab}^2}$
$(\tau_L^-\ ,\ \tau_R^+)\ (\tau_R^+\ ,\ \tau_L^-)$	$2(1-u)$	$2(1-v)$	$A_a + A_b + A_c + A_e$
$(\tau_L^-\ ,\ \tau_L^+)\ (\tau_R^+\ ,\ \tau_R^-)$	$2(1-u)$	$2v$	$B_a + B_b + B_c + B_e$
$(\tau_R^-\ ,\ \tau_R^+)\ (\tau_L^+\ ,\ \tau_L^-)$	$2u$	$2(1-v)$	$C_a + C_b + C_c + C_e$
$(\tau_R^-\ ,\ \tau_L^+)\ (\tau_L^+\ ,\ \tau_R^-)$	$2u$	$2v$	$D_a + D_b + D_c + D_e$

Table 6.2: $\frac{1}{\Gamma}\frac{\mathrm{d}\Gamma}{\mathrm{d}m_{ab}^2}$ for mass scenario II ($b_B < b_C$)

$(\tau_b\ ,\ \tau_a)$	$f_{\beta\,\mathcal{P}_\beta}(u)$	$g_{\alpha\,\mathcal{P}_\alpha}(v)$	$\frac{1}{\Gamma}\frac{\mathrm{d}\Gamma}{\mathrm{d}m_{ab}^2}$
$(\tau_L^-\ ,\ \tau_R^+)\ (\tau_R^+\ ,\ \tau_L^-)$	$2(1-u)$	$2(1-v)$	$A_a + A_b + A_d + A_e$
$(\tau_L^-\ ,\ \tau_L^+)\ (\tau_R^+\ ,\ \tau_R^-)$	$2(1-u)$	$2v$	$B_a + B_b + B_d + B_e$
$(\tau_R^-\ ,\ \tau_R^+)\ (\tau_L^+\ ,\ \tau_L^-)$	$2u$	$2(1-v)$	$C_a + C_b + C_d + C_e$
$(\tau_R^-\ ,\ \tau_L^+)\ (\tau_L^+\ ,\ \tau_R^-)$	$2u$	$2v$	$D_a + D_b + D_d + D_e$

6.3 Results and discussion

The invariant mass distributions are plotted in Figures 6.4 and 6.5, along with the familiar triangle distribution of a corresponding dilepton cascade (identical for all lepton helicities). Once again we note that there is a factor $2m_{ab}$ relating the m_{ab} distributions plotted in the figures to the m_{ab}^2 distributions given in the tables. All distributions have associated labels of the general form $(\tau_b\,,\,\tau_a)$, specifying the exact tau content of the cascade. Due to the CP invariance of tau decays each distribution represents two possible choices for $(\tau_b\,,\,\tau_a)$.

Studying the plots in Fig. 6.4 we first note that cascades with right-handed taus and left-handed antitaus result in relatively high invariant masses (red distribution). This is what one would expect as the scalar (a, b) is primarily emitted along the tau direction in such decays, leading to large scalar energies. Correspondingly, in decays of left-handed taus and right-handed antitaus the scalar is usually emitted opposite to the tau direction, resulting in a distribution shifted towards lower invariant masses (light blue distribution).

For the two distributions containing taus from both 'categories' mentioned above, the difference is generally much smaller (yellow and dark blue distributions). Their relative separation is mostly due to the helicity of the highest energy tau as seen from the rest frame of B. Which of the two taus is the most energetic one is given by the mass scenario: In the rest frame of B the energies of τ_b and τ_a are

$$E^B_{\tau_b} \;=\; \frac{m_C^2 - m_B^2 - m_\tau^2}{2m_B} \tag{6.29}$$

$$E^B_{\tau_a} \;=\; \frac{m_B^2 - m_A^2 + m_\tau^2}{2m_B} \tag{6.30}$$

Thus, for mass scenario I we have

$$b_C \;<\; b_B \qquad \Leftrightarrow \qquad m_B^2 \;<\; \frac{1}{2}(m_C^2 + m_A^2) - m_\tau^2 \qquad \Leftrightarrow \qquad E^B_{\tau_a} \;<\; E^B_{\tau_b} \tag{6.31}$$

while mass scenario II gives

$$b_C \;>\; b_B \qquad \Leftrightarrow \qquad m_B^2 \;>\; \frac{1}{2}(m_C^2 + m_A^2) - m_\tau^2 \qquad \Leftrightarrow \qquad E^B_{\tau_a} \;>\; E^B_{\tau_b} \tag{6.32}$$

This explains why the yellow and dark blue distributions 'switch places' when going from low to high values of m_B. The relative difference between these two distributions

vanishes when both $(m_C - m_B)$ and $(m_B - m_A)$ are large compared to m_τ, as can be seen in Fig. 6.4(b)

In order to illustrate the behaviour of the analytical expressions in all four m_{ab} ranges, a set of masses where all mass differences are small has been chosen for Fig. 6.5(a). Finally we note that an unweighted, normalised sum of all four distributions reproduce the result obtained in the spin-0 approximation (Fig. 6.5(b)). Below we give a list of all terms contributing to $\mathrm{d}\Gamma/\,\mathrm{d}m_{ab}^2$, as referred to in Tables 6.1 and 6.2.

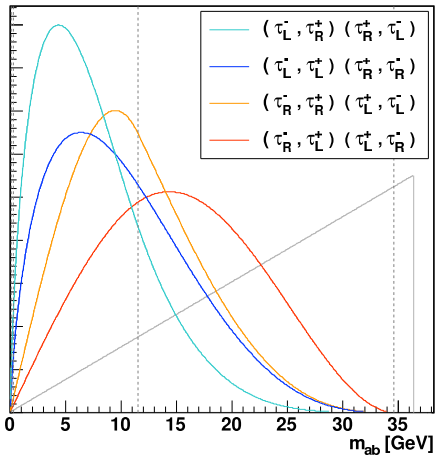

(a) $m_C = 180,\ m_B = 100,\ m_A = 97$ (GeV)
scenario I

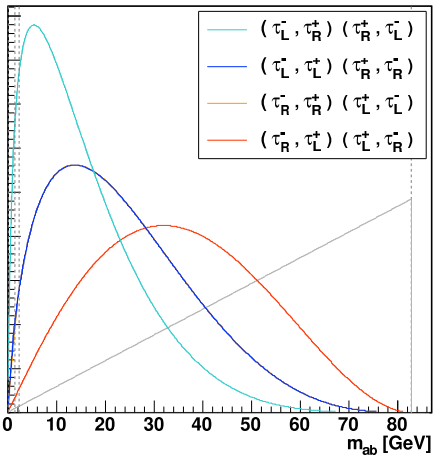

(b) $m_C = 180,\ m_B = 135,\ m_A = 97$ (GeV)
scenario I

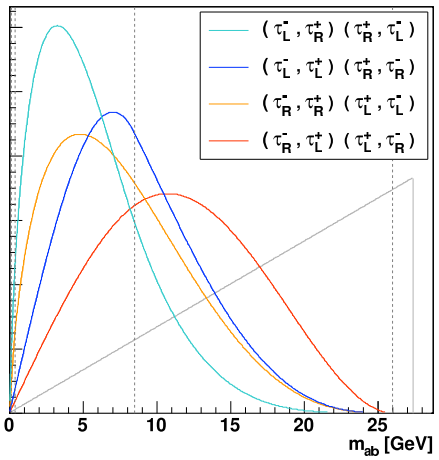

(c) $m_C = 180,\ m_B = 177,\ m_A = 97$ (GeV)
scenario II

Figure 6.4: $(1/\Gamma)(\,\mathrm{d}\Gamma/\,\mathrm{d}m_{ab})$ plotted for three different sets of masses. The labels specifying the tau content are of the general form $(\tau_b\,,\,\tau_a)$ and L/R indices refer to helicity. Dotted vertical lines mark the points where the functional form of the distributions change. In (b) the yellow and dark blue distributions are almost identical. All plots use $m_\tau = 1.78$ GeV.

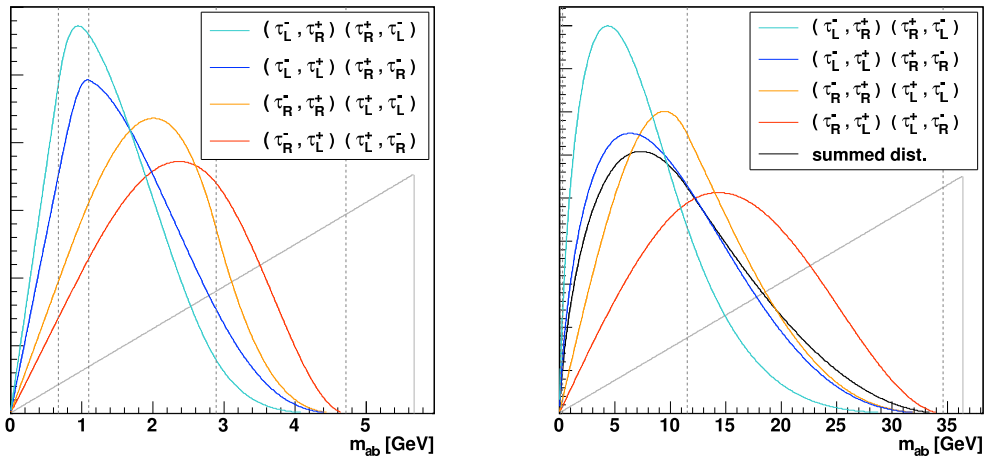

(a) $m_C = 180,\ m_B = 176,\ m_A = 174$ (GeV) scenario I

(b) $m_C = 180,\ m_B = 100,\ m_A = 97$ (GeV) scenario I

Figure 6.5: In (a) the set of masses is chosen such that the general behaviour of $(1/\Gamma)(\,\mathrm{d}\Gamma/\,\mathrm{d}m_{ab})$ for all four m_{ab} ranges is illustrated. In (b) an unweighted sum of the four helicity dependent distributions is included (black), reproducing the spin-0 distribution. Both plots use $m_\tau = 1.78$ GeV.

$$
\begin{aligned}
A_a \;=\; \frac{4}{M^2}\Bigg\{ \quad & (b_B+1)(b_C+1)\ln\!\left(\frac{b_B+1}{b_B}\right)\ln\!\left(\frac{b_C+1}{b_C}\right) \\
& -\,(b_B+1)\ln\!\left(\frac{b_B+1}{b_B}\right) \;-\; (b_C+1)\ln\!\left(\frac{b_C+1}{b_C}\right) \;+\; 1 \quad \Bigg\}
\end{aligned}
$$

$$
\text{for}\;\begin{cases} 0 \;<\; m_{ab}^2 \;<\; b_B\, b_C\, M^2 & \text{scenario I} \\ 0 \;<\; m_{ab}^2 \;<\; b_B\, b_C\, M^2 & \text{scenario II} \end{cases}
$$

$$
\begin{aligned}
A_b \;=\; \frac{4}{M^2}\Bigg\{ \quad & \frac{1}{2}(b_B+1)(b_C+1)\left(\left[\ln\!\left(\frac{b_B+1}{b_B}\right)\right]^2 - \left[\ln\!\left(\frac{(b_B+1)b_C M^2}{m_{ab}^2}\right)\right]^2\right) \\
& +\,(b_B+1)(b_C+1)\ln\!\left(\frac{b_B+1}{b_B}\right)\ln\!\left(\frac{b_B(b_C+1)M^2}{m_{ab}^2}\right) \\
& +\left(\frac{m_{ab}^2}{M^2}+2b_Bb_C+b_B+b_C\right)\ln\!\left(\frac{b_Bb_CM^2}{m_{ab}^2}\right) \\
& -\,(b_C+1)\ln\!\left(\frac{b_C+1}{b_C}\right) \;-\; (b_B+1)\ln\!\left(\frac{b_B+1}{b_B}\right) \\
& +\left(\frac{m_{ab}^2}{b_Bb_CM^2}-1\right)\left(3b_Bb_C+b_B+b_C\right) \;+\; 1 \quad \Bigg\}
\end{aligned}
$$

$$
\text{for}\;\begin{cases} b_B\, b_C\, M^2 \;<\; m_{ab}^2 \;<\; (b_B+1)\, b_C\, M^2 & \text{scenario I} \\ b_B\, b_C\, M^2 \;<\; m_{ab}^2 \;<\; b_B\, (b_C+1)\, M^2 & \text{scenario II} \end{cases}
$$

$$
\begin{aligned}
A_c \;=\; \frac{4}{M^2}\Bigg\{ \quad & \frac{1}{2}(b_B+1)(b_C+1)\left[\ln\!\left(\frac{b_B+1}{b_B}\right)\right]^2 \\
& +\,(b_B+1)(b_C+1)\ln\!\left(\frac{b_B+1}{b_B}\right)\ln\!\left(\frac{b_B(b_C+1)M^2}{m_{ab}^2}\right) \\
& -\,(b_C+1)\ln\!\left(\frac{b_B(b_C+1)M^2}{m_{ab}^2}\right) \\
& -\left(\frac{m_{ab}^2}{M^2}+2(b_B+1)(b_C+1)\right)\ln\!\left(\frac{b_B+1}{b_B}\right) \\
& +\,\frac{m_{ab}^2}{b_BM^2} \;+\; 2(b_C+1) \quad \Bigg\}
\end{aligned}
$$

$$
\text{for}\;\Big\{\; (b_B+1)\, b_C\, M^2 \;<\; m_{ab}^2 \;<\; b_B\, (b_C+1)\, M^2 \quad \text{scenario I}
$$

$$
\begin{aligned}
A_d \;=\; \frac{4}{M^2}\Bigg\{ \quad & \frac{1}{2}(b_B+1)(b_C+1)\left[\ln\!\left(\frac{(b_B+1)(b_C+1)M^2}{m_{ab}^2}\right)\right]^2 \\
& - \frac{1}{2}(b_B+1)(b_C+1)\left[\ln\!\left(\frac{(b_B+1)b_C M^2}{m_{ab}^2}\right)\right]^2 \\
& - \left(\frac{m_{ab}^2}{M^2} + 2b_B b_C + b_B + 2b_C + 1\right)\ln\!\left(\frac{b_C+1}{b_C}\right) \\
& - (b_B+1)\ln\!\left(\frac{(b_B+1)(b_C+1)M^2}{m_{ab}^2}\right) \\
& + \frac{m_{ab}^2}{b_C M^2} \;+\; 2(b_B+1) \quad \Bigg\}
\end{aligned}
$$

$$
\text{for} \left\{ b_B\,(b_C+1)\,M^2 \;<\; m_{ab}^2 \;<\; (b_B+1)\,b_C\,M^2 \quad \text{scenario II} \right.
$$

$$
\begin{aligned}
A_e \;=\; \frac{4}{M^2}\Bigg\{ \quad & \frac{1}{2}(b_B+1)(b_C+1)\left[\ln\!\left(\frac{(b_B+1)(b_C+1)M^2}{m_{ab}^2}\right)\right]^2 \\
& - \left(\frac{m_{ab}^2}{M^2} + 2(b_B+1)(b_C+1)\right)\ln\!\left(\frac{(b_B+1)(b_C+1)M^2}{m_{ab}^2}\right) \\
& + 3\left((b_B+1)(b_C+1) - \frac{m_{ab}^2}{M^2}\right) \quad \Bigg\}
\end{aligned}
$$

$$
\text{for} \begin{cases} b_B\,(b_C+1)\,M^2 \;<\; m_{ab}^2 \;<\; (b_B+1)\,(b_C+1)\,M^2 & \text{scenario I} \\ (b_B+1)\,b_C\,M^2 \;<\; m_{ab}^2 \;<\; (b_B+1)\,(b_C+1)\,M^2 & \text{scenario II} \end{cases}
$$

$$
\begin{aligned}
B_a \;=\; \frac{4}{M^2}\Bigg\{ \quad & (b_C+1)\ln\!\left(\frac{b_C+1}{b_C}\right) \;+\; b_B\ln\!\left(\frac{b_B+1}{b_B}\right) \\
& - b_B(b_C+1)\ln\!\left(\frac{b_B+1}{b_B}\right)\ln\!\left(\frac{b_C+1}{b_C}\right) \;-\; 1 \quad \Bigg\}
\end{aligned}
$$

$$
\text{for}\ \begin{cases} 0 \;<\; m_{ab}^2 \;<\; b_B\, b_C\, M^2 & \text{scenario I} \\ 0 \;<\; m_{ab}^2 \;<\; b_B\, b_C\, M^2 & \text{scenario II} \end{cases}
$$

$$
\begin{aligned}
B_b \;=\; \frac{4}{M^2}\Bigg\{ \quad & \frac{1}{2}b_B(b_C+1)\left(\left[\ln\!\left(\frac{(b_B+1)b_C M^2}{m_{ab}^2}\right)\right]^2 - \left[\ln\!\left(\frac{b_B+1}{b_B}\right)\right]^2\right) \\
& - b_B(b_C+1)\ln\!\left(\frac{b_B+1}{b_B}\right)\ln\!\left(\frac{b_B(b_C+1)M^2}{m_{ab}^2}\right) \\
& - \left(\frac{m_{ab}^2}{M^2}+2b_Bb_C+b_B\right)\ln\!\left(\frac{b_Bb_CM^2}{m_{ab}^2}\right) \\
& + (b_C+1)\ln\!\left(\frac{b_C+1}{b_C}\right) \;+\; b_B\ln\!\left(\frac{b_B+1}{b_B}\right) \\
& + 3\left(b_Bb_C-\frac{m_{ab}^2}{M^2}\right) \;-\; \frac{m_{ab}^2}{b_CM^2} \;+\; b_B \;-\; 1 \quad \Bigg\}
\end{aligned}
$$

$$
\text{for}\ \begin{cases} b_B\, b_C\, M^2 \;<\; m_{ab}^2 \;<\; (b_B+1)\, b_C\, M^2 & \text{scenario I} \\ b_B\, b_C\, M^2 \;<\; m_{ab}^2 \;<\; b_B\,(b_C+1)\, M^2 & \text{scenario II} \end{cases}
$$

$$
\begin{aligned}
B_c \;=\; \frac{4}{M^2}\Bigg\{ & -\frac{1}{2}b_B(b_C+1)\left[\ln\!\left(\frac{b_B+1}{b_B}\right)\right]^2 \\
& - b_B(b_C+1)\ln\!\left(\frac{b_B+1}{b_B}\right)\ln\!\left(\frac{b_B(b_C+1)M^2}{m_{ab}^2}\right) \\
& + (b_C+1)\ln\!\left(\frac{b_B(b_C+1)M^2}{m_{ab}^2}\right) \\
& + \left(\frac{m_{ab}^2}{M^2}+2b_Bb_C+2b_B+b_C+1\right)\ln\!\left(\frac{b_B+1}{b_B}\right) \\
& - \frac{m_{ab}^2}{(b_B+1)M^2} \;-\; 2(b_C+1) \quad \Bigg\}
\end{aligned}
$$

$$
\text{for}\ \left\{ (b_B+1)\, b_C\, M^2 \;<\; m_{ab}^2 \;<\; b_B\,(b_C+1)\, M^2 \quad \text{scenario I} \right.
$$

$$
\begin{aligned}
B_d \;=\; \frac{4}{M^2}\Bigg\{ \quad & \frac{1}{2}b_B(b_C+1)\left[\ln\!\left(\frac{(b_B+1)b_C M^2}{m_{ab}^2}\right)\right]^2 \\
& -\frac{1}{2}b_B(b_C+1)\left[\ln\!\left(\frac{(b_B+1)(b_C+1)M^2}{m_{ab}^2}\right)\right]^2 \\
& +\left(\frac{m_{ab}^2}{M^2}+2b_Bb_C+b_B+b_C+1\right)\ln\!\left(\frac{b_C+1}{b_C}\right) \\
& +b_B\ln\!\left(\frac{(b_B+1)(b_C+1)M^2}{m_{ab}^2}\right) \\
& -\frac{m_{ab}^2}{b_CM^2}\;-\;2b_B\;-\;1 \quad \Bigg\}
\end{aligned}
$$

$$
\text{for}\;\Big\{\; b_B\,(b_C+1)\,M^2 \;<\; m_{ab}^2 \;<\; (b_B+1)\,b_C\,M^2 \quad \text{scenario II}
$$

$$
\begin{aligned}
B_e \;=\; \frac{4}{M^2}\Bigg\{ & -\frac{1}{2}b_B(b_C+1)\left[\ln\!\left(\frac{(b_B+1)(b_C+1)M^2}{m_{ab}^2}\right)\right]^2 \\
& +\left(\frac{m_{ab}^2}{M^2}+2b_Bb_C+2b_B+b_C+1\right)\ln\!\left(\frac{(b_B+1)(b_C+1)M^2}{m_{ab}^2}\right) \\
& +2\Big(\frac{m_{ab}^2}{M^2}-(b_B+1)(b_C+1)\Big)\;+\;b_B\Big(\frac{m_{ab}^2}{(b_B+1)M^2}-(b_C+1)\Big) \quad \Bigg\}
\end{aligned}
$$

$$
\text{for}\;\begin{cases} b_B\,(b_C+1)\,M^2 \;<\; m_{ab}^2 \;<\; (b_B+1)\,(b_C+1)\,M^2 & \text{scenario I} \\ (b_B+1)\,b_C\,M^2 \;<\; m_{ab}^2 \;<\; (b_B+1)\,(b_C+1)\,M^2 & \text{scenario II} \end{cases}
$$

$$
\begin{aligned}
C_a \;=\; \frac{4}{M^2}\Bigg\{ & \;(b_B+1)\ln\!\left(\frac{b_B+1}{b_B}\right) \;+\; b_C\ln\!\left(\frac{b_C+1}{b_C}\right) \\
& -(b_B+1)b_C\ln\!\left(\frac{b_B+1}{b_B}\right)\ln\!\left(\frac{b_C+1}{b_C}\right) \;-\; 1 \quad \Bigg\}
\end{aligned}
$$

$$
\text{for}\;\begin{cases} 0 \;<\; m_{ab}^2 \;<\; b_B\, b_C\, M^2 & \text{scenario I} \\ 0 \;<\; m_{ab}^2 \;<\; b_B\, b_C\, M^2 & \text{scenario II} \end{cases}
$$

$$
\begin{aligned}
C_b \;=\; \frac{4}{M^2}\Bigg\{ & \;\frac{1}{2}(b_B+1)b_C\left(\left[\ln\!\left(\frac{(b_B+1)b_C M^2}{m_{ab}^2}\right)\right]^2 - \left[\ln\!\left(\frac{b_B+1}{b_B}\right)\right]^2\right) \\
& -(b_B+1)b_C\ln\!\left(\frac{b_B+1}{b_B}\right)\ln\!\left(\frac{b_B(b_C+1)M^2}{m_{ab}^2}\right) \\
& -\left(\frac{m_{ab}^2}{M^2}+2b_Bb_C+b_C\right)\ln\!\left(\frac{b_Bb_CM^2}{m_{ab}^2}\right) \\
& +(b_B+1)\ln\!\left(\frac{b_B+1}{b_B}\right) \;+\; b_C\ln\!\left(\frac{b_C+1}{b_C}\right) \\
& +3\left(b_Bb_C-\frac{m_{ab}^2}{M^2}\right) \;-\; \frac{m_{ab}^2}{b_BM^2} \;+\; b_C \;-\; 1 \quad \Bigg\}
\end{aligned}
$$

$$
\text{for}\;\begin{cases} b_B\, b_C\, M^2 \;<\; m_{ab}^2 \;<\; (b_B+1)\, b_C\, M^2 & \text{scenario I} \\ b_B\, b_C\, M^2 \;<\; m_{ab}^2 \;<\; b_B\,(b_C+1)\, M^2 & \text{scenario II} \end{cases}
$$

$$
\begin{aligned}
C_c \;=\; \frac{4}{M^2}\Bigg\{ & -\frac{1}{2}(b_B+1)b_C\left[\ln\!\left(\frac{b_B+1}{b_B}\right)\right]^2 \\
& -(b_B+1)b_C\ln\!\left(\frac{b_B+1}{b_B}\right)\ln\!\left(\frac{b_B(b_C+1)M^2}{m_{ab}^2}\right) \\
& +b_C\ln\!\left(\frac{b_B(b_C+1)M^2}{m_{ab}^2}\right) \\
& +\left(\frac{m_{ab}^2}{M^2}+2b_Bb_C+b_B+2b_C+1\right)\ln\!\left(\frac{b_B+1}{b_B}\right) \\
& -\frac{m_{ab}^2}{b_BM^2} \;-\; 2b_C \;-\; 1 \quad \Bigg\}
\end{aligned}
$$

$$
\text{for}\;\Big\{\; (b_B+1)\, b_C\, M^2 \;<\; m_{ab}^2 \;<\; b_B\,(b_C+1)\, M^2 \quad \text{scenario I}
$$

$$
\begin{aligned}
C_d \;=\; \frac{4}{M^2}\Bigg\{ \quad & \frac{1}{2}(b_B+1)b_C\left[\ln\!\left(\frac{(b_B+1)b_C M^2}{m_{ab}^2}\right)\right]^2 \\
& -\frac{1}{2}(b_B+1)b_C\left[\ln\!\left(\frac{(b_B+1)(b_C+1)M^2}{m_{ab}^2}\right)\right]^2 \\
& +\left(\frac{m_{ab}^2}{M^2}+2b_Bb_C+2b_C\right)\ln\!\left(\frac{b_C+1}{b_C}\right) \\
& +(b_B+1)\ln\!\left(\frac{(b_B+1)(b_C+1)M^2}{m_{ab}^2}\right) \\
& -\frac{m_{ab}^2}{(b_C+1)M^2} \;-\; 2(b_B+1) \quad \Bigg\}
\end{aligned}
$$

$$
\text{for } \Big\{\; b_B\,(b_C+1)\,M^2 \;<\; m_{ab}^2 \;<\; (b_B+1)\,b_C\,M^2 \quad \text{scenario II}
$$

$$
\begin{aligned}
C_e \;=\; \frac{4}{M^2}\Bigg\{ & -\frac{1}{2}(b_B+1)b_C\left[\ln\!\left(\frac{(b_B+1)(b_C+1)M^2}{m_{ab}^2}\right)\right]^2 \\
& +\left(\frac{m_{ab}^2}{M^2}+2b_Bb_C+b_B+2b_C+1\right)\ln\!\left(\frac{(b_B+1)(b_C+1)M^2}{m_{ab}^2}\right) \\
& +2\left(\frac{m_{ab}^2}{M^2}-(b_B+1)(b_C+1)\right) \;+\; b_C\left(\frac{m_{ab}^2}{(b_C+1)M^2}-(b_B+1)\right) \quad \Bigg\}
\end{aligned}
$$

$$
\text{for } \begin{cases} b_B\,(b_C+1)\,M^2 \;<\; m_{ab}^2 \;<\; (b_B+1)\,(b_C+1)\,M^2 & \text{scenario I} \\ (b_B+1)\,b_C\,M^2 \;<\; m_{ab}^2 \;<\; (b_B+1)\,(b_C+1)\,M^2 & \text{scenario II} \end{cases}
$$

$$
\begin{aligned}
D_a \;=\; \frac{4}{M^2}\Bigg\{ \;& b_B b_C \ln\!\left(\frac{b_B+1}{b_B}\right)\ln\!\left(\frac{b_C+1}{b_C}\right) \\
& - b_B \ln\!\left(\frac{b_B+1}{b_B}\right) \;-\; b_C \ln\!\left(\frac{b_C+1}{b_C}\right) \;+\; 1 \;\Bigg\}
\end{aligned}
$$

$$
\text{for } \begin{cases} 0 \;<\; m_{ab}^2 \;<\; b_B\, b_C\, M^2 & \text{scenario I} \\ 0 \;<\; m_{ab}^2 \;<\; b_B\, b_C\, M^2 & \text{scenario II} \end{cases}
$$

$$
\begin{aligned}
D_b \;=\; \frac{4}{M^2}\Bigg\{ \;& \frac{1}{2} b_B b_C \left(\left[\ln\!\left(\frac{b_B+1}{b_B}\right)\right]^2 - \left[\ln\!\left(\frac{(b_B+1)b_C M^2}{m_{ab}}\right)\right]^2 \right) \\
& + b_B b_C \ln\!\left(\frac{b_B+1}{b_B}\right)\ln\!\left(\frac{b_B(b_C+1)M^2}{m_{ab}^2}\right) \\
& + \left(\frac{m_{ab}^2}{M^2} + 2b_B b_C\right)\ln\!\left(\frac{b_B b_C M^2}{m_{ab}^2}\right) \\
& - b_B \ln\!\left(\frac{b_B+1}{b_B}\right) \;-\; b_C \ln\!\left(\frac{b_C+1}{b_C}\right) \\
& + 3\left(\frac{m_{ab}^2}{M^2} \;-\; b_B b_C\right) \;+\; 1 \;\Bigg\}
\end{aligned}
$$

$$
\text{for } \begin{cases} b_B\, b_C\, M^2 \;<\; m_{ab}^2 \;<\; (b_B+1)\, b_C\, M^2 & \text{scenario I} \\ b_B\, b_C\, M^2 \;<\; m_{ab}^2 \;<\; b_B\, (b_C+1)\, M^2 & \text{scenario II} \end{cases}
$$

$$
\begin{aligned}
D_c \;=\; \frac{4}{M^2}\Bigg\{ \;& \frac{1}{2} b_B b_C \left[\ln\!\left(\frac{b_B+1}{b_B}\right)\right]^2 \\
& + b_B b_C \ln\!\left(\frac{b_B+1}{b_B}\right)\ln\!\left(\frac{b_B(b_C+1)M^2}{m_{ab}^2}\right) \\
& - b_C \ln\!\left(\frac{b_B(b_C+1)M^2}{m_{ab}^2}\right) \\
& - \left(\frac{m_{ab}^2}{M^2} + 2b_B b_C + b_B + b_C\right)\ln\!\left(\frac{b_B+1}{b_B}\right) \\
& + \frac{m_{ab}^2}{(b_B+1)M^2} \;+\; 2b_C \;+\; 1 \;\Bigg\}
\end{aligned}
$$

$$
\text{for } \left\{ \; (b_B+1)\, b_C\, M^2 \;<\; m_{ab}^2 \;<\; b_B\, (b_C+1)\, M^2 \quad \text{scenario I} \right.
$$

$$
\begin{aligned}
D_d \;=\; \frac{4}{M^2}\Bigg\{ \quad & \frac{1}{2} b_B b_C \left[\ln\!\left(\frac{(b_B+1)(b_C+1)M^2}{m_{ab}^2}\right)\right]^2 \\
& - \frac{1}{2} b_B b_C \left[\ln\!\left(\frac{(b_B+1) b_C M^2}{m_{ab}^2}\right)\right]^2 \\
& - \left(\frac{m_{ab}^2}{M^2} + 2 b_B b_C + b_C\right) \ln\!\left(\frac{b_C+1}{b_C}\right) \\
& - b_B \ln\!\left(\frac{(b_B+1)(b_C+1)M^2}{m_{ab}^2}\right) \\
& + \frac{m_{ab}^2}{(b_C+1)M^2} \;+\; 2 b_B \;+\; 1 \quad \Bigg\}
\end{aligned}
$$

$$
\text{for} \left\{ b_B\,(b_C+1)\,M^2 \;<\; m_{ab}^2 \;<\; (b_B+1)\,b_C\,M^2 \quad \text{scenario II} \right.
$$

$$
\begin{aligned}
D_e \;=\; \frac{4}{M^2}\Bigg\{ \quad & \frac{1}{2} b_B b_C \left[\ln\!\left(\frac{(b_B+1)(b_C+1)M^2}{m_{ab}^2}\right)\right]^2 \\
& - \left(\frac{m_{ab}^2}{M^2} + 2 b_B b_C + b_B + b_C\right) \ln\!\left(\frac{(b_B+1)(b_C+1)M^2}{m_{ab}^2}\right) \\
& + \Big(3 b_B b_C + 2 b_B + 2 b_C + 1\Big)\Big(1 - \frac{m_{ab}^2}{(b_B+1)(b_C+1)M^2}\Big) \quad \Bigg\}
\end{aligned}
$$

$$
\text{for} \left\{ \begin{array}{ll}
b_B\,(b_C+1)\,M^2 \;<\; m_{ab}^2 \;<\; (b_B+1)\,(b_C+1)\,M^2 & \text{scenario I} \\
(b_B+1)\,b_C\,M^2 \;<\; m_{ab}^2 \;<\; (b_B+1)\,(b_C+1)\,M^2 & \text{scenario II}
\end{array} \right.
$$

6.4 The limit $\mathbf{m_\tau = 0}$

As for the spin-0 distribution in Section 4.4, taking $m_\tau = 0$ implies

$$\begin{aligned} b_C &= 0 \\ b_B &= 0 \\ M^2 &= \frac{(m_C^2 - m_B^2)(m_B^2 - m_A^2)}{m_B^2} \end{aligned} \tag{6.33}$$

Consequently, the distinction between the two mass scenarios disappears and the m_{ab} range corresponding to integration region e) of the xy plane now covers the entire allowed m_{ab} range

$$0 \,<\, m_{ab} \,<\, M \tag{6.34}$$

That is, only the last terms of the exact distributions (A_e, B_e, C_e, D_e) 'survive' as we take the taus to be massless. Furthermore, as b_B and b_C vanish the two terms B_e and C_e become identical, thus merging two of the four distributions contained in the exact result. When we take the above simplifications into account the helicity dependent m_{ab} distributions reduce to

1. $\left(\tau_b\,,\,\tau_a\right) \;=\; \left(\tau_L^-\,,\,\tau_R^+\right),\,\left(\tau_R^+\,,\,\tau_L^-\right)$

$$\frac{1}{\Gamma}\frac{\mathrm{d}\Gamma}{\mathrm{d}m_{ab}} \;=\; \frac{8\,m_{ab}}{M^2}\left\{\frac{1}{2}\left[\ln\!\left(\frac{M^2}{m_{ab}^2}\right)\right]^2 - \left(2+\frac{m_{ab}^2}{M^2}\right)\ln\!\left(\frac{M^2}{m_{ab}^2}\right) \,+\, 3\left(1-\frac{m_{ab}^2}{M^2}\right)\right\}$$

2. $\left(\tau_b\,,\,\tau_a\right) \;=\; \left(\tau_R^-\,,\,\tau_R^+\right),\,\left(\tau_L^+\,,\,\tau_L^-\right),\,\left(\tau_L^-\,,\,\tau_L^+\right),\,\left(\tau_R^+\,,\,\tau_R^-\right)$

$$\frac{1}{\Gamma}\frac{\mathrm{d}\Gamma}{\mathrm{d}m_{ab}} \;=\; \frac{8\,m_{ab}}{M^2}\left\{\left(1+\frac{m_{ab}^2}{M^2}\right)\ln\!\left(\frac{M^2}{m_{ab}^2}\right) \,+\, 2\left(\frac{m_{ab}^2}{M^2}-1\right)\right\}$$

3. $\left(\tau_b\,,\,\tau_a\right) \;=\; \left(\tau_R^-\,,\,\tau_L^+\right),\,\left(\tau_L^+\,,\,\tau_R^-\right)$

$$\frac{1}{\Gamma}\frac{\mathrm{d}\Gamma}{\mathrm{d}m_{ab}} \;=\; \frac{8\,m_{ab}}{M^2}\left\{\left(1-\frac{m_{ab}^2}{M^2}\right) \,-\, \frac{m_{ab}^2}{M^2}\ln\!\left(\frac{M^2}{m_{ab}^2}\right)\right\}$$

$$\text{for} \quad 0 \,<\, m_{ab}^2 \,<\, M^2$$

In Figures 6.6 and 6.7 these approximate distributions (solid curves) are compared to the exact results (dashed curves). As expected, we see good agreement as long as the mass differences $(m_C - m_B)$ and $(m_B - m_A)$ are not close to m_τ (Fig. 6.6(b)). If either one or both of these mass differences are small, the approximate distributions are enlarged for minimum and maximum m_{ab} values relative to the exact distributions (Figs. 6.6(a), 6.6(c) and 6.7(a)). As discussed in Section 4.4, this effect is due to the energy ranges of particles a and b being expanded when we take $m_\tau = 0$.

Finally, in Fig. 6.7(b) an unweighted sum of the three distributions is included (black) reproducing the spin-0 distribution in the massless tau limit, which we derived in Section 4.4. From comparison with the spin-0 distribution it is evident that the m_{ab} distribution has a strong spin dependence. Even with spins not being measured directly this dependence might still be exploited experimentally, as we comment on in the following section.

6.5 Measuring SUSY mixing parameters

The perhaps most interesting feature of the spin dependent distributions is that as long as the mass differences $(m_C - m_B)$ and $(m_B - m_A)$ make the tau mass negligible, the distribution shapes are independent of m_A, m_B and m_C. (The parameter M only sets the overall scale.) As spins are not observed, a realistic m_{ab} distribution will be a weighted combination of the three approximate distributions given in Section 6.4. With the distribution shapes fixed it is therefore possible to fit an experimental distribution using the weights as parameters. These weights will correspond to the probabilities of producing different tau helicities at the two vertices, which again can be related to the mixing parameters in a general SUSY theory [26, 27].

In order to be more specific we introduce some simplifying notation: First, recall that in the limit of massless taus we may use helicity and chirality interchangeably, keeping in mind that chirality and helicity are of opposite sign for antiparticles. The approximate distributions numbered 1, 2 and 3 in Section 6.4 may therefore be labelled according to tau chiralities as $(L_c\, L_c)$, $(R_c\, L_c\, =\, L_c\, R_c)$ and $(R_c\, R_c)$, respectively. Thus,

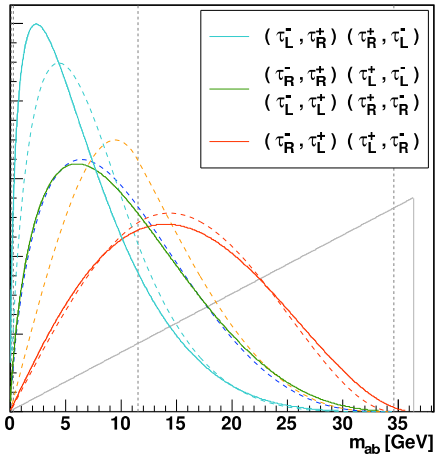

(a) $m_C = 180,\ m_B = 100,\ m_A = 97$ (GeV)
(scenario I)

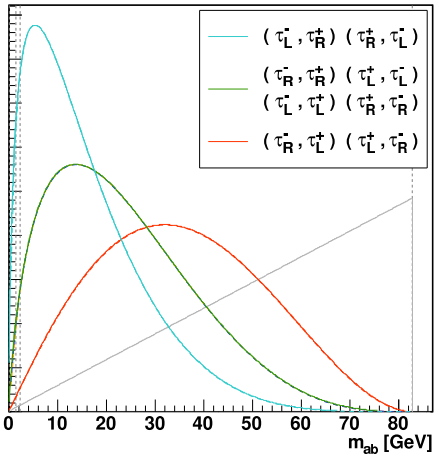

(b) $m_C = 180,\ m_B = 135,\ m_A = 97$ (GeV)
(scenario I)

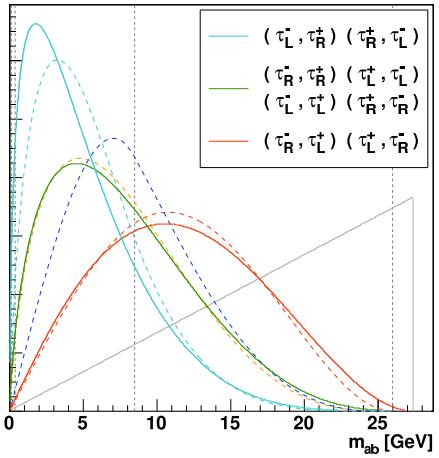

(c) $m_C = 180,\ m_B = 177,\ m_A = 97$ (GeV)
(scenario II)

Figure 6.6: $(1/\Gamma)(\,\mathrm{d}\Gamma/\,\mathrm{d}m_{ab})$ in the limit $m_\tau = 0$ (solid) compared to the exact distributions (dashed). As the taus are assumed massless the yellow and dark blue dashed distributions merge into the solid green distribution. The functional shapes of the solid distributions are independent of the masses m_A, m_B and m_C.

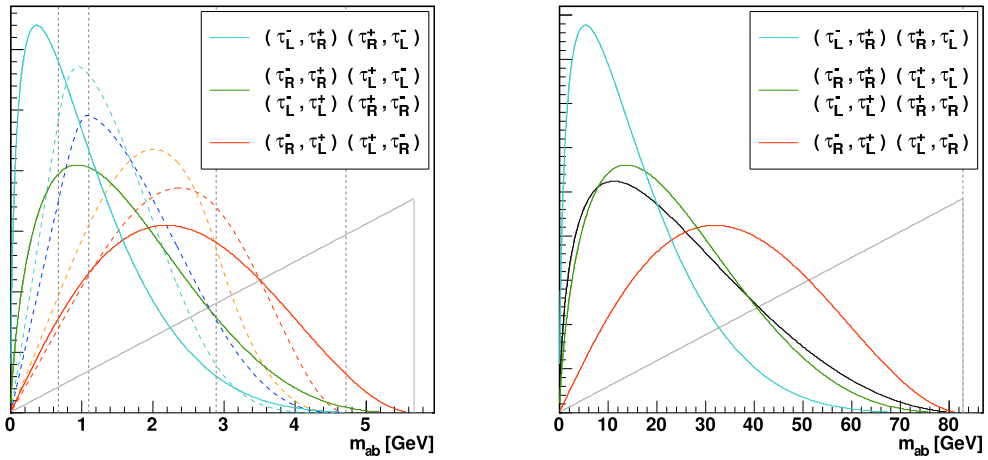

(a) $m_C = 180,\ m_B = 176,\ m_A = 174$ (GeV) (scenario I)

(b) $m_C = 180,\ m_B = 135,\ m_A = 97$ (GeV)

Figure 6.7: $(1/\Gamma)(\mathrm{d}\Gamma/\,\mathrm{d}m_{ab})$ in the limit $m_\tau = 0$. In (b) an unweighted sum of the three helicity dependent distributions is included (black), reproducing the spin-0 distribution in the massless tau limit.

referring to the numbered distributions, we define

$$\textbf{1.} \quad \frac{1}{\Gamma}\frac{\mathrm{d}\Gamma}{\mathrm{d}m_{ab}} \equiv f(m_{ab})_{L_c\,L_c} \qquad \text{(light blue)}$$

$$\textbf{2.} \quad \frac{1}{\Gamma}\frac{\mathrm{d}\Gamma}{\mathrm{d}m_{ab}} \equiv f(m_{ab})_{R_c\,L_c} \qquad \text{(green)}$$

$$\textbf{3.} \quad \frac{1}{\Gamma}\frac{\mathrm{d}\Gamma}{\mathrm{d}m_{ab}} \equiv f(m_{ab})_{R_c\,R_c} \qquad \text{(red)}$$

Second, we denote the probability of producing a right-chiral tau in the first vertex by $\cos^2\beta$, and in the second vertex by $\cos^2\alpha$. Consequently, the probabilities of producing left-chiral taus in the first and second vertices are respectively $\sin^2\beta$ and $\sin^2\alpha$. A general m_{ab} distribution might then be expressed as

$$\begin{aligned} f(m_{ab})_{\mathrm{tot}} \;=\;& \cos^2\beta\,\cos^2\alpha\, f(m_{ab})_{R_c\,R_c} \\ &+ (\cos^2\beta\,\sin^2\alpha + \sin^2\beta\,\cos^2\alpha)\, f(m_{ab})_{R_c\,L_c} \\ &+ \sin^2\beta\,\sin^2\alpha\, f(m_{ab})_{L_c\,L_c} \end{aligned} \tag{6.35}$$

One could in principle fit this function to an observed distribution using α and β as fit parameters. This would measure the probabilities of producing different tau chiralities in the two vertices, which could in turn be translated into measurements of mixing parameters for the stau sector ($\widetilde{\tau}_L$-$\widetilde{\tau}_R$) and neutralino sector ($\widetilde{W}^0$-$\widetilde{B}^0$-$\widetilde{H}^0$) in a general SUSY theory.

Although the idea presented above is simple enough, there are several complications related to performing such a study. In the following we will mention a few of these complicating aspects, referring the reader to [27] for further details. First of all, in an experimental analysis it will be preferable to include all tau decays resulting in a single charged hadron ('one-prong'), not just the two-body decay into a scalar (pion) and a neutrino. The dominant additional contributions will come from tau decays into ρ's and a_1's, with subsequent decays into pions. As ρ and a_1 are vector mesons, this will complicate the relation between the taus' chiralities and the energy spectra of the final state particles. The resulting invariant mass distributions will consequently not be as clearly separated as in Figures 6.6 and 6.7. On the other hand, including additional decay modes results in better statistics that may more than compensate for this decrease in separation.

Second, selection criteria on the transverse momenta of the visible particles will shift the invariant mass distributions towards higher m_{ab} values. Due to the soft energy spectra of particles resulting from left-chiral taus, such criteria will have a greater impact on $f(m_{ab})_{L_c\,L_c}$ compared to $f(m_{ab})_{L_c\,R_c}$ and $f(m_{ab})_{R_c\,R_c}$, and thus reduce the difference between the distributions.

A third complication in performing a fit to an experimentally observed distribution arises due to the poorly defined endpoints of $f(m_{ab})_{L_c\,L_c}$, $f(m_{ab})_{L_c\,R_c}$ and $f(m_{ab})_{R_c\,R_c}$. With the endpoint being difficult to determine experimentally, it may not be feasible to use it to anchor the theoretical distributions. In [27] a solution is proposed where one exploits the fact that the common endpoint (M) of the theoretical distributions is (for each distribution) uniquely determined by the position of the peak. As the peak should be well defined in an experimental distribution, one can define rescaled theoretical distributions that all have their peaks located at the observed position while their relative endpoints are allowed to vary. By using these rescaled distributions one can perform the fit without prior knowledge of the endpoint position. However, as

this rescaling procedure must reproduce the total area of the observed distribution, the total number of observed events must be well understood.

Chapter 7

Conclusion

Supersymmetry has for many years been regarded as one of the most promising theories for physics beyond the Standard Model. With the experiments at the LHC up and running, the question of whether supersymmetry is manifest at the TeV scale may soon be settled. If supersymmetric particles are detected, the next step will be to determine masses and other parameters as precisely as possible. One way this can be achieved is by extracting information from invariant mass distributions of the visible particles in supersymmetric cascade decays. In this thesis, shape formulas have been derived for distributions resulting from cascades with decaying taus in the final state.

In Chapter 4 the ditau cascade

$$\widetilde{\chi}_2^0 \;\rightarrow\; \tau_n^{\pm}\,\widetilde{\tau}^{\mp} \;\rightarrow\; (\pi_n^{\pm}\,\nu)\,(\tau_f^{\mp}\,\widetilde{\chi}_1^0) \;\rightarrow\; \pi_n^{\pm}\,\nu\,\pi_f^{\mp}\,\nu\,\widetilde{\chi}_1^0 \tag{7.1}$$

was considered.[1] An analytical expression for the $m_{\pi\pi}$ distribution resulting from phase space alone was derived. Due to the energy lost to the neutrinos, the $m_{\pi\pi}$ distribution is rounded and weighted towards lower invariant mass values relative to the dilepton triangle distribution. By comparison with the distribution obtained by setting $m_\tau = 0$, the effect of non-zero tau masses was shown only to be significant for scenarios where $(m_{\widetilde{\chi}_2^0} - m_{\widetilde{\tau}})$ or $(m_{\widetilde{\tau}} - m_{\widetilde{\chi}_1^0})$ are close to m_τ. Including non-zero tau masses leads to a slightly narrower distribution due to a more restricted range of allowed pion energies. The $m_{\pi\pi}$ distribution might seem unsuited for endpoint measurements due its slow decrease at high invariant mass values. However, with negligible tau masses

[1] We now return to a notation in terms of particle and sparticle labels rather than the simplified notation used for the derivations in Chapters 4 – 6.

the distribution shape is fixed, implying that the necessary information can be obtained from other, more distinct features of the distribution (e.g. the maximum).

In Chapter 5 we studied the extended ditau cascade

$$\widetilde{q} \;\rightarrow\; q\,\widetilde{\chi}_2^0 \;\rightarrow\; q\,\tau_n^{\pm}\,\widetilde{\tau}^{\mp} \;\rightarrow\; q\,(\pi_n^{\pm}\,\nu)\,(\tau_f^{\mp}\,\widetilde{\chi}_1^0) \;\rightarrow\; q\,\pi_n^{\pm}\,\nu\,\pi_f^{\mp}\,\nu\,\widetilde{\chi}_1^0 \tag{7.2}$$

We derived a shape formula for the distribution of the invariant mass variable m_{high}, defined in (5.3). As in Chapter 4, the effects of particle spins were ignored. Due to the compositeness of m_{high}, the resulting distribution exhibits substantial structure, with the shape depending strongly on the two mass differences $(m_{\widetilde{\chi}_2^0} - m_{\widetilde{\tau}})$ and $(m_{\widetilde{\tau}} - m_{\widetilde{\chi}_1^0})$. This is analogous to the corresponding distribution for the extended dilepton cascade [24]. As a consistency check, the m_{high} distribution was compared to the shapes of the underlying $m_{q\pi_n}$ and $m_{q\pi_f}$ distributions. For intermediate to low values of $m_{\widetilde{\tau}}$, relative to the kinematically allowed range $(m_{\widetilde{\chi}_1^0}, m_{\widetilde{\chi}_2^0})$, the endpoint of the m_{high} distribution is quite pronounced. For larger $m_{\widetilde{\tau}}$ values, a 'foot'-like structure close to the endpoint is manifest. The mass scenarios for which this distribution foot is evident were identified. Finally, and not surprisingly, non-zero tau masses were found to have a nearly vanishing impact on the distribution shape as long as not *both* $(m_{\widetilde{\chi}_2^0} - m_{\widetilde{\tau}})$ and $(m_{\widetilde{\tau}} - m_{\widetilde{\chi}_1^0})$ are close to m_τ.

For Chapter 6 we returned to the cascade in (7.1), but this time incorporating the effects of particle spins. Shape formulas were derived for the four different $m_{\pi\pi}$ distributions corresponding to the four possible combinations of tau helicities. Except for the two distributions corresponding to both taus having the same helicity, the distribution shapes were found to be clearly separated, showing a strong dependence on the tau helicity configuration. Further, it was verified that an unweighted sum of the four distributions reproduces the spin-independent distribution derived in Chapter 4. In the limit of negligible tau masses (when neither $(m_{\widetilde{\chi}_2^0} - m_{\widetilde{\tau}})$ nor $(m_{\widetilde{\tau}} - m_{\widetilde{\chi}_1^0})$ are close to m_τ) the two least separated distributions merge, leaving a total of three clearly distinct distribution shapes. These distributions seem to be in good agreement with corresponding distributions shown in [26]. Similar to what we found in Chapter 4, the distribution shapes are fixed in the limit of massless taus.

The strong spin dependence in ditau cascades is a complicating aspect from the viewpoint of mass measurements. On the other hand, this dependence may be exploited

to extract information on the mixing parameters of the stau and gaugino sectors, as shown in [26, 27].

The work presented here can clearly be extended in both the theoretical and the experimental direction: On the theoretical side, shape formulas for the m_{low} and $m_{q\pi\pi}$ distributions can be derived. When considering phase space alone, a derivation of the m_{low} distribution will follow in exact analogy with the derivation of m_{high} in Chapter 5. Further, spin effects should be taken into account for all distributions. The fact that the m_{high} distribution of Chapter 5 is nearly unaffected by non-zero tau masses, indicates that subsequent derivations safely can be performed in the limit of $m_\tau = 0$. Although conceptually straightforward, the derivation of spin-dependent m_{high}, m_{low} and $m_{q\pi\pi}$ distributions may become quite involved due to the amount of bookkeeping necessary to cover all integration regions for all possible helicity combinations. Furthermore, it should be possible to derive a 'threshold version' of the $m_{q\pi\pi}$ distribution (a $m_{q\pi\pi}$ distribution including arbitrary selection criteria on the m_{ll} value), as was done for the extended dilepton cascade in [25].

From an experimental point of view, the most important extension would be to compare the derived shapes to simulated data, and further investigate to what extent the theoretical and experimental distributions will differ due to selection criteria, detector effects, combinatorial background and other limiting factors. Additionally, the potential for extracting sparticle mass information from complete distribution fits should be studied, similar to what was done in [22] for the extended dilepton cascade.

Appendix A

The $\mathbf{m_{ac}}$ and $\mathbf{m_{bc}}$ Distributions in the Spin-0 Approximation

During the derivation of the m_{high} distribution in Chapter 5 we found that the invariant masses m_{ac} and m_{bc} can be expressed as

$$m_{ac}^2 \;=\; \big[a_C - (b_C + v)\big]\,(b_B + u)\,w\,M^2\,, \qquad 0 \;\leq\; (u, v, w) \;\leq\; 1 \tag{A.1}$$

$$m_{bc}^2 \;=\; a_B\,(b_C + v)\,t\,M^2\,, \qquad 0 \;\leq\; (t, v) \;\leq\; 1 \tag{A.2}$$

The angular variables t, u, v and w are defined in (5.13) and (5.21), while the mass parameters a_B, a_C, b_B, b_C and M^2 are defined in (5.14). Making use of the spin-0 approximation in which t, u, v and w all have flat distributions, the analytical expressions for $\mathrm{d}\Gamma/\,\mathrm{d}m_{ac}$ and $\mathrm{d}\Gamma/\,\mathrm{d}m_{bc}$ can be obtained in a way completely analogous to the derivation of $\mathrm{d}\Gamma/\,\mathrm{d}m_{ab}$ in Chapter 4. In the following sections we will therefore simply state the analytical results along with the simplified expressions found for the limit $m_\tau = 0$.

A.1 The $\mathbf{m_{ac}}$ distribution in the spin-0 approximation

For the m_{ac} distribution we must differentiate between the two mass scenarios

$$b_B \;<\; a_C - (b_C + 1) \qquad \text{Scenario I}$$

$$b_B \;>\; a_C - (b_C + 1) \qquad \text{Scenario II}$$

Here scenario I is the most 'common' as scenario II only applies if m_B is very close to $(m_A + m_\tau)$.

A. The m_{ac} and m_{bc} Distributions

Scenario I

$$\frac{1}{\Gamma}\frac{\mathrm{d}\Gamma}{\mathrm{d}m_{ac}} = \begin{cases} \frac{m_{ac}}{M^2}\left\{ 2\ln\left(\frac{b_B+1}{b_B}\right)\ln\left(\frac{a_C-b_C}{a_C-(b_C+1)}\right)\right\} & \text{for (1)} \\ \frac{m_{ac}}{M^2}\left\{ \left[\ln\left(\frac{a_C-b_C}{a_C-(b_C+1)}\right)\right]^2 - \left[\ln\left(\frac{(a_C-b_C)b_BM^2}{m_{ac}^2}\right)\right]^2 \right. & \\ \qquad \left. + \; 2\ln\left(\frac{(a_C-(b_C+1))(b_B+1)M^2}{m_{ac}^2}\right)\ln\left(\frac{a_C-b_C}{a_C-(b_C+1)}\right)\right\} & \text{for (2)} \\ \frac{m_{ac}}{M^2}\left\{ \left[\ln\left(\frac{a_C-b_C}{a_C-(b_C+1)}\right)\right]^2 \right. & \\ \qquad \left. + \; 2\ln\left(\frac{(a_C-(b_C+1))(b_B+1)M^2}{m_{ac}^2}\right)\ln\left(\frac{a_C-b_C}{a_C-(b_C+1)}\right)\right\} & \text{for (3)} \\ \frac{m_{ac}}{M^2}\left\{ \left[\ln\left(\frac{(a_C-b_C)(b_B+1)M^2}{m_{ac}^2}\right)\right]^2\right\} & \text{for (4)} \end{cases}$$

$$\begin{array}{lrcccl} (1) & 0 & < & m_{ac} & < & \sqrt{(a_C-(b_C+1))b_BM^2} \\ (2) & \sqrt{(a_C-(b_C+1))b_BM^2} & < & m_{ac} & < & \sqrt{(a_C-b_C)b_BM^2} \\ (3) & \sqrt{(a_C-b_C)b_BM^2} & < & m_{ac} & < & \sqrt{(a_C-(b_C+1))(b_B+1)M^2} \\ (4) & \sqrt{(a_C-(b_C+1))(b_B+1)M^2} & < & m_{ac} & < & \sqrt{(a_C-b_C)(b_B+1)M^2} \end{array}$$

Scenario II

$$\frac{1}{\Gamma}\frac{\mathrm{d}\Gamma}{\mathrm{d}m_{ac}} = \begin{cases} \frac{m_{ac}}{M^2}\left\{ 2\ln\left(\frac{b_B+1}{b_B}\right)\ln\left(\frac{a_C-b_C}{a_C-(b_C+1)}\right)\right\} & \text{for (1)} \\ \frac{m_{ac}}{M^2}\left\{ \left[\ln\left(\frac{a_C-b_C}{a_C-(b_C+1)}\right)\right]^2 - \left[\ln\left(\frac{(a_C-b_C)b_BM^2}{m_{ac}^2}\right)\right]^2 \right. & \\ \qquad \left. + \; 2\ln\left(\frac{(a_C-(b_C+1))(b_B+1)M^2}{m_{ac}^2}\right)\ln\left(\frac{a_C-b_C}{a_C-(b_C+1)}\right)\right\} & \text{for (2)} \\ \frac{m_{ac}}{M^2}\left\{ \left[\ln\left(\frac{(a_C-b_C)(b_B+1)M^2}{m_{ac}^2}\right)\right]^2 - \left[\ln\left(\frac{(a_C-b_C)b_BM^2}{m_{ac}^2}\right)\right]^2\right\} & \text{for (3)} \\ \frac{m_{ac}}{M^2}\left\{ \left[\ln\left(\frac{(a_C-b_C)(b_B+1)M^2}{m_{ac}^2}\right)\right]^2\right\} & \text{for (4)} \end{cases}$$

$$
\begin{array}{lrcccl}
(1) & 0 & < & m_{ac} & < & \sqrt{(a_C-(b_C+1))b_B M^2} \\
(2) & \sqrt{(a_C-(b_C+1))b_B M^2} & < & m_{ac} & < & \sqrt{(a_C-(b_C+1))(b_B+1)M^2} \\
(3) & \sqrt{(a_C-(b_C+1))(b_B+1)M^2} & < & m_{ac} & < & \sqrt{(a_C-b_C)b_B M^2} \\
(4) & \sqrt{(a_C-b_C)b_B M^2} & < & m_{ac} & < & \sqrt{(a_C-b_C)(b_B+1)M^2}
\end{array}
$$

A.1.1 The limit $m_\tau = 0$

We recall from Section 5.4 that setting the tau mass to zero has the following implications for the mass parameters:

$$
\begin{aligned}
a_B &= \frac{m_B^2}{m_B^2-m_A^2} \qquad & b_B &= 0 \\
a_C &= \frac{m_C^2}{m_C^2-m_B^2} \qquad & b_C &= 0 \\
M^2 &= \frac{(m_D^2-m_C^2)(m_C^2-m_B^2)(m_B^2-m_A^2)}{m_B^2\, m_C^2}
\end{aligned}
\tag{A.3}
$$

Consequently, mass scenario II vanishes and the number of split points along the m_{ac} axis is reduced, leaving only the two upper ranges of the scenario I distribution. Thus, in the limit of massless taus the m_{ac} distribution is reduced to

$$
\frac{1}{\Gamma}\frac{\mathrm{d}\Gamma}{\mathrm{d}m_{ac}}\bigg|_{m_\tau=0} = \begin{cases} \frac{m_{ac}}{M^2}\left\{\left[\ln\left(\frac{a_C}{a_C-1}\right)\right]^2 + 2\ln\left(\frac{(a_C-1)M^2}{m_{ac}^2}\right)\ln\left(\frac{a_C}{a_C-1}\right)\right\} & \text{for (1)} \\ \frac{m_{ac}}{M^2}\left\{\left[\ln\left(\frac{a_C M^2}{m_{ac}^2}\right)\right]^2\right\} & \text{for (2)} \end{cases}
$$

$$
\begin{array}{lrcccl}
(1) & 0 & < & m_{ac} & < & \sqrt{(a_C-1)M^2} \\
(2) & \sqrt{(a_C-1)M^2} & < & m_{ac} & < & \sqrt{a_C M^2}
\end{array}
$$

The full m_{ac} distribution (black) and the $m_\tau = 0$ approximation (red) are compared in Figure A.1, using the same sets of masses as in Chapter 5. It is worth noticing that even though taking $(m_C - m_B)$ close to m_τ increases the parameter b_C, the distribution with massless taus ($b_C = 0$) shows good agreement with the complete distribution

(Fig. A.1(e)). This behaviour is explained by the fact that $\mathrm{d}\Gamma/\,\mathrm{d}m_{ac}$ only depends on b_C through the difference $(a_C - b_C)$, and as $(m_C - m_B)$ decreases the parameter a_C increases faster than b_C, making $(a_C - b_C) \simeq a_C$ a good approximation.

A.2 The m_{bc} distribution in the spin-0 approximation

As particles b and c are produced in the decays $D \to c\,C$ and $C \to \tau_b\,B \to b\,\nu\,B$, their invariant mass m_{bc} is independent of the subsequent decay $B \to \tau_a\,A$. Consequently, we expect the distribution $\mathrm{d}\Gamma/\,\mathrm{d}m_{bc}$ to be independent of m_A. To see that this is indeed the case, despite the appearance of $a_B = m_B^2/\sqrt{\lambda_{B\tau A}}$ in (A.2), we note that

$$a_B\,M^2 \;=\; \frac{m_B^2}{\sqrt{\lambda_{B\tau A}}}\,\frac{(m_D^2 - m_C^2)\sqrt{\lambda_{B\tau A}}\sqrt{\lambda_{C\tau B}}}{m_B^2 m_C^2} \;=\; \frac{(m_D^2 - m_C^2)\sqrt{\lambda_{C\tau B}}}{m_C^2} \tag{A.4}$$

Evidently the parameters for the m_{bc} distribution could be chosen more economically, but to ease comparison with the m_{ac} and m_{high} distributions we will keep all parameters as previously defined. Deriving $\mathrm{d}\Gamma/\,\mathrm{d}m_{bc}$ from (A.2), we obtain

$$\frac{1}{\Gamma}\frac{\mathrm{d}\Gamma}{\mathrm{d}m_{bc}} \;=\; \begin{cases} \dfrac{2\,m_{bc}}{a_B\,M^2}\ln\!\left(\dfrac{b_C+1}{b_C}\right) & \text{for (1)} \\[2ex] \dfrac{2\,m_{bc}}{a_B\,M^2}\ln\!\left(\dfrac{a_B(b_C+1)M^2}{m_{bc}^2}\right) & \text{for (2)} \end{cases}$$

$$\begin{array}{lccccc} (1) & 0 & < & m_{ac} & < & \sqrt{a_B b_C M^2} \\ (2) & \sqrt{a_B b_C M^2} & < & m_{ac} & < & \sqrt{a_B(b_C+1)M^2} \end{array}$$

A.2.1 The limit $m_\tau = 0$

Since b_C vanishes in the limit of massless taus, the m_{bc} distribution reduces to

$$\left.\frac{1}{\Gamma}\frac{\mathrm{d}\Gamma}{\mathrm{d}m_{bc}}\right|_{m_\tau=0} \;=\; \frac{2\,m_{bc}}{a_B\,M^2}\ln\!\left(\frac{a_B M^2}{m_{bc}^2}\right) \qquad \text{for} \quad 0 \,<\, m_{bc} \,<\, \sqrt{a_B M^2}$$

As expected, the agreement between the complete and approximate m_{bc} distributions is good as long as $(m_C - m_B)$ is not close to m_τ (Fig. A.2).

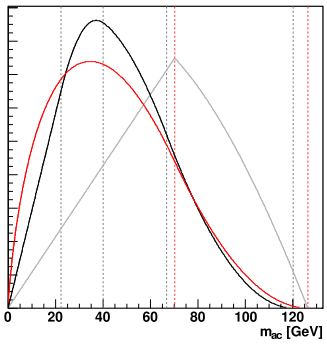

(a) $m_D = 550,\ m_C = 180,$
$m_B = 100,\ m_A = 97$ (GeV)
scenario I

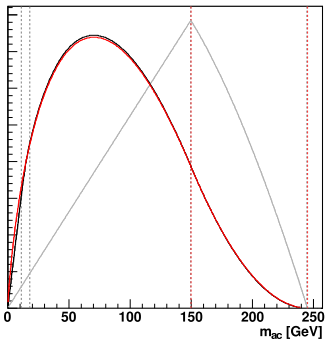

(b) $m_D = 550,\ m_C = 180,$
$m_B = 110,\ m_A = 97$ (GeV)
scenario I

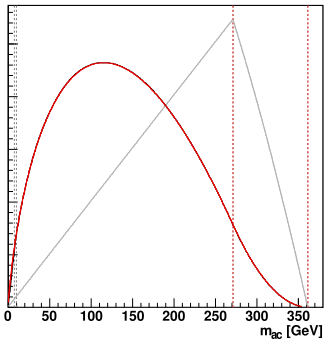

(c) $m_D = 550,\ m_C = 180,$
$m_B = 135,\ m_A = 97$ (GeV)
scenario I

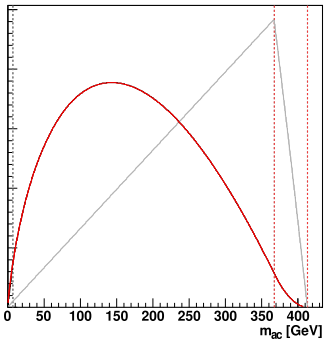

(d) $m_D = 550,\ m_C = 180,$
$m_B = 160,\ m_A = 97$ (GeV)
scenario I

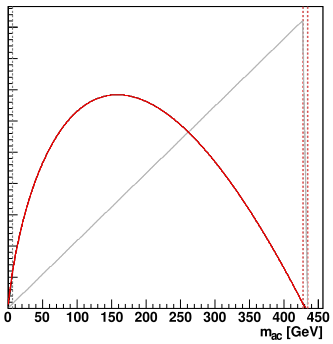

(e) $m_D = 550,\ m_C = 180,$
$m_B = 177,\ m_A = 97$ (GeV)
scenario I

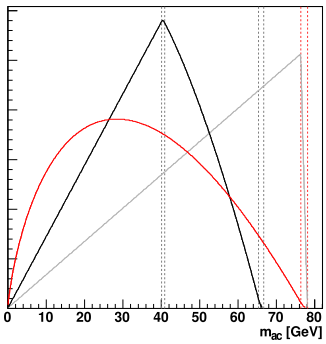

(f) $m_D = 550,\ m_C = 180,$
$m_B = 176,\ m_A = 174$ (GeV)
scenario I

Figure A.1: The $(1/\Gamma)(\,\mathrm{d}\Gamma/\,\mathrm{d}m_{ac})$ distribution (black) along with the $m_\tau = 0$ approximation (red) plotted for the same sets of masses used for m_{high} in Chapter 5. The corresponding distribution for a dilepton cascade is shown in grey [24].

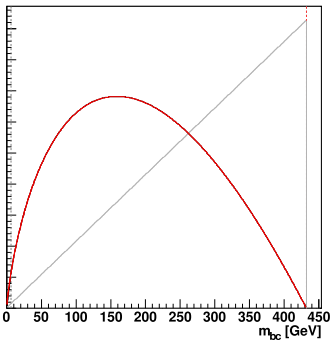

(a) $m_D = 550,\ m_C = 180,$
$m_B = 100$ (GeV)

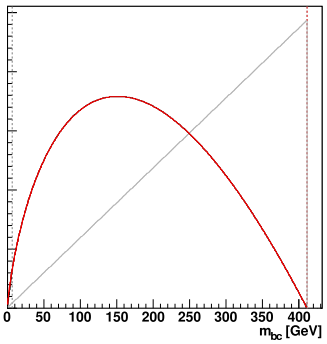

(b) $m_D = 550,\ m_C = 180,$
$m_B = 110$ (GeV)

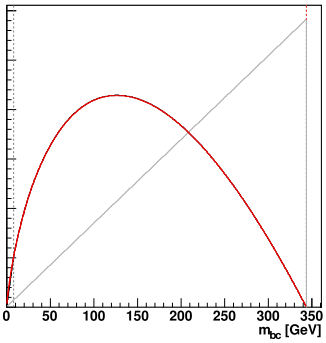

(c) $m_D = 550,\ m_C = 180,$
$m_B = 135$ (GeV)

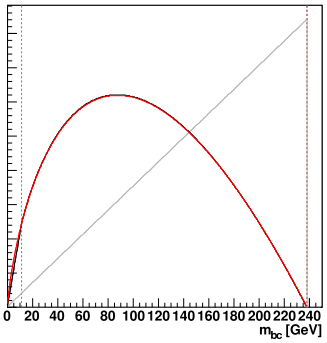

(d) $m_D = 550,\ m_C = 180,$
$m_B = 160$ (GeV)

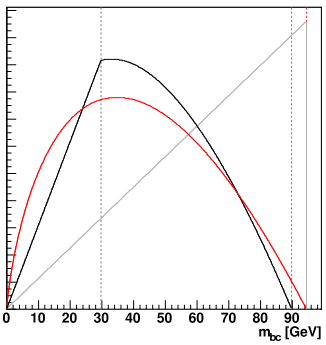

(e) $m_D = 550,\ m_C = 180,$
$m_B = 177$ (GeV)

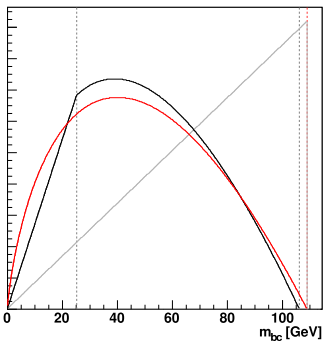

(f) $m_D = 550,\ m_C = 180,$
$m_B = 176$ (GeV)

Figure A.2: The $(1/\Gamma)(\,\mathrm{d}\Gamma/\,\mathrm{d}m_{bc})$ distribution (black) along with the $m_\tau = 0$ approximation (red) plotted for the same sets of masses used for m_{high} in Chapter 5. Note that the m_{bc} distribution is independent of m_A. The corresponding distribution for a dilepton cascade is shown in grey [24].

Appendix B

The Spin Dependent m_{ab} Distribution in the Collinear Approximation

In what follows we will illustrate an alternative derivation of the spin dependent m_{ab} distribution in the limit of massless taus. This derivation is outlined in [26, 27] and makes use of the 'collinear approximation' in which the visible tau products a and b are assumed to move in the directions of their respective taus, viewed from the lab frame.

In Section 6.2.1 we saw that the angular distribution in the decay $\tau_b \to b\,\nu$ is

$$\frac{1}{\Gamma}\frac{\mathrm{d}\Gamma}{\mathrm{d}\cos\theta_b} \;=\; \frac{1}{2}\left(1 - \beta\,\mathcal{P}_\beta\cos\theta_b\right) \tag{B.1}$$

Here $\beta = \pm$ and $\mathcal{P}_\beta = \pm$ specify the charge and polarisation of τ_b, respectively, while θ_b is the angle between the τ_b spin quantization axis and the three-momentum of b in the τ_b rest frame. (In Section 6.2.1 this angle was referred to as $\theta_{b\,\tau_b}^{\tau_b}$. See Figure 6.2 for illustration.) The spin axis can be chosen to coincide with the τ_b direction in the lab frame. With the lab-frame directions of a and b given by the directions of their parent taus, the spin dependent m_{ab} distributions will only differ from the linear $m_{\tau\tau}$ distribution due to the energy lost to the neutrinos. As noted earlier, the $m_{\tau\tau}$ distribution is identical for all spin configurations. Defining the energy fractions

$$z_a \;\equiv\; \frac{E_a^{\mathrm{lab}}}{E_{\tau_a}^{\mathrm{lab}}} \tag{B.2}$$

$$z_b \;\equiv\; \frac{E_b^{\mathrm{lab}}}{E_{\tau_b}^{\mathrm{lab}}} \tag{B.3}$$

we can obtain the desired m_{ab} distributions by folding the $m_{\tau\tau}$ distribution with the distributions of z_a and z_b. If we can express $\cos\theta_b$ in terms of z_b, the distribution of z_b can be found from from (B.1) by a change of variable. The procedure for deriving the z_a distribution from the distribution of $\cos\theta_a$ is completely analogous.

In finding an expression for $\cos\theta_b$ in terms of the energy fraction z_b, we start by defining the x-axis as the common direction of $\boldsymbol{p}_{\tau_b}^{\text{lab}}$ and spin quantization in the τ_b rest frame. From the definition of $\cos\theta_b$ it now follows that

$$\cos\theta_b \;=\; \frac{(p_b^{\tau_b})_x}{p_b^{\tau_b}} \tag{B.4}$$

With the lab frame and the τ_b rest frame being related by a boost $\beta_\tau = p_{\tau_b}^{\text{lab}}/E_{\tau_b}^{\text{lab}}$ along the x-axis, we can write down the following Lorentz transformations for particle b:

$$E_b^{\tau_b} \;=\; \gamma E_b^{\text{lab}} - \beta_\tau\gamma(p_b^{\text{lab}})_x \tag{B.5}$$

$$(p_b^{\tau_b})_x \;=\; -\beta_\tau\gamma E_b^{\text{lab}} + \gamma(p_b^{\text{lab}})_x \tag{B.6}$$

Solving (B.5) for $(p_b^{\text{lab}})_x$ and inserting the resulting expression into (B.6) leaves us with

$$(p_b^{\tau_b})_x \;=\; \frac{E_b^{\text{lab}}/\gamma - E_b^{\tau_b}}{\beta_\tau} \tag{B.7}$$

Thus, $\cos\theta_b$ can be expressed as

$$\cos\theta_b \;=\; \frac{E_b^{\text{lab}}/\gamma - E_b^{\tau_b}}{\beta_\tau p_b^{\tau_b}} \tag{B.8}$$

By squaring the four-momentum relation $P_\nu = P_{\tau_b} - P_b$ and evaluating the cross term in the rest frame of τ_b, we find (including the mass of b)

$$E_b^{\tau_b} \;=\; \frac{m_\tau^2 + m_b^2}{2\,m_\tau} \;=\; \frac{m_\tau}{2}\left(1 + \frac{m_b^2}{m_\tau^2}\right) \tag{B.9}$$

$$p_b^{\tau_b} \;=\; \frac{m_\tau^2 - m_b^2}{2\,m_\tau} \;=\; \frac{m_\tau}{2}\left(1 - \frac{m_b^2}{m_\tau^2}\right) \tag{B.10}$$

In addition, the term E_b^{lab}/γ appearing in the numerator in (B.8) can be rewritten as

$$\frac{E_b^{\text{lab}}}{\gamma} \;=\; \frac{m_\tau}{2}\left(\frac{2\,E_b^{\text{lab}}}{m_\tau\gamma}\right) \;=\; \frac{m_\tau}{2}\left(2\,\frac{E_b^{\text{lab}}}{E_{\tau_b}^{\text{lab}}}\right) \;=\; \frac{m_\tau}{2}\big(2\,z_b\big) \tag{B.11}$$

By inserting the results of (B.9) – (B.11) into (B.8) and cancelling the common factor $m_\tau/2$ we arrive at

$$\cos\theta_b \;=\; \frac{2\,z_b - 1 - m_b^2/m_\tau^2}{\beta_\tau\left(1 - m_b^2/m_\tau^2\right)} \tag{B.12}$$

As we have assumed b to me massless in all previous derivations, we now drop the terms m_b^2/m_τ^2. (If b is a pion, $m_b^2/m_\tau^2 \sim 0.6\,\%$.) Further, going to the collinear approximation corresponds to taking $\beta_\tau \to 1$. We are then left with the simple relation

$$\cos\theta \;=\; 2\,z_b - 1 \tag{B.13}$$

Using (B.13) to perform a change of variable in (B.1) we find the z_b distribution in the collinear limit:

$$\frac{1}{\Gamma}\frac{\mathrm{d}\Gamma}{\mathrm{d}z_b} \;=\; 1 - \beta\,\mathcal{P}_\beta\,(2\,z_b - 1) \tag{B.14}$$

Similarly, the distribution of $z_a = (E_a^{\mathrm{lab}}/E_{\tau_a}^{\mathrm{lab}})$ for the decay $\tau_a \to a\,\nu$ is given by

$$\frac{1}{\Gamma}\frac{\mathrm{d}\Gamma}{\mathrm{d}z_a} \;=\; 1 - \alpha\,\mathcal{P}_\alpha\,(2\,z_a - 1) \tag{B.15}$$

where $\alpha = \pm$ and $\mathcal{P}_\alpha = \pm$ specify the charge and polarisation of τ_a. Due to the assumed collinearity in the lab frame, we have that

$$\cos\theta_{ab}^{\mathrm{lab}} \;=\; \cos\theta_{\tau\tau}^{\mathrm{lab}} \tag{B.16}$$

With the taus treated as massless in the lab frame, the invariant mass m_{ab}^2 is related to the ditau invariant mass $m_{\tau\tau}^2$ by

$$\begin{aligned} m_{ab}^2 \;&=\; 2\,E_a^{\mathrm{lab}}\,E_b^{\mathrm{lab}}\left(1 - \cos\theta_{ab}^{\mathrm{lab}}\right) \\ &=\; 2\,z_a\,z_b\,E_{\tau_a}^{\mathrm{lab}}\,E_{\tau_b}^{\mathrm{lab}}\left(1 - \cos\theta_{\tau\tau}^{\mathrm{lab}}\right) \\ &=\; z_a\,z_b\,m_{\tau\tau}^2 \end{aligned} \tag{B.17}$$

The distribution of the squared ditau mass is simply

$$\frac{1}{\Gamma}\frac{\mathrm{d}\Gamma}{\mathrm{d}m_{\tau\tau}^2} \;=\; \frac{1}{M^2} \tag{B.18}$$

which corresponds to the well-known linear distribution of $m_{\tau\tau}$. Here M^2 denotes the maximum value of $m_{\tau\tau}^2$, given by

$$M^2 \;=\; \frac{(m_C^2 - m_B^2)(m_B^2 - m_A^2)}{m_B^2} \tag{B.19}$$

As the various normalised differential decay rates are nothing but probability density functions, and the variables m_{ab}^2, $m_{\tau\tau}^2$, z_a and z_b are related by (B.17), the desired m_{ab}^2 distribution can be obtained by folding $(1/\Gamma)(\,\mathrm{d}\Gamma/\,\mathrm{d}m_{\tau\tau}^2)$ with the z_a and z_b distributions. For notational convenience we define

$$\frac{1}{\Gamma}\frac{\mathrm{d}\Gamma}{\mathrm{d}m_{ab}^2} \;\equiv\; f(m_{ab}^2) \tag{B.20}$$

$$\frac{1}{\Gamma}\frac{\mathrm{d}\Gamma}{\mathrm{d}z_a} \;\equiv\; g_a(z_a) \tag{B.21}$$

$$\frac{1}{\Gamma}\frac{\mathrm{d}\Gamma}{\mathrm{d}z_b} \;\equiv\; g_b(z_b) \tag{B.22}$$

$$\frac{1}{\Gamma}\frac{\mathrm{d}\Gamma}{\mathrm{d}m_{\tau\tau}^2} \;\equiv\; h(m_{\tau\tau}^2) \tag{B.23}$$

The probability of observing m_{ab}^2 in the range $[\,m_{ab}^2\,,\,m_{ab}^2+\,\mathrm{d}m_{ab}^2\,]$ can now be expressed as [30]

$$f(m_{ab}^2)\,\mathrm{d}m_{ab}^2 \;=\; \iiint\limits_{\mathrm{d}S} g_a(z_a)\,g_b(z_b)\,h(m_{\tau\tau}^2)\;\mathrm{d}m_{\tau\tau}^2\,\mathrm{d}z_b\,\mathrm{d}z_a \tag{B.24}$$

where integration is over the infinitesimal volume $\mathrm{d}S$ of $(z_a, z_b, m_{\tau\tau}^2)$ space that corresponds to m_{ab}^2 values in $[\,m_{ab}^2\,,\,m_{ab}^2+\,\mathrm{d}m_{ab}^2\,]$. As we specify the order of integration we get

$$f(m_{ab}^2)\,\mathrm{d}m_{ab}^2 \;=\; \int\limits_{\frac{m_{ab}^2}{M^2}}^{1} g_a(z_a) \int\limits_{\frac{m_{ab}^2}{z_a\,M^2}}^{1} g_b(z_b) \int\limits_{\frac{m_{ab}^2}{z_a\,z_b}}^{\frac{m_{ab}^2+\mathrm{d}m_{ab}^2}{z_a\,z_b}} h(m_{\tau\tau}^2)\;\mathrm{d}m_{\tau\tau}^2\,\mathrm{d}z_b\,\mathrm{d}z_a \tag{B.25}$$

From (B.18) we know that $h(m_{\tau\tau}^2) = 1/M^2$, which makes the integration over $m_{\tau\tau}^2$ trivial:

$$\int\limits_{\frac{m_{ab}^2}{z_a\,z_b}}^{\frac{m_{ab}^2+\mathrm{d}m_{ab}^2}{z_a\,z_b}} h(m_{\tau\tau}^2)\;\mathrm{d}m_{\tau\tau}^2 \;=\; \frac{1}{M^2}\frac{\mathrm{d}m_{ab}^2}{z_a\,z_b} \tag{B.26}$$

Inserting this result back into (B.25) we see that m_{ab}^2 is distributed according to

$$f(m_{ab}^2) \;=\; \frac{1}{M^2}\int\limits_{\frac{m_{ab}^2}{M^2}}^{1}\int\limits_{\frac{m_{ab}^2}{z_a\,M^2}}^{1} g_a(z_a)\,g_b(z_b)\,\frac{1}{z_a\,z_b}\;\mathrm{d}z_b\,\mathrm{d}z_a \tag{B.27}$$

Obtaining the m_{ab}^2 distribution for various combinations of tau charges and helicities is now just a matter of inserting the corresponding z_a and z_b distributions (Equations (B.14) and (B.15)) and perform the remaining integrations. The explicit $g_a(z_a)$ and $g_b(z_b)$ expressions for the different tau configurations are are given below:

$$\tau_b \;=\; \begin{cases} \tau_L^-, \tau_R^+ & \Rightarrow \quad g_b(z_b) \;=\; 2\,(1-z_b) \\ \tau_R^-, \tau_L^+ & \Rightarrow \quad g_b(z_b) \;=\; 2\,z_b \end{cases} \tag{B.28}$$

$$\tau_a \;=\; \begin{cases} \tau_L^-, \tau_R^+ & \Rightarrow \quad g_a(z_a) \;=\; 2\,(1-z_a) \\ \tau_R^-, \tau_L^+ & \Rightarrow \quad g_a(z_a) \;=\; 2\,z_a \end{cases} \tag{B.29}$$

We recall that particles A and C are assumed to be neutral, implying that τ_a and τ_b must be of opposite charge. As integrating (B.27) for various choices of $g_a(z_a)$ and $g_b(z_b)$ is straightforward, further details will be omitted.

After all integrations have been performed the spin dependent m_{ab}^2 distributions in the collinear approximation are obtained. Returning to the notation of differential decay rates and expressing the distributions in terms of m_{ab} (rather than m_{ab}^2), we have:

1. $\left(\tau_b\,,\,\tau_a\right) \;=\; \left(\tau_L^-\,,\,\tau_R^+\right),\,\left(\tau_R^+\,,\,\tau_L^-\right)$

$$\frac{1}{\Gamma}\frac{\mathrm{d}\Gamma}{\mathrm{d}m_{ab}} \;=\; \frac{8\,m_{ab}}{M^2}\left\{\frac{1}{2}\left[\ln\!\left(\frac{M^2}{m_{ab}^2}\right)\right]^2 - \left(2+\frac{m_{ab}^2}{M^2}\right)\ln\!\left(\frac{M^2}{m_{ab}^2}\right) \;+\; 3\left(1-\frac{m_{ab}^2}{M^2}\right)\right\}$$

2. $\left(\tau_b\,,\,\tau_a\right) \;=\; \left(\tau_R^-\,,\,\tau_R^+\right),\,\left(\tau_L^+\,,\,\tau_L^-\right),\,\left(\tau_L^-\,,\,\tau_L^+\right),\,\left(\tau_R^+\,,\,\tau_R^-\right)$

$$\frac{1}{\Gamma}\frac{\mathrm{d}\Gamma}{\mathrm{d}m_{ab}} \;=\; \frac{8\,m_{ab}}{M^2}\left\{\left(1+\frac{m_{ab}^2}{M^2}\right)\ln\!\left(\frac{M^2}{m_{ab}^2}\right) \;+\; 2\left(\frac{m_{ab}^2}{M^2}-1\right)\right\}$$

3. $\left(\tau_b\,,\,\tau_a\right) \;=\; \left(\tau_R^-\,,\,\tau_L^+\right),\,\left(\tau_L^+\,,\,\tau_R^-\right)$

$$\frac{1}{\Gamma}\frac{\mathrm{d}\Gamma}{\mathrm{d}m_{ab}} \;=\; \frac{8\,m_{ab}}{M^2}\left\{\left(1-\frac{m_{ab}^2}{M^2}\right) \;-\; \frac{m_{ab}^2}{M^2}\ln\!\left(\frac{M^2}{m_{ab}^2}\right)\right\}$$

$$\text{for} \quad 0 \;<\; m_{ab}^2 \;<\; M^2$$

As expected, the above distributions are identical to those derived in Section 6.4, where further discussion of these results can be found.

Appendix C

The Differential Decay Rate

As the main quantity of interest in this thesis is the differential decay rate, we present here an outline of how this quantity is derived from field theory. For this purpose we first briefly introduce the *Interaction Picture* of quantum mechanics, along with the concept of the *S-matrix*. The following treatment is largely based on Mandl & Shaw [2].

C.1 The Interaction Picture

When treating particle interactions it is convenient to work in the so called Interaction Picture (I.P.). This picture is based on a division of the Hamiltonian H into a free part H_0 describing free fields, and an interaction part H_I:

$$H \;=\; H_0 \,+\, H_I \tag{C.1}$$

The advantage of employing the interaction picture is that the time evolution of a system is split between states and operators: operators evolve according to H_0, while states are evolved by H_I. More precisely, the equation of motion for states is the I.P. version of the Scrödinger equation, given by

$$i\frac{\mathrm{d}}{\mathrm{d}t}\,|\Phi(t)\rangle \;=\; H_I(t)\,|\Phi(t)\rangle \tag{C.2}$$

while for operators the equation of motion is the I.P. version of the Heisenberg equation

$$i\frac{\mathrm{d}}{\mathrm{d}t}O(t) \;=\; \big[\,O(t)\,,\,H_0\,\big] \tag{C.3}$$

In what follows we will focus on the time evolution of states. With the initial condition that the system is in a well-defined state $|i\rangle$ at time $t = t_0$, that is $|\Phi(t_0)\rangle = |i\rangle$, a formal solution of (C.2) is

$$|\Phi(t)\rangle = U(t)\,|i\rangle = T\exp\left(-i\int_{t_0}^{t}\mathrm{d}t'\,H_I(t')\right)|i\rangle \tag{C.4}$$

Here T denotes time-ordering of the operator products $H_I(t')H_I(t'')(\ldots)$ resulting from expanding the exponential. As $H_I(t)$ is Hermitian, it follows that $U(t)$ is unitary. Thus, the normalisation of states is preserved under time evolution by $U(t)$:

$$\langle\Psi(t)\,|\,\Psi(t)\rangle = \langle i|\,U^{\dagger}(t)U(t)\,|i\rangle = \langle i|\,U^{-1}(t)U(t)\,|i\rangle = \langle i\,|\,i\rangle = 1 \tag{C.5}$$

C.2 The S-matrix

For a particle interaction we are interested in connecting the known initial state 'long' before the interaction (relative to the interaction time span)

$$|\Phi(-\infty)\rangle = |i\rangle \tag{C.6}$$

with the state 'long' after the interaction, $|\Phi(\infty)\rangle$. For this purpose we define the S-matrix to be the operator evolving states from $t = -\infty$ to $t = \infty$:

$$|\Phi(\infty)\rangle = S\,|\Phi(-\infty)\rangle = S\,|i\rangle \tag{C.7}$$

In this definition $|\Phi(\infty)\rangle$ contains *all* possible final states that can result from $|i\rangle$ undergoing the interaction given by $H_I(t)$. Note that S is nothing but a special version of the unitary operator $U(t)$ (defined in (C.4)) for the case $t_0 = -\infty$ and $t = \infty$. If we let a specific final state be denoted $|f\rangle$, the probability of observing the system in exactly this state long after the interaction is given by

$$\left|\,\langle f\,|\,\Phi(\infty)\rangle\,\right|^2 = \left|\,\langle f|\,S\,|i\rangle\,\right|^2 \equiv |S_{fi}|^2 \tag{C.8}$$

where we have defined the S-matrix element S_{fi}. It is from this probability that we will obtain observables like cross sections and decay rates. With the specific final states $|f\rangle$ forming a complete, orthonormal set of states, $|\Phi(\infty)\rangle$ can be expanded as

$$|\Phi(\infty)\rangle = \sum_f |f\rangle\,\langle f\,|\,\Phi(\infty)\rangle = \sum_f S_{fi}\,|f\rangle \tag{C.9}$$

Using this expansion we can see that the unitarity of S implies conservation of probability:

$$\begin{aligned} 1 \;&=\; \langle i \,|\, i \rangle \;=\; \langle i |\, S^\dagger S \,| i \rangle \;=\; \langle \Phi(\infty) \,|\, \Phi(\infty) \rangle \\ &= \Big(\sum_{f'} \langle f' |\, S^*_{f'i} \Big) \Big(\sum_{f} S_{fi} \,| f \rangle \Big) \\ &= \sum_{f'} \sum_{f} S^*_{f'i} \, S_{fi} \, \delta_{f'f} \\ &= \sum_{f} |S_{fi}|^2 \end{aligned} \tag{C.10}$$

As stated earlier, we are interested in obtaining the probability $|S_{fi}|^2$ for a specific process $|i\rangle \to |f\rangle$. From the definition of $U(t)$ in (C.4) we know that S can be expressed as

$$S \;=\; T \exp\left(-i \int_{-\infty}^{\infty} \mathrm{d}t' \, H_I(t') \right) \tag{C.11}$$

By writing S in terms of Hamiltonian densities rather than Hamiltonians, using

$$H_I(t) \;=\; \int \mathrm{d}^3x \, \mathcal{H}_I(t) \tag{C.12}$$

we arrive at an explicitly covariant expression:

$$\begin{aligned} S \;&=\; T \exp\left(-i \int \mathrm{d}^4x \, \mathcal{H}_I(t') \right) \\ &=\; 1 \,+\, \sum_{n=1}^{\infty} \frac{(-i)^n}{n!} \int \ldots \int \mathrm{d}^4x_1 \ldots \mathrm{d}^4x_n \, T\big\{ \mathcal{H}_I(x_1) \ldots \mathcal{H}_I(x_n) \big\} \end{aligned} \tag{C.13}$$

The above expansion of the S-matrix is known as the Dyson expansion. It forms the basis for doing calculations in perturbation theory, as, given a small interaction energy of H_I, the series can be truncated when the desired accuracy is obtained.

There are, however, several complications connected to extracting the desired matrix element $\langle f |\, S \,| i \rangle$, and we will just briefly mention some here. First, the initial and final states $|i\rangle$ and $|f\rangle$ used are stationary states of the free field Hamiltonian H_0, which describes fields as non-interacting. Using these states may seem invalid as we are developing a formalism for particle interactions. However, this conceptual difficulty can be remedied by assuming that the interaction only is of importance when the particles are relatively close together, such that $H_I \to 0$ when $t \to \infty$. Second, the fields

contained in $\mathcal{H}_I(x)$ are subject to normal-ordering (absorption operators to the right of creation operators), thus to be able to expand S in a meaningful way we must know how to deal with time-ordered products of normal-ordered operators. The solution to this problem is found in Wick's theorem, where it is shown that such time-orderings can be expanded to give sums of normal-ordered operator products combined with vacuum expectation values of time-ordered operators. A general term in this sum will thus contain normal-ordered annihilation and creation operators for a set of initial and final external particles, along with vacuum expectation values which can be interpreted as propagators. Upon calculating $\langle f| S |i\rangle$, only the terms that exactly annihilate $|i\rangle$ and create $|f\rangle$ give non-zero contributions.

C.3 From matrix elements to observable decay rates

Studying the matrix element S_{fi} for various processes, the resulting expressions can be seen to exhibit a common structure:

$$\begin{aligned} S_{fi} \;=\; \delta_{fi} + (2\pi)^4 \delta^{(4)}\Big(\sum P_i - \sum P_f\Big) \prod_i \left(\frac{1}{2VE_i}\right)^{1/2} \\ \times \prod_f \left(\frac{1}{2VE_f}\right)^{1/2} \prod_l (2\,m_l)^{1/2}\, \mathcal{M} \end{aligned} \tag{C.14}$$

Here indices i and f run over all initial- and final-state particles, respectively, while l runs over all fermions involved. The Kronecker delta in front is for the case of no interaction, $|i\rangle = |f\rangle$. The four-dimensional delta function ensures conservation of four-momentum, while V represents a normalisation volume used in plane-wave expansions of fields. Being a non-physical volume, V must of course drop out of all measurable quantities, and we will shortly see that this is indeed the case. All the process-specific dynamics are contained in the Feynman amplitude $\mathcal{M}$.

For a particle decay $P \to P_1 + P_2 + \ldots + P_N$ the expression for S_{fi} simplifies to

$$\begin{aligned} S_{fi} \;=\; \delta_{fi} + (2\pi)^4 \delta^{(4)}\Big(P - \sum P_f\Big) \left(\frac{1}{2VE}\right)^{1/2} \\ \times \prod_f \left(\frac{1}{2VE_f}\right)^{1/2} \prod_l (2\,m_l)^{1/2}\, \mathcal{M} \end{aligned} \tag{C.15}$$

In what follows we will leave out the term δ_{fi}. As the integrations in (C.13) are over all of spacetime, the above expressions for S_{fi} correspond to the limit of infinite time

T and infinite normalisation volume V. To aid the following derivation we will assume V and T to be large but finite, before taking the limits $V \to \infty$ and $T \to \infty$ at the end. With T finite, the transition probability per unit time, w_{fi}, is

$$w_{fi} \;=\; \frac{|S_{fi}|^2}{T} \tag{C.16}$$

Before we can write out the expression for w_{fi} explicitly, the delta function $\delta^{(4)}(P - \sum P_f)$ in (C.15) must be replaced with its counterpart for finite T and V, $\delta^{(4)}_{TV}(P - \sum P_f)$. The two functions are related by

$$\delta^{(4)}\Big(P - \sum P_f\Big) \;=\; \lim_{\substack{T\to\infty \\ V\to\infty}} \delta^{(4)}_{TV}\Big(P - \sum P_f\Big) \tag{C.17}$$

A finite delta function $\delta_L(x)$ (working in one dimension for simplicity) satisfying the one-dimensional analogue of (C.17) can be defined as **[ref?]**

$$\delta_L(x) \;=\; \frac{1}{(2\pi)} \int_{-\infty}^{\infty} \mathrm{d}y\, e^{ixy}\, e^{-2|y|/L} \tag{C.18}$$

for which we have that

$$\delta_L(0) \;=\; \frac{L}{(2\pi)} \tag{C.19}$$

The squared four-dimensional delta function appearing in $|S_{fi}|^2$ can thus be expressed as

$$\begin{aligned} \Big[\delta^{(4)}_{TV}\Big(P - \sum P_f\Big)\Big]^2 \;&=\; \Big[\delta^{(4)}_{TV}(0)\Big]\Big[\delta^{(4)}_{TV}\Big(P - \sum P_f\Big)\Big] \\ &=\; \frac{TV}{(2\pi)^4}\, \delta^{(4)}_{TV}\Big(P - \sum P_f\Big) \end{aligned} \tag{C.20}$$

Using the above result the transition rate w_{fi} defined in (C.16) becomes

$$w_{fi} \;=\; (2\pi)^4 V\, \delta^{(4)}\Big(P - \sum P_f\Big) \Big(\frac{1}{2\,VE}\Big) \prod_f \Big(\frac{1}{2\,VE_f}\Big) \prod_l (2\,m_l)\, |\mathcal{M}|^2 \tag{C.21}$$

This is the transition rate from $|i\rangle$ to the exact final state $|f\rangle$. However, what we can observe are transitions to final states where the outgoing particles have three-momenta within the intervals $[\,\boldsymbol{p}_f\,,\ \boldsymbol{p}_f + \mathrm{d}\boldsymbol{p}_f\,]$. Therefore, in order to obtain a physical transition

rate, w_{fi} must be multiplied by the number of such states. For a large but finite normalisation volume V this number of states is given by

$$\prod_f \frac{V\,\mathrm{d}^3\boldsymbol{p}_f}{(2\pi)^3} \tag{C.22}$$

Upon multiplying w_{fi} by (C.22) we note that all factors of the non-physical volume V cancel. Thus, when we now let T and V become infinite again, all that changes is $\delta^{(4)}_{TV}(\ldots) \to \delta^{(4)}(\ldots)$. This leaves us with the physically meaningful differential decay rate $\mathrm{d}\Gamma$:

$$\mathrm{d}\Gamma \;=\; (2\pi)^4\delta^{(4)}\Big(P - \sum P_f\Big)\left(\frac{1}{2\,E}\right)|\mathcal{M}|^2\prod_l\big(2m_l\big)\prod_f\left(\frac{\mathrm{d}^3\boldsymbol{p}_f}{(2\pi)^3 2\,E_f}\right) \tag{C.23}$$

From (C.23) the differential decay rate with respect to some observable kinematical property (x) of the final-state particles can be obtained by integrating over all other final-state variables. Moreover, if we divide by the total decay rate Γ we arrive at a normalised differential decay rate

$$\frac{1}{\Gamma}\frac{\mathrm{d}\Gamma}{\mathrm{d}x} \;=\; f(x) \tag{C.24}$$

which can be interpreted as a probability density for the observable x in the decay $P \to P_1 + P_2 + \ldots + P_N$. The results derived in Chapters 4 – 6 are all in the general form of (C.24), with x being the invariant mass of two visible final-state particles.

References

[1] K. Nakamura *et al.*, "Particle Data Group," *Journal of Physics G* **37** (2010) 075021. `http://pdg.lbl.gov`. 3, 4, 47

[2] F. Mandl and G. Shaw, *Quantum Field Theory*. John Wiley & Sons, 2010. 7, 151

[3] V. Barger and R. Phillips, *Collider Physics*. Frontiers in physics. Addison-Wesley Pub. Co., 1997. 7

[4] **Gfitter** Collaboration, A. Hoecker, "Status of the Global Electroweak Fit of the Standard Model," *PoS* **EPS-HEP2009** (2009) 366, `arXiv:0909.0961 [hep-ph]`. 28, 29

[5] S. P. Martin, "A Supersymmetry Primer," `arXiv:hep-ph/9709356`. 28, 31, 37, 40, 47

[6] A. D. Sakharov, "Violation of CP Invariance, C Asymmetry, and Baryon Asymmetry of the Universe," *Pisma Zh. Eksp. Teor. Fiz.* **5** (1967) 32–35. 29

[7] V. C. Rubin, N. Thonnard, and W. K. Ford, Jr., "Rotational properties of 21 SC galaxies with a large range of luminosities and radii, from NGC 4605 /R = 4kpc/ to UGC 2885 /R = 122 kpc/," *Astrophys. J.* **238** (1980) 471. 29

[8] A. N. Taylor, S. Dye, T. J. Broadhurst, N. Benitez, and E. van Kampen, "Gravitational Lens Magnification and the Mass of Abell 1689," `arXiv:astro-ph/9801158`. 29

[9] N. Jarosik *et al.*, "Seven-Year Wilkinson Microwave Anisotropy Probe (WMAP) Observations: Sky Maps, Systematic Errors, and Basic Results," *Astrophys. J. Suppl.* **192** (2011) 14, `arXiv:1001.4744 [astro-ph.CO]`. 29, 30

[10] A. Liddle, *An Introduction to Modern Cosmology*. Wiley, 2003. 30

[11] U. Amaldi, W. de Boer, and H. Furstenau, "Comparison of Grand Unified Theories with Electroweak and Strong Coupling Constants Measured at LEP," *Phys. Lett.* **B260** (1991) 447–455. 30

[12] I. Aitchison, *Supersymmetry in Particle Physics: An Elementary Introduction*. Cambridge University Press, 2007. 31

[13] S. R. Coleman and J. Mandula, "All Possible Symmetries of the S Matrix," *Phys. Rev.* **159** (1967) 1251–1256. 32

[14] R. Haag, J. T. Lopuszanski, and M. Sohnius, "All Possible Generators of Supersymmetries of the S Matrix," *Nucl. Phys.* **B88** (1975) 257. 32

[15] **Super-Kamiokande** Collaboration, H. Nishino *et al.*, "Search for Proton Decay via $p \to e^+\pi^0$ and $p \to \mu^+\pi^0$ in a Large Water Cherenkov Detector," *Phys. Rev. Lett.* **102** (2009) 141801, arXiv:0903.0676 [hep-ex]. 41

[16] F. E. Paige, "Determining SUSY Particle Masses at LHC," arXiv:hep-ph/9609373. 43

[17] I. Hinchliffe, F. E. Paige, M. D. Shapiro, J. Soderqvist, and W. Yao, "Precision SUSY Measurements at CERN LHC," *Phys. Rev.* **D55** (1997) 5520–5540, arXiv:hep-ph/9610544. 43

[18] B. C. Allanach, C. G. Lester, M. A. Parker, and B. R. Webber, "Measuring Sparticle Masses in Non-Universal String Inspired Models at the LHC," *JHEP* **09** (2000) 004, arXiv:hep-ph/0007009. 43, 45

[19] H. Bachacou, I. Hinchliffe, and F. E. Paige, "Measurements of Masses in SUGRA Models at CERN LHC," *Phys. Rev.* **D62** (2000) 015009, arXiv:hep-ph/9907518. 43, 44

[20] B. K. Gjelsten, D. J. Miller, and P. Osland, "Measurement of SUSY Masses via Cascade Decays for SPS 1a," *JHEP* **12** (2004) 003, arXiv:hep-ph/0410303. 43, 44, 45

[21] B. K. Gjelsten, D. J. Miller, and P. Osland, "Determining Masses of Supersymmetric Particles," arXiv:hep-ph/0511008. 46

[22] B. K. Gjelsten, D. J. Miller, P. Osland, and A. R. Raklev, "Mass Determination in Cascade Decays Using Shape Formulas," *AIP Conf. Proc.* **903** (2007) 257–260, arXiv:hep-ph/0611259. 47, 137

[23] B. K. Gjelsten, D. J. Miller, P. Osland, and A. R. Raklev, "Mass Ambiguities in Cascade Decays," arXiv:hep-ph/0611080. 47

[24] D. J. Miller, P. Osland, and A. R. Raklev, "Invariant Mass Distributions in Cascade Decays," *JHEP* **03** (2006) 034, arXiv:hep-ph/0510356. 47, 50, 82, 136, 143, 144

[25] C. G. Lester, "Constrained Invariant Mass Distributions in Cascade Decays: The Shape of the 'm(qll)-threshold' and Similar Distributions," *Phys. Lett.* **B655** (2007) 39–44, arXiv:hep-ph/0603171. 47, 137

[26] S. Y. Choi, K. Hagiwara, Y. G. Kim, K. Mawatari, and P. M. Zerwas, "Tau Polarization in SUSY Cascade Decays," *Phys. Lett.* **B648** (2007) 207–212, arXiv:hep-ph/0612237. 48, 107, 128, 136, 137, 145

[27] M. Graesser and J. Shelton, "Probing Supersymmetry With Third-Generation Cascade Decays," *JHEP* **06** (2009) 039, arXiv:0811.4445 [hep-ph]. 48, 107, 110, 128, 129, 130, 137, 145

[28] P. Richardson, "Spin Correlations in Monte Carlo Simulations," *JHEP* **11** (2001) 029, arXiv:hep-ph/0110108. 64

[29] A. J. Barr, "Using Lepton Charge Asymmetry to Investigate the Spin of Supersymmetric Particles at the LHC," *Phys. Lett.* **B596** (2004) 205–212, arXiv:hep-ph/0405052. 64, 65

[30] G. Cowan, *Statistical Data Analysis*. Oxford science publications. Clarendon Press, 1998. 148